September 2015

Bio-Photoelectrochemical Solar Cells Incorporating Reaction Center and Reaction Center Plus Light Harvesting Complexes

Houman Yaghoubi
University of South Florida, hyaghoubi@mail.usf.edu

Bio-Photoelectrochemical Solar Cells Incorporating Reaction Center and Reaction Center Plus Light

Harvesting Complexes

by

Houman Yaghoubi

A dissertation submitted in partial fulfillment
of the requirements for the degree of
Doctor of Philosophy in Electrical Engineering
Department of Electrical Engineering
College of Engineering
University of South Florida

Major Professor: Arash Takshi, Ph.D.
Rudy Schlaf, Ph.D.
Shengqian Ma, Ph.D.
Jing Wang, Ph.D.
Nathan Gallant, Ph.D.

Date of Approval:
February 27, 2015

Keywords: Solar Energy Conversion, Photoactive Films, Rhodobacter Sphaeroides, Photosynthetic
Protein Complexes

DEDICATION

To my mother, father, and brother, Mahin Mehdizadeh, Yousef Yaghoubi, and Shayan Yaghoubi for their

unconditional love, support, dedication, and inspiration.

ACKNOWLEDGMENTS

TABLE OF CONTENTS

LIST OF TABLES

LIST OF FIGURES

ABSTRACT

Harvesting solar energy can potentially be a promising solution to the energy crisis now and in the future. However, material and processing costs continue to be the most important limitations for the commercial devices. A key solution to these problems might lie within the development of bio-hybrid solar cells that seeks to mimic photosynthesis to harvest solar energy and to take advantage of the low material costs, negative carbon footprint, and material abundance. The bio-photoelectrochemical cell technologies exploit biomimetic means of energy conversion by utilizing plant-derived photosystems which can be inexpensive and ultimately the most sustainable alternative. Plants and photosynthetic bacteria harvest light, through special proteins called reaction centers (RCs), with high efficiency and convert it into electrochemical energy. In theory, photosynthetic RCs can be used in a device to harvest solar energy and generate 1.1 V open circuit voltage and $\sim$1 mA cm^{-2} short circuit photocurrent. Considering the nearly perfect quantum yield of photo-induced charge separation, efficiency of a protein-based solar cell might exceed 20%. In practice, the efficiency of fabricated devices has been limited mainly due to the challenges in the electron transfer between the protein complex and the device electrodes as well as limited light absorption. The overarching goal of this work is to increase the power conversion efficiency in protein-based solar cells by addressing those issues (*i.e.* electron transfer and light absorption). This work presents several approaches to increase the charge transfer rate between the photosynthetic RC and underlying electrode as well as increasing the light absorption to eventually enhance the external quantum efficiency (EQE) of bio-hybrid solar cells. The first approach is to decrease the electron transfer distance between one of the redox active sites in the RC and the underlying electrode by direct attachment of the of protein complex onto Au electrodes *via* surface exposed cysteine residues. This resulted in photocurrent densities as large as $\sim$600 nA cm^{-2} while still the incident photon to generated electron quantum efficiency was as low as %3 $\times$ 10^{-4}. 2- The second approach is to immobilize wild type RCs of *Rhodobacter sphaeroides* on

the surface of a Au underlying electrode using self-assembled monolayers of carboxylic acid terminated

oligomers and cytochrome *c* charge mediating layers, with a preferential orientation from the primary

electron donor site. This approach resulted in EQE of up to 0.06%, which showed 200 times efficiency

improvement comparing to the first approach. In the third approach, instead of isolated protein complexes,

RCs plus light harvesting (LH) complexes were employed for a better photon absorption. Direct attachment

of RC-LH1 complexes on Au working electrodes, resulted in 0.21% EQE which showed 3.5 times

efficiency improvement over the second approach (700 times higher than the first approach). The main

impact of this work is the harnessing of biological RCs for efficient energy harvesting in man-made

structures. Specifically, the results in this work will advance the application of RCs in devices for energy

harvesting and will enable a better understanding of bio and nanomaterial interfaces, thereby advancing the

application of biological materials in electronic devices. At the end, this work offers general guidelines that

can serve to improve the performance of bio-hybrid solar cells.

CHAPTER 1 : INTRODUCTION

1.1. Visionary Scenario of Electricity Generation in Future

Humankind has burnt a wide variety of energy sources so far, mainly carbon fossil fuels, which has led to environmental catastrophes due to greenhouse gas emissions. CO_2 is the major greenhouse gas emitted through humankind activities. Coal-fired power plants remain the major source of electricity generation in 2014 and the goal of restraining climate warming to 2 °C is becoming increasingly onerous with every passing year. The amount of CO_2 which is being produced annually creates chronic diseases over time, inflames lung tissue (asthma), reduces lung function, increases the risk of blood clots, reduces oxygen saturation, increases the risk of brain stroke, alters cardiac autonomic function, and reduces the ability of cardiac cells to repair themselves.[1] This should be added to CO_2 environmental adverse effects such as air pollution, global climate change due to the accumulation of greenhouse gases in the earth's atmosphere, and creation of acidic gases and rain, which kills plant life, pollutes rivers and streams, and erodes stonework. The following diagram demonstrates how coal power plants emission in 27 European countries, impacts annual health of people. The following diagram illustrates that the coal power generation in these countries in 2009 caused €15.5-€42.8 billion total health costs per year.
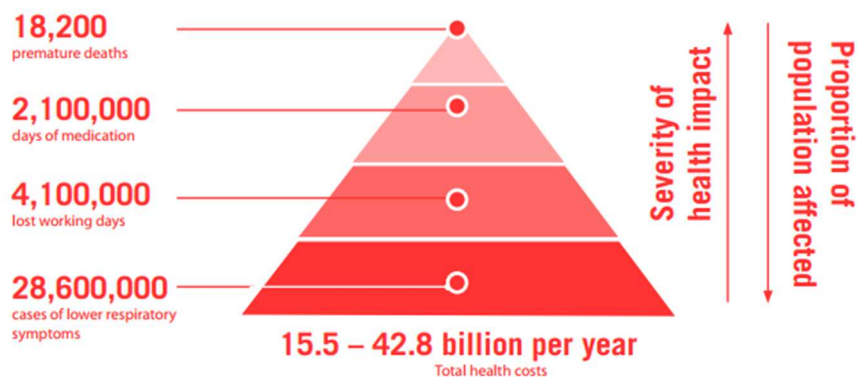
Figure 1.1 Annual health impacts caused by coal power plants in the EU, 27 countries (used with permission[1]).

Currently 40% of world electricity comes from combustion.[2] In the meantime, it is well known now that the earth's oil reserves could run out during this century. We should add the above facts to the public concern such as environmental pollution arising from frequent oil spills such as the British Petroleum (BP) oil spill incident in 2010. In the meantime, the energy need would be almost doubled over the next 50 years. Hence, evidently new systems and strategies are crucial for generation of electricity.

The increasing demand for the production of energy without a direct link to combustion of fossil fuels and the accompanying production of CO_2 has brought attention to the clean renewable energies.[3] Figure 1.2 shows the US electricity generation by energy source in 2013.
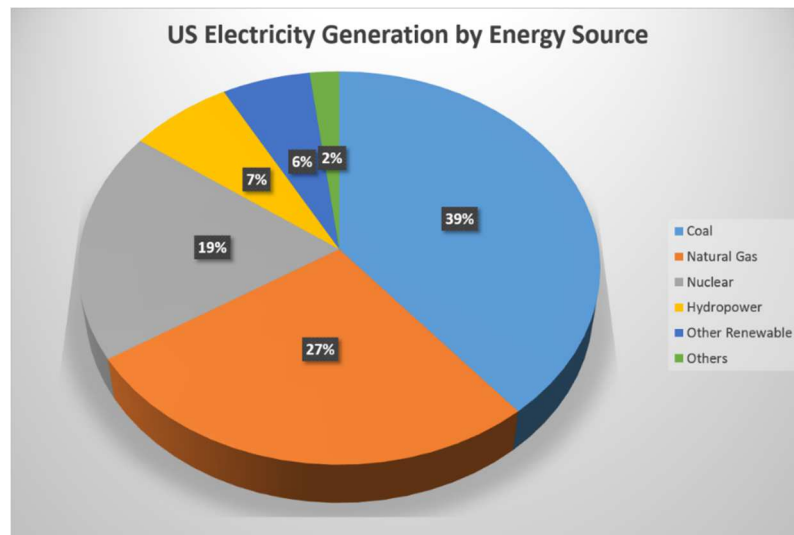
Figure 1.2 The US electricity generation by energy source in 2013. Reproduced from the data presented by US Energy Information Administration.

Revolution in the future sources of electricity simply means that the share of renewables should be increased significantly for the future sources of electricity. It seems harvesting of solar energy as a carbon free source can potentially be a promising solution to the energy crises and environmental pollution. Almost 1.2×10^5 TW of energy strikes at the earth surface from the sun out of which 600 TW is useable, when subtracting the amount that is being absorbed by ocean, mountains, *etc.* Hence, there is this vast excess of energy reaching the earth from the sun to our already vast global electricity demand. Additionally, this source is free and clean. However, the solar production of electricity compares to the utilization of all energy

sources is unfortunately tiny. One of the main problems on the road of utilizing solar energy is cost. The associated cost of electricity generation using solar energy is more than what we currently pay for electricity using coal. The US Department of Energy (DOE) has set an ambitious target of reaching the cost of 5 cents per kWh (or 1$/Wp). This means that to achieve this goal, various types of solar cell technologies should be developed, so each can play a role in providing the electricity need for the global future demand. To address both the sustainability in energy production from renewable sources and the increasing demand for photovoltaic devices, a potential approach is to use natural materials from photosynthetic cells to fabricate solar cells. This dissertation mainly focuses on a few challenges in employing photosynthetic reaction center (RC) proteins for solar energy harvesting in photovoltaic devices.

In this chapter, the principles of photoelectrochemical cell technologies with a brief summary of dye sensitized solar cells are reviewed. Also, in a greater detail, some basics of photosynthesis are explained with a comprehensive review of different strategies implemented to date for fabrication of solar energy harvesting electrochemical cells using photosynthetic proteins. The second chapter is about the materials and methods used in this work. Chapter 3 is about a new method of attaching the protein complexes on an underlying electrode without any use of linker which showed potential application in solar energy harvesting. Chapter 4 shows a new layer-by-layer assembly technique to preferentially orient photosynthetic reaction center complexes on an electrode using hybrids of oligomers and a protein charge mediating layer, which resulted in higher electron transfer (ET) rate between photosynthetic protein and underlying substrate. Chapter 5 shows how to directly adsorb photosynthetic plus light harvesting complexes on a surface of a Au electrode which showed an improved external quantum efficiency. Chapter 6 presents conclusion of this dissertation and suggests several approaches for future works.

1.2. Solar Cell Technologies

1.2.1. Photoelectrochemical Cells

Until 2001, photovoltaic industry was dominated by solid-state devices that were often made of silicon or thin-film semiconductors. As Michael Gratzel denoted, "this dominance was challenged by a new generation of solar cells", the third one, which utilizes nanocrystalline materials and conducting polymer

films.[4] The following section talks about photoelectrochemical solar cells using nanocrystalline materials. Since the science of photoelectrochemial cells is likely similar to the bio-photoelectrochemical cells incorporating reaction centers and reaction center plus light harvesting complexes, we briefly review them in the following section which is the subject of the current dissertation.

1.2.2. Photoelectrochemical Dye Sensitized Solar Cells

The advantages of devices using nanocrystalline material as well as the fabrication processes that are not involved in the expensive and energy-intensive high-temperature and high-vacuum processes, inspired various research groups to extensively put effort on developing efficient photoelectrochemical cells for utilizing solar energy.[4] The first semiconductor-electrolyte interface study in electrochemical and photoelectrochemical cells was performed by Brattain and Garret,[5] and later by Gerischer.[6] As represented in a review article by Gratzel,[4] the emphasis was on two types of cells: 1- regenerative cells and 2- photosynthetic cells. The operation mechanism of regenerative cells is shown in Figure 1.3.
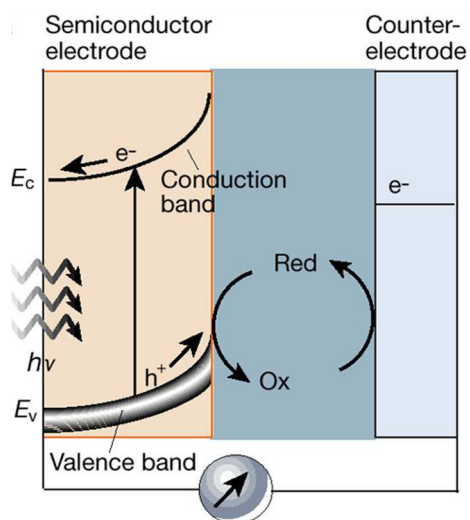
Figure 1.3 Principle of operation of regenerative photoelectrochemical cells based on n-type semiconductors producing electric current from sunlight (used with permission[4]).

In regenerative cells, upon exposure to sunlight, the light would be converted into electrical energy without leaving any net chemical changes behind. Any photon with an energy larger than the bandgap of the semiconductor, forms an unbound electron-hole pair. The separation happens through the presented electric field in the space-charge layer. The electrons will be collected by the semiconductor electrode. The

created holes will move through the bulk of semiconductor to its surface where they can be scavenged with the reduced form of the redox molecules in the electrolyte ($h^+ + R \rightarrow O$). The electrons that re-enter the cell from the external circuit can consequently reduce O which is the oxidized form of the redox to R which is the reduced form. This process can be repeated many times. The operation mechanism of photosynthetic cell is similar to the regenerative cells except the fact that instead of one redox system, this structure deals with two redox systems: one interacting with the holes at the surface of the semiconductor and the other with the electrons re-entering the cell from the external circuit.[4]

The motivation for absorbing photons in a wide range led to utilization of ET sensitizers that can absorb light in the visible range and inject charge carriers across the semiconductor-electrolyte junction into a substrate with a wide bandgap semiconductor.[4] This was the beginning of photoelectrochemical cells knows as dye sensitized solar cells (DSSCs) or Gratzel cells. Figure 1.4 shows the operation mechanism of and charge transfer path in such cells.
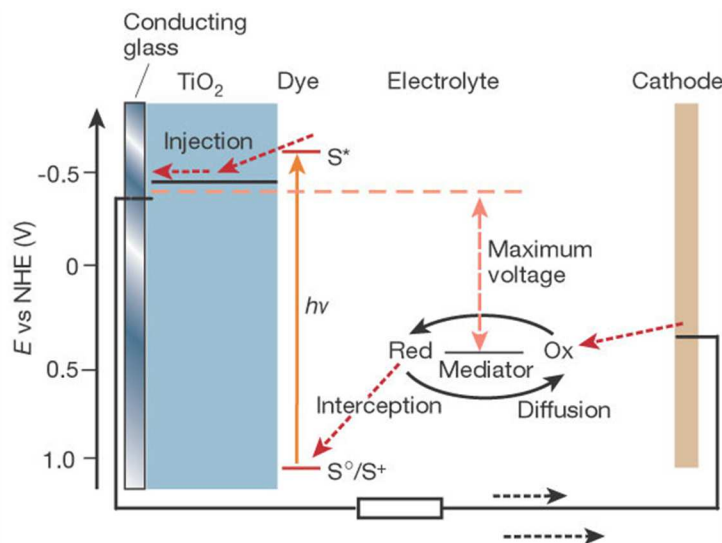
Figure 1.4 Operation mechanism of a DSSCs (used with permission[4]).

The TiO_2 photoanode is sensitized with a dye material that is capable of absorbing lower energy photons. The dye has two energy levels: lowest unoccupied molecular orbital (LUMO) and highest occupied molecular orbital (HOMO). Typically a ruthenium metalorganic dye (Ru-centered) is used as a monolayer of light-absorbing material. Upon exposure of the electrochemical cell to sun light, photons are

absorbed by the dye material. Accordingly, the generated electrons in the dye's excited state (S^*) can be injected into the E_C of TiO_2. In return, dye can oxidize the redox mediator in the electrolyte. The redox mediator can be regenerated at the cathode by receiving electrons through the external circuit. Various efforts have been carried out to optimize the morphology and surface area of TiO_2 photoanode as well as the cathode, the dye material, and the redox electrolyte.[7-11] The photovoltage in a DSSC is the results of contribution from the potential drop across the back contact of the nanocrystalline film with the conducting glass and the Fermi level shift of the TiO_2 nanoparticle.[12-14]

1.3. Bio-photoelectrochemical Cells using Protein Complexes

As mentioned in section 1.1, to reduce the share of fossil fuels in electricity generation, clean energy should be scaled up to the TW level of deployment.[15] To reach this goal, different ways and strategies of harvesting solar energy should be utilized. Photosynthesis, which is the process used by plants and other organisms to capture sunlight and convert it into chemical forms of energy (with the use of CO_2 and water), has been the source of energy on earth since the evolutionary history of life.[16] The average rate of energy capture *via* photosynthesis globally is almost 130 TW,[17,18] which is higher than the current global power consumption. Additionally, through the photosynthetic process almost 110 billion metric tons of carbon are converted into biomass annually.[19] Photosynthetic plants and bacteria convert solar energy into electrochemical energy with high efficiency.[20] In photosynthesis, the visible light conversion to utilizable chemical energy--*i.e.* adenosine triphosphate (ATP) and nicotinamide adenine dinucleotide phosphate (NADPH)--occurs with an efficiency of 53.2%.[21] The photosynthesis process might seem to be simple at first look. But if we take a closer look at the process, the route is much more complicated. Photosynthesis occurs in two steps: the light-dependent and the light-independent reactions, while the light-dependent reactions occur in the thylakoid membrane and the light-independent reactions take place in stroma, the fluid-filled area of a chloroplast outside of the thylakoid membranes.[22,23] Figure 1.5 shows light-dependent reactions of photosynthesis, which happen in the thylakoid membranes of chloroplasts.
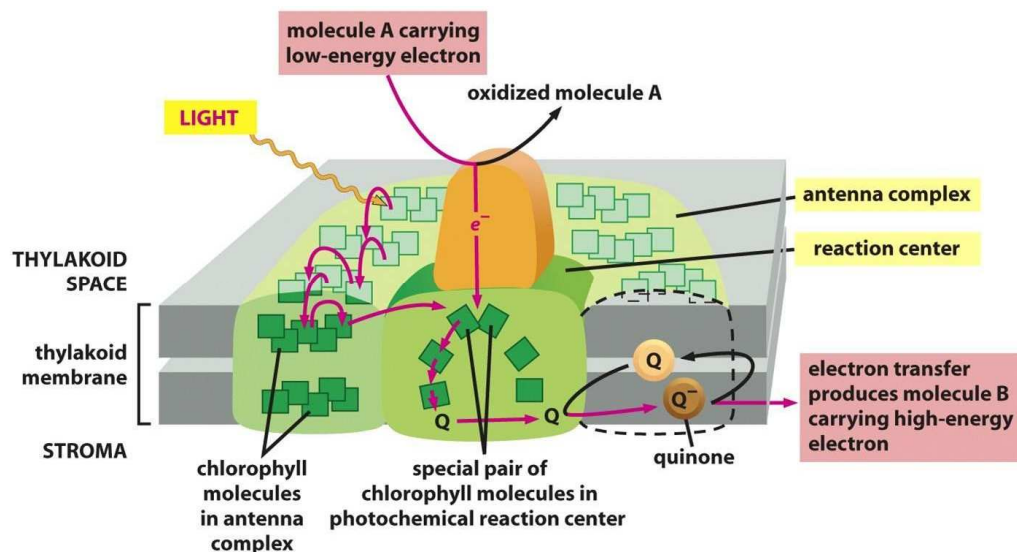
Figure 1.5 Light-dependent reactions in thylakoid membranes (used with permission[23]).

A thylakoid is a membrane-bound section inside chloroplasts and cyanobacteria. In the leaf cells of green plants, there are special subunits called chloroplasts. Chloroplasts have high concentration of green pigments called chlorophyll. The chlorophyll job is to absorb the photons from sunlight and to transfer them to another subunit called reaction center (RC). In the light-dependent reactions, some energy is used to convert water, for example to oxygen. Additionally, other compounds such as reduced NADPH and ATP are generated. In plants, algae, and cyanobacteria as photoautotrophs organisms, sequence of light-independent reactions called the Calvin cycle, leads to production of sugar. What happens in the Calvin cycle is that the atmospheric CO_2 is incorporated into existing organic carbon compounds in the plant, and using the ATP and NADPH further carbohydrates such as glucose would form. It is interesting to mention that some bacteria such as *Rhodobacter (Rb.) sphaeroides* which is the main subject of current dissertation, do not evolve oxygen as they utilize H_2S instead of water as electron donors.[22]

Mimicking the nature to utilize solar energy can potentially be a cheap and sustainable technology which could help speed up the transition from fossil fuels into clean energy. The key advantage of solar energy instead of covering vast swathes of desert in solar panels and piping the energy hundreds of miles through high-voltage transmission lines, maybe that it can cover houses, buildings, and other urban structures, enabling them to generate their own power. Unfortunately, current solar cell technologies are

7

too expensive, especially for homeowners. The other often ignored topic in renewable energy strategies is the sustainability of the renewable energy technology itself.

Interest in the potential application of biological photosystems has been fueled by the discovery of the 3-D crystal structures of these membrane protein complexes, and the quantitative understanding of the primary ET processes of photosynthesis.[24-26] In the succeeding years, among several intriguing applications of photosynthetic proteins,[27-29] solar energy harvesting has achieved prominence due to an increasing demand for the production of clean energy.[20,30] The bio-photoelectrochemical cell uses technologies that exploit biomimetic means of energy conversion by utilizing plant-derived photosystems.[30,31] In a photosynthetic organism, the primary energy conversion reactions take place in a RC protein. Different types of protein complexes may be employed to fabricate a bio-photoelectrochemical cell, including RCs from the *Rb. sphaeroides* bacterium, plant photosystems, and bacteriorhodopsin proteins.[3,32-48] In the rest of this chapter, various types of bio-photoelectrochemical cells developed so far have been reviewed.

1.3.1. Reaction Center and Reaction Center plus Light Harvesting Complexes

1.3.1.1. The Structure of Photosynthetic Reaction Center Complex in Purple Photosynthetic Bacteria

In purple photosynthetic bacteria, photochemical energy conversion initiates in a pigment-protein complex spanning the cytoplasmic membrane, the RC.[49] The RC protein complex in photosynthetic bacteria harvests photons and generates spatially separated positive and negative charges. The RC of the bacterium *Rb. sphaeroides* is the simplest and perhaps the most resilient photosynthetic complex, with ~200 times longer recombination time of the separated charges compared to that in silicon-based devices.[50] Through Förster resonance energy transfer, photon energy initially absorbed by antenna complexes, such as the bacterial light-harvesting complexes 1 and 2 (LH1 and LH2), is transferred to the RC, where a charge-separated state is generated with ~100% quantum efficiency.[51] The charge separation and stabilization occur in a complex of ~7 nm diameter and lead to the formation of a local electric field of more than 1.2×10^6 V cm^{-1}, which corresponds to approximately 10% of the total local electric field around primary donor site of the RC.[52] The RC of *Rb. sphaeroides* is a transmembrane complex comprised of three protein subunits (called L, M and H) ligate the pigment and other cofactors that make up the RC with a donor (P)

8

and an acceptor (Q) side. The cofactors, which constitute an ET pathway, include a bacteriochlorophyll (BChl) dimer (termed as P, the primary donor), two monomer bacteriochlorophylls (BChl$_A$ and BChl$_B$), two bacteriopheophytins (BPhe$_A$ and BPhe$_B$), two quinones (Q$_A$ and Q$_B$) known as electron acceptors, and one non-heme iron are symmetrically arranged in the L and M subunits.[53-55] All cofactors are non-covalently bound to the polypeptides. Figure 1.6(a) shows a block view of the photosynthetic RC protein complex from purple bacteria and the ET pathway through the cofactors. Additionally, Figure 1.6(a) shows a bowl (cavity) in the RC, based on the RC–cytochrome (cyt) c co-complex crystal structure.[56] C92, C234, and C156 show the approximate location of surface exposed cysteine residues. Cysteine which can be abbreviated as Cys or C is an α-amino acid with the chemical formula of HO$_2$CCH(NH$_2$)CH$_2$SH.
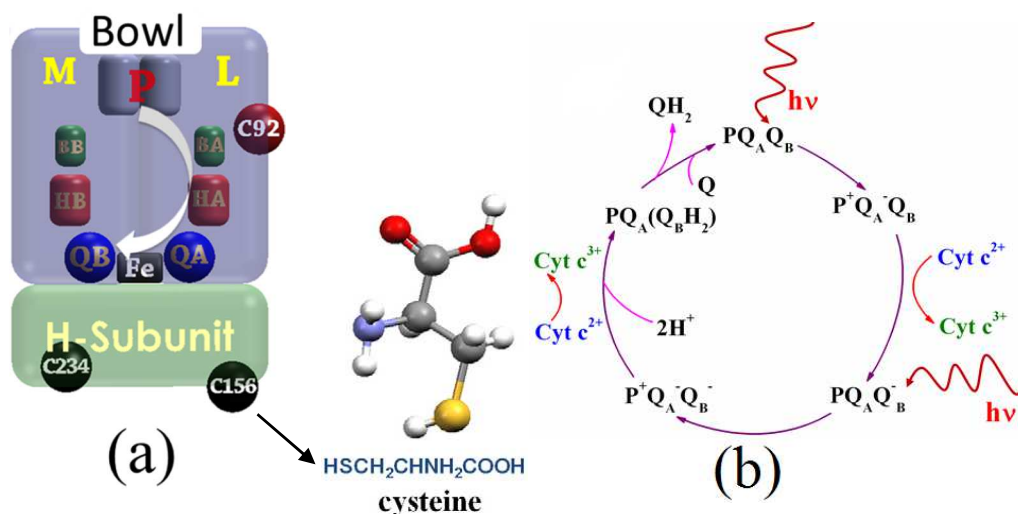
Figure 1.6 (a) Representation of the RC, protein subunits and cofactors, and approximate location of surface-exposed cysteine groups, of which C156 is the most externally exposed. White arrow shows the ET path from P to QB. (b) Charge transfer cycle in the RC (used with permission[33]).

The X-ray crystallographic structures of photosynthetic RCs have contributed significantly to the understanding of the kinetics of ET, and biological ET processes in general.[57-59] The charge separation in the RC occurs by generation of an excited state (P*) in a pair of bacteriochlorophylls (BChls), called the special pair (P). An electron is then transferred to an accessory BChl (B$_A$), then to a bacteriopheophytin (BPhe), and subsequently to a primary (Q$_A$) and secondary (Q$_B$) quinone in a series of steps (Figure 1.6(b)).[33] *In vivo*, cyt c acts as a diffusible ET mediator to reach to the P-side of RC and donate an electron to P. Therefore, oxidized cyt c is the mediator, carrying the positive charge. After absorption of two photons

and receiving two protons, a quinol (QH_2) is produced at the Q_B site. QH_2 diffuses out from the protein and acts as an electron carrier mediator. The photosynthetic cycle repeats after the Q_B vacancy is filled with a fresh quinone (*i.e.* Q) (Figure 1.6(b)).

The distinctive three Q_y RC cofactor absorption peaks, *i.e.*, BPhe, monomeric BChl, and the BChl "special pair", are present at 760, 804 and 867 nm, respectively, while the most intense peak is at 804 nm.[44] Figure 1.7 shows the absorption spectrum of purified RC in a phosphate buffer.
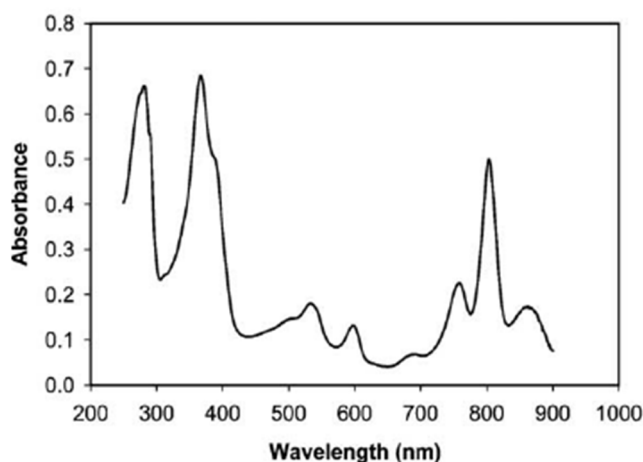
Figure 1.7 Absorption spectrum of purified RC in 10 mM phosphate buffer at pH 7.4 (used with permission[44]).

The bacterial photosynthetic RC shows great promise for solar energy harvesting because of nearly 100% quantum yield of primary charge separation and an efficient stabilization of separated charges. The long recombination time and the high quantum efficiency,[60] have inspired several research groups to utilize RCs in photoelectrochemical cells for harvesting solar energy.[3,32-37,43,61,62] In addition, active photosynthetic elements can be obtained at a low cost from cultivated algae or agricultural remains, such as leaf stalks.

The common approach is to make a bio-hybrid device by coating the surface of an electrode with a monolayer of photosynthetic RC protein complexes and applying the electrode in an electrochemical cell. The coating or immobilization of RC protein complex on the electrode can happen using linkers or directly without any linker. In such devices, diffusible mediators are used to transfer light-induced charges from the RCs to the electrodes through reversible redox reactions.[33] Figure 1.8 shows schematics of a bio-hybrid photosynthetic solar cell device.
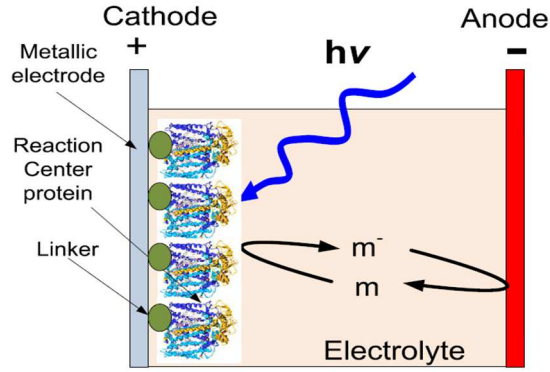
Figure 1.8 Schematics of a bio-hybrid photosynthetic solar cell device. m shows the redox mediator system in the electrolyte.

However, there are some challenges on the road of integrating biomaterials in electronic devices including: the adoption and the interface between biomaterials and synthetic materials as well as the stability of biomaterials in a device. Because of the aforementioned challenges, majority of studies so far have been focused on the structure of devices using photosynthetic proteins. The criteria to evaluate these type of devices is mainly based on the ET and external quantum efficiency (EQE). The EQE can be measured in a photovoltaic device as the ratio of collected electrons to incident photons. The equation for calculation is thus:

$$EQE = 100 \times \frac{J.\hbar\omega}{e.I} \qquad \text{Eq. 1.1}$$

where J is the current density in A cm^{-2}, e is the electron charge in C, I is the incident photon power density in W cm^{-2}, and $\hbar\omega$ is the energy per photon in Joules, all at the wavelength λ. The ratio of J/e is equal to the number of electrons transferred to the electrode per unit area (the electrode area) per unit time. Similarly, the ratio of $I/\hbar\omega$ is equal to the number of incident photons per unit area per unit time (monochromic light). Considering that J and I are measured for monochromic lights at different wavelengths, the above equation is then the number of collected electrons to the number of incident photons, at the wavelength λ. This will only reach 100% when every incident photon is absorbed and every absorbed photon generates an electron and every generated electron is collected in the form of current through the circuit.

1.3.1.2. Standard Immobilization Strategies

Typically, bio-photoelectrochemical cells have been fabricated using RCs immobilized from either the H-side or the P-side on the surface of one of the cell's electrode.[32,33,44,45,61-65] Figure 1.9 shows the protein orientation on a metallic electrode from H-side which is suitable for receiving electrons from the cathode. Upon illumination, a photocurrent can be generated by transferring one of the charges from the RC to the electrode. The opposite charges are moved to the counter electrode *via* a redox mediator in the electrolyte.

One of the early examples of bio-photoelectrochemical cells using photosynthetic RCs goes back to 1994 when Katz performed random and oriented immobilization of photosynthetic RCs on carbon electrode, using bifunctional reagents.[38]
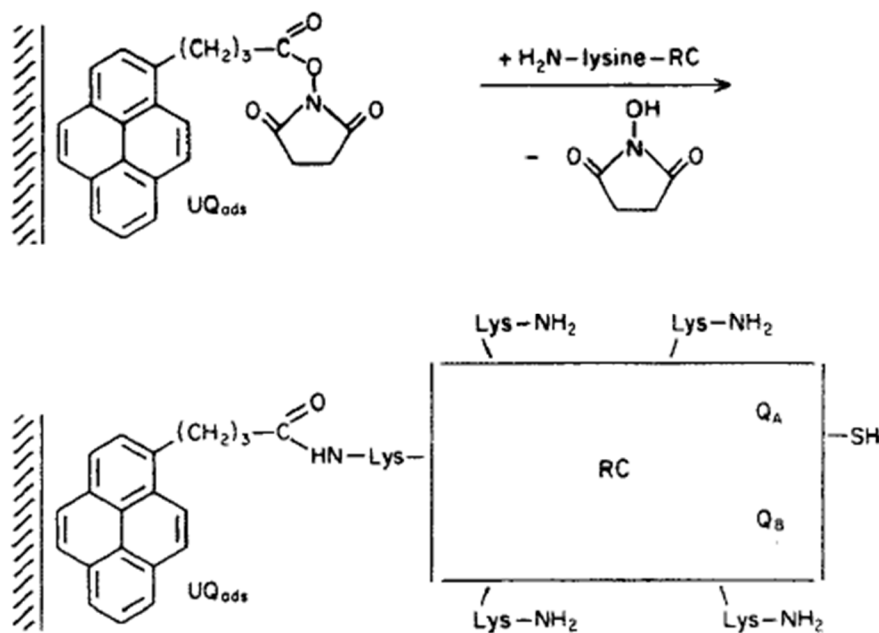
Figure 1.9 Schematic of the RC immobilization *via* lysine residual once bifunctional reagent (1) was used. (used with permission[38]).

The cysteine residual located at RCs' accepting sides (H-side) was used to orient RCs on a carbon electrode surface activated for thiol binding.[38] In his experiments, Katz used two different bifunctional reagents for covalent coupling with amino or thiol groups: (1) N-hydroxysuccinimidyl ester and (2) iodoacetamidyl. After immobilization of linker (1) or (2) on a highly ordered pyrolytic graphite (HOPG) electrode, the RCs were incubated on top.[38] A series of systematic experiments were performed and it was

shown that using bifunctional reagent 1 leads to random orientation of RCs on the electrode's surface due to many lysine residuals around RC globula.[38] Figure 1.9 shows schematic orientation of RCs on the HOPG's surface once reagent (1) was used.

In the meantime using iodoacetoamidyl (bifunctional reagent (2)) resulted in RCs preferential orientation on the surface from H-side *via* cysteine residuals. Figure 1.10 shows the schematics of such structure.
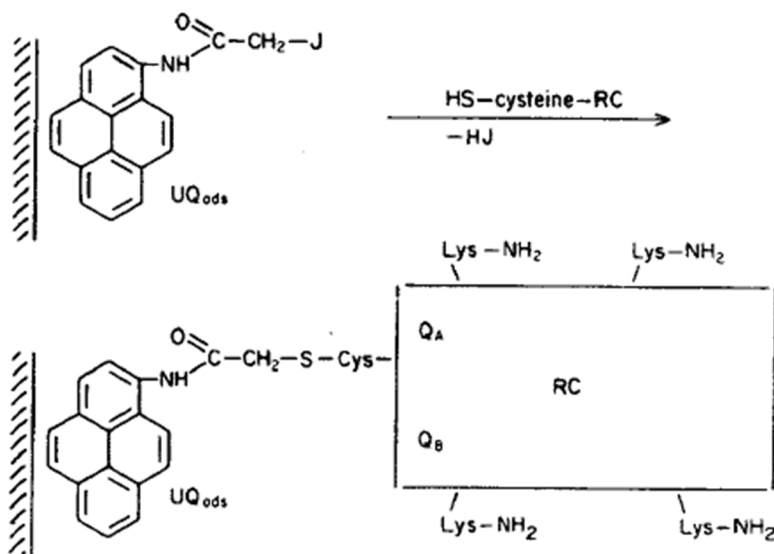
Figure 1.10 Schematic of covalent immobilization of RCs via cysteine residual once bifunctional reagent (2) was used. (used with permission[38]).

It was reasoned since in the random orientation of the RCs using bifunctional reagent 1, the distance between Q_B in RC (Figure 1.11(a)) and the electrode is not short enough for tunneling to be effective. Hence, without any additional exogenous ubiquinone in the electrolyte, the photocurrent under illumination was negligible in such a case. Figure 1.11 shows the photocurrent associated with the above described structures.
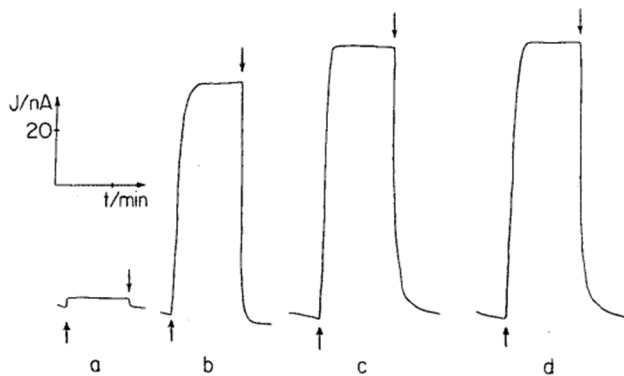
Figure 1.11 Changes in the photocurrent induced by switching the illumination of the RC-modified electrodes. (↑) on and (↓) off. (a) reagent 1, (b) reagent 1 plus additional exogenous ubiquinone-10 in the electrolyte, (c) reagent 1 plus additional exogenous ubiquinone-10 in the electrolyte, (c) reagent 2, and (d) reagent 2 plus additional exogenous ubiquinone-10 in the electrolyte. (used with permission[38]).

Katz' early study can be considered as the building block of later in-depth studies on the application of photosynthetic RCs in solar energy harvesting. In 2002, Zhao and her coworkers could show a successful ordered self-assemble of 24 RC layers using alternate electrostatic adsorption with positively charged poly dimethyldiallylammonium chloride (PDDA) and negatively charged protein.[66] The assembly of many layers of RC was mainly performed to improve the light absorption. Their results (presented in Figure 1.12) suggested that there is a good linearity between the number of assembled RCs and the photocurrent results. Such a structure with 24 layers of RC could produce ∼80 nA cm^{-2} photocurrent density.[66]
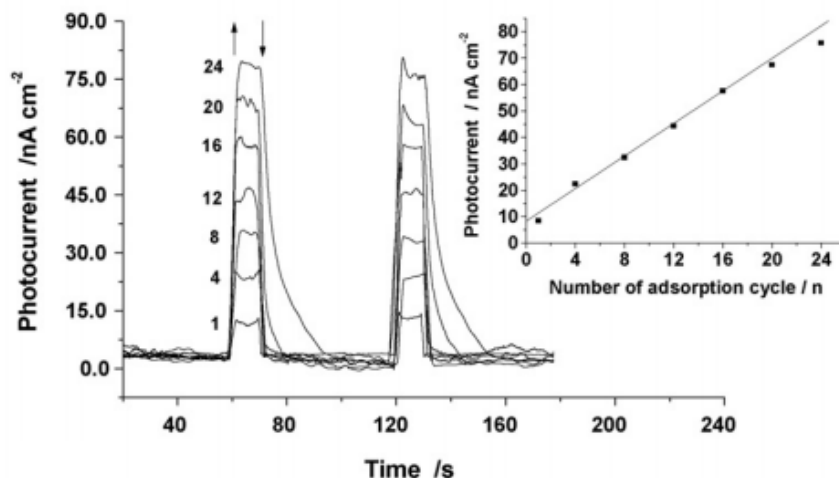
Figure 1.12 Short-circuit photocurrent for 1 to 24 layers of RC assembled PDDA induced by switching on (↑) and off (↓) the illumination. The insert showed the relationship between the photocurrent and the number of the adsorption cycles (used with permission[66]).

14

In 2002, Zhao *et al.* could show that the RCs orientation can be controlled using other types of self-assembled linkers such as 2-mercaptoethylamine (MEA) and 4-aminothiophenol (ATP).[67] Figure 1.13 shows schematic diagrams of self-assembled monolayers (SAMs) of RC-MEA and RC-ATP films. As shown, the RCs can be oriented from either the P (primary donor) or the H-side on a Au surface using MEA and ATP SAMs, respectively.[67]
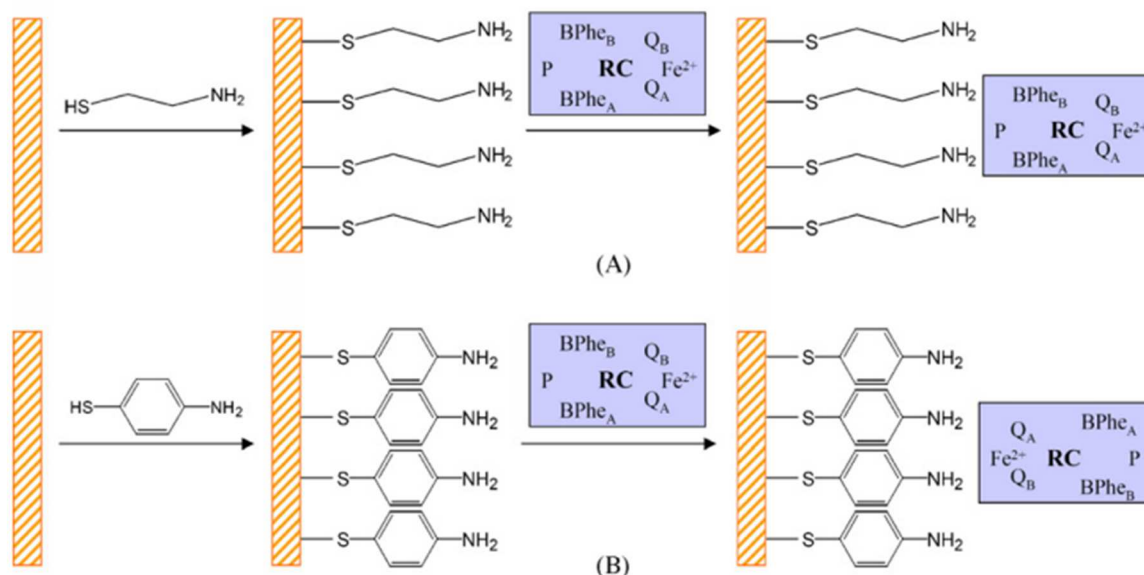
Figure 1.13 The schematic diagrams of self-assembled monolayers for (A) RC-MEA film and (B) RC-ATP film (used with permission[67]).

In 2004 Trammel of Naval Research Laboratory and his coworkers demonstrated successful immobilization of photosynthetic RCs on a Au surface with the RC primary donor (P-side) facing towards the substrate by using a genetically engineered poly-histidine tag (His7) at the C-terminal end of the M-subunit and a Ni–nitrillotriacetic acid (NTA) terminated SAM.[44] The photoelectrochemical cell was fabricated with applying the above explained electrode in an electrolyte with one redox system, ubiquinone-10 as an electron acceptor, Pt counter electrode, and a reference electrode. The measurements were performed in a three electrode setup using an Ag-AgCl reference electrode. Figure 1.14(a) shows the orientation of RC on Ni-NTA SAM. Figure 1.14(b) shows the energetics and kinetics of photo-induced charge separation in RC.
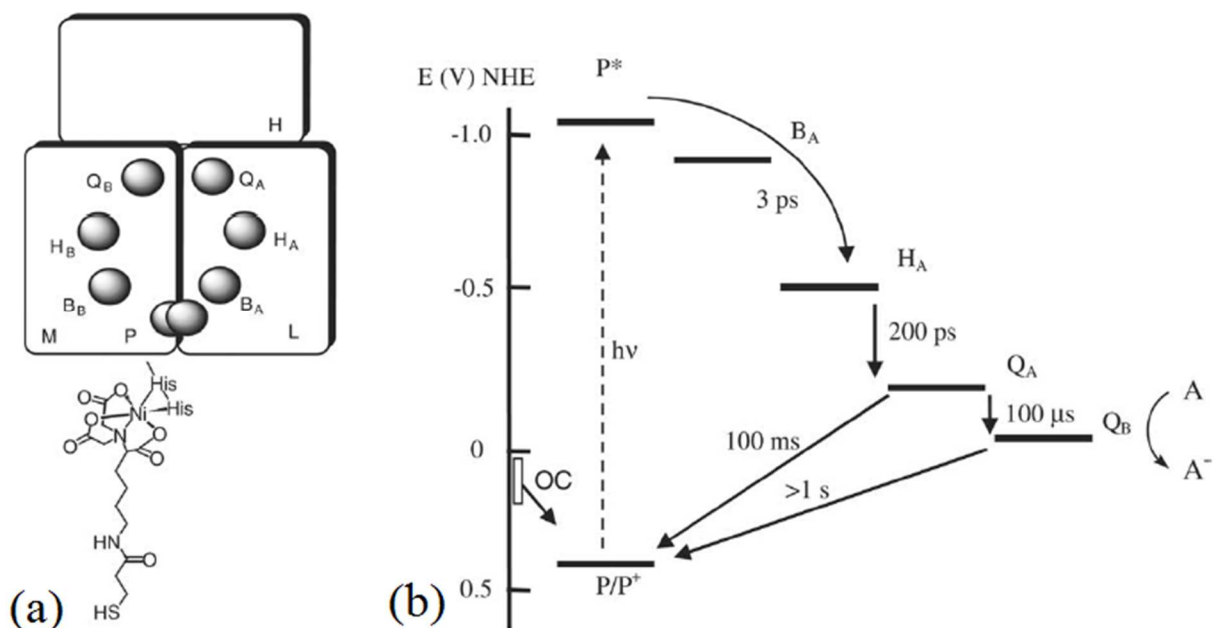
Figure 1.14 (a) The orientation of RC on a Ni–NTA SAM. (b) The energetics and kinetics of photo-induced charge separation in RC. The photochemical excitation is indicated by a dashed arrow and the ET reactions are shown with arrows. The range of open circuit potentials (in the dark) of the working electrodes are marked as OC (used with permission[44]).

Figure 1.14(b) shows that under illumination, the electron in P is raised to its excited singlet state (P^*) and an electron is transferred to the primary quinone (Q_A) in ~200 ps and forms the charge separated state $P^+Q_A^-$. The ET between Q_A to Q_B takes about 100 µs.[44] As a result Q_B can act as electron donor and the primary donor (P) end of RC can accept electrons from cyt complexes.[24,44,68] Under monochromic illumination (λ=800 nm) a cathodic photocurrent density of ~30 nA.cm^{-2} was achieved from the structure shown in Figure 1.14(a).

Although Trammell *et al.* showed that the coverage of the electrode with the photosynthetic RC using NI-NTA SAM was not perfect, the photochemical activity of the assembled RCs through linker implied no structural deformation or degradation of protein complexes.[44] Not long after, in 2006, the same group, oriented RCs from both primary donor and acceptor sides on a carbon electrode using two different linkers.[65] Their work showed the effect of the protein orientation on ET between photosynthetic RC and carbon electrodes.[65] Although their study was somehow similar to the early study by Katz in 1994,[38] no adsorbed quinone was used after treating the electrode's surface with a linker.[38] Additionally this in-depth

16

study could strongly show that the direction of ET changes upon changing the orientation of immobilized RC on the surface. Figure 1.15(a) shows different orientation of RCs on a carbon electrode from H-side *via* cysteine residues using 4 A° thick N-(1-pyrene)iodoacetamide (linker 1) and from P-side *via* polyhistidine tag using 12 A° Ni-NTA linker. Figure 1.15(b) shows photocurrent *vs* time for both orientations.
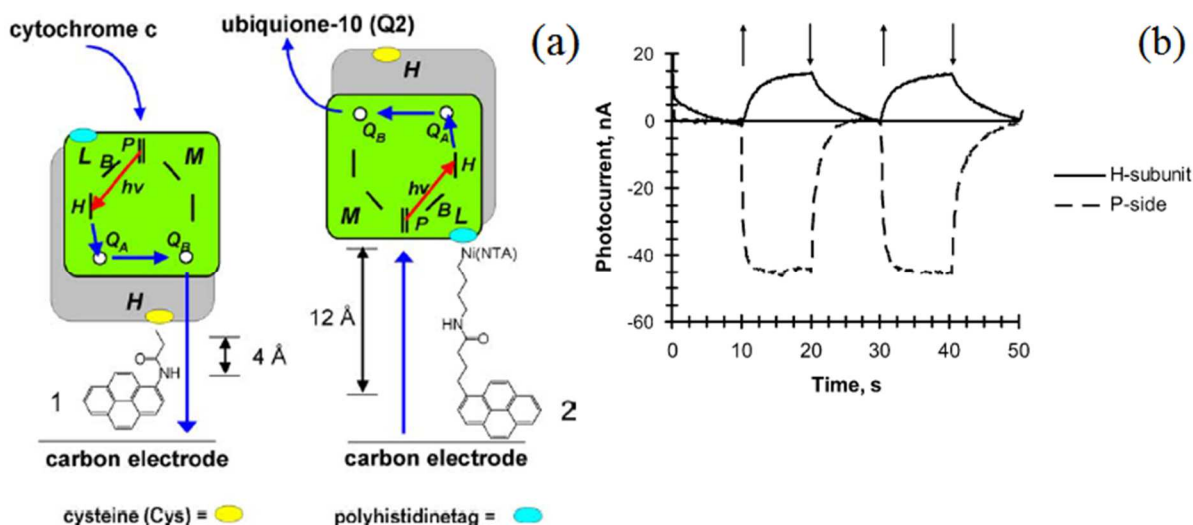
Figure 1.15 (a) A schematic presentation showing two possible ways of RC binding and ET pathways between RC and electrode. The structure of the bifunctional linkers used for binding to carbon electrodes are labeled 1 and 2. (b) Photoinduced electric current in carbon electrodes having RC bound through the cysteine at the top of the H-subunit, and through the polyhistidine at the close proximity of the primary donor (P side). (Light on, ↑, off, ↓) (used with permission[65]).

The surface coverage estimation results showed that in both configurations, the RC coverage approached 75–80% of the ideal theoretical coverage.[65] The significance of Trammell's result is that the photocurrent response (Figure 1.16(b)) suggested lower ET rate for the attached proteins from the H-subunit side, despite the shorter linker molecule used for the immobilization. The reason was explained by estimating the ET distance in those structures. Considering the thickness of the H-subunit (~24 A°),[44] and the thickness of the SAM 1 (4 A°) , there is a 28 A° distance for ET between RC and carbon electrode, while RCs are being oriented from H-side on the surface. In case of RCs orientation from P side there is a 19 A° ET distance between RC and the electrode, as the special pair is buried at a distance of 7 °A from the protein surface and the length of linker is about 12 A° (Figure 1.15 (a)).[65] Therefore, the larger distance between the ET molecules--*i.e.* RC--and the electrodes due to the presence of H subunit, caused a slower

rate.[65] In contrast, higher rate of ET and larger photocurrents can be obtained by orientating RCs from P-side onto a surface. Comprehending the effect of distance between the RC's redox active sites and the electrodes, Trammell *et al.* demonstrated in 2007 that the electron tunneling rates between redox centers in RC protein complexes and the underlying electrodes depend exponentially on the tunneling distance.[63] Figure 1.16 shows a schematic of photosynthetic RCs immobilized on a Au electrode through linkers with different (3, 6, 10, and 15) number of methylene units in the linker's alkane bridge, in the dark and under illumination.
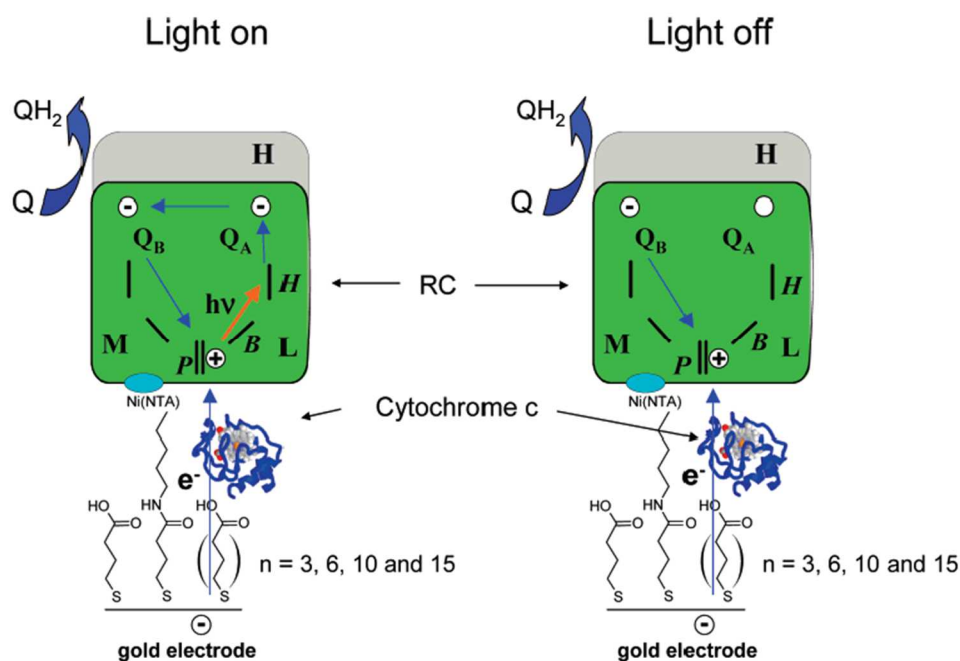
Figure 1.16 Schematic presentation of photoinduced and "dark" ETs in RC-cyt-SAM-Gold electrode (used with permission[63]).

Trammell *et al.* measured the photocurrent as a function of the applied potential to the working electrode and the number of methylene units in the linker's alkane bridge for the structures in Figure 1.16. Based on Marcus formalism, density of electronic states in the metal, the estimation of midpoint potential of the primary donor, and the reorganization energy, the rate constant of electron tunneling between the RC and the electrode for various electrode potentials, and the different number of methylene units in the linker, it was shown the highest kinetic of charge transfer and largest photocurrent density can be obtained once the length of the linker is the shortest (n=3).[63] This earlier work demonstrated an 0.8 distance dependence

factor of electron tunneling for RC immobilized with alkane bridges per methylene unit.[63] This implies the significance of the protein proximity to the electrode for an efficient ET between RC and the electrode. The maximal tunneling rate constant for ET from the flat Au electrode to RC primary donor was about 10^4-10^5 s^{-1}.[63]

Later, Trammell *et al.* used the same Ni-NTA-terminated type of SAM in their previous work,[65] for immobilizing the proteins through polyHis tag located at the C-terminal end of M-subunit in another study.[69] This allowed protein orientation with the primary donor (P-side) facing the Au electrode. To improve the ET between the RC primary donor and the underlying Au electrode, cyt *c* was injected into the electrolyte. In an earlier work by Lebedev *et al.*,[69] it was demonstrated that the charge transfer at the RC-electrode interface in the orientation, shown in Figure 1.17, is complicated by a bowl or a cavity on the P-side that introduces a gap between the electrode and the protein (Figure 1.6(a)). Lebedev *et al.* revealed a higher photocurrent can be achieved if the bowl of at least some of the RCs may be filled by diffusion of cyt *c* into the space between a 7-His-tagged RC and an NTA terminated SAM on a Au electrode.[69] Figure 1.17(a) shows the schematic presentation of RC and cyt *c* on NTA SAM.

a Red = α-helices, yellow = β-strands, green = chlorophylls, brown = heme, blue = his-tag). Inset shows the possible RC orientation relative to SAM surface (violet = RC, brown = cytochrome)
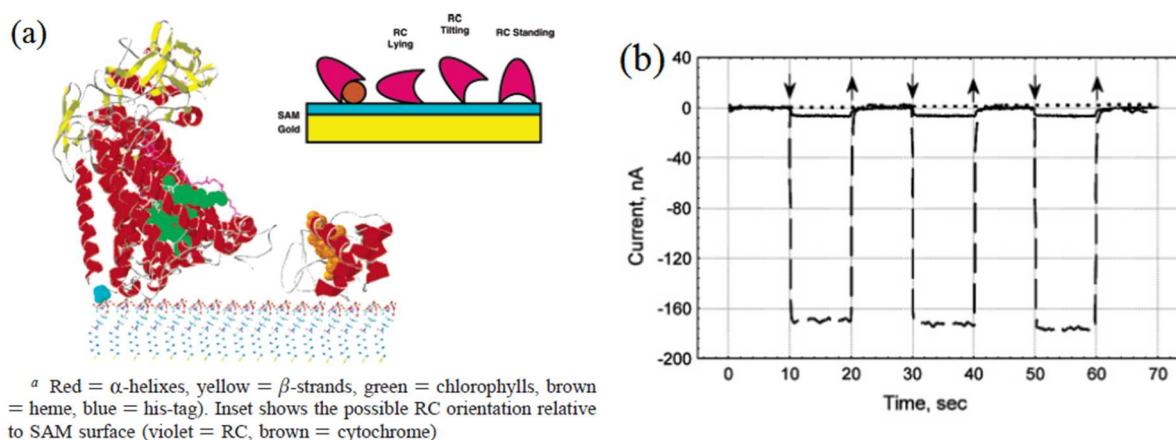
Figure 1.17 (a) Schematic presentation of RC and cyt *c* on NTA SAM. (b) Steady-state photocurrent at RC-NTA-electrode with (---) and without (-) 1 µM cyt *c* and NTA electrode incubated with cyt *c* without RC (…). The arrows indicate light on (↓) and off (↑) (used with permission[69]).

Figure 1.17(b) shows the steady state photocurrent at RC-NTA-electrode with and without cyt *c*. Also a control experiment was performed without any RC and just with cyt *c*, to prove that the generated photocurrent is the result of immobilized RCs on the surface. Lebedev *et al.* considered three different

orientation of RCs on the surface: tilting, lying, and standing (Figure 1.17(a)).[69] It was demonstrated that in the tilting orientation, the ET between RC and Au is ~2×10^6 higher with cyt *c* as a conductive wire comparing to no wiring mechanism.[69]

As it was shown earlier, the electron tunneling rates between redox centers in RCs and the underlying electrode depend exponentially on the tunneling distance.[69,70] In an attempt to further improve the ET between RC's redox active sites and the electrodes, an earlier study genetically modified the *Rb. sphaeroides* RC with the aim of achieving shortened tunneling distances between the RC's redox sites and the underlying electrodes.[71] In Mahmoudzadeh *et al.*'s study, the mutant RCs were directly attached from the P-side to a Au electrode, in which electrons tunneled from the Au to the immobilized proteins.[71] However, the results demonstrated a very low photocurrent density of 5 nA cm^{-2}, mainly due to a low success rate in controlling the orientation of the RCs directly in contact with the electrode.[71] Figure 1.18(a) shows a schematic representation of such a structure with the associate photocurrent graph shown in Figure 1.18(b).
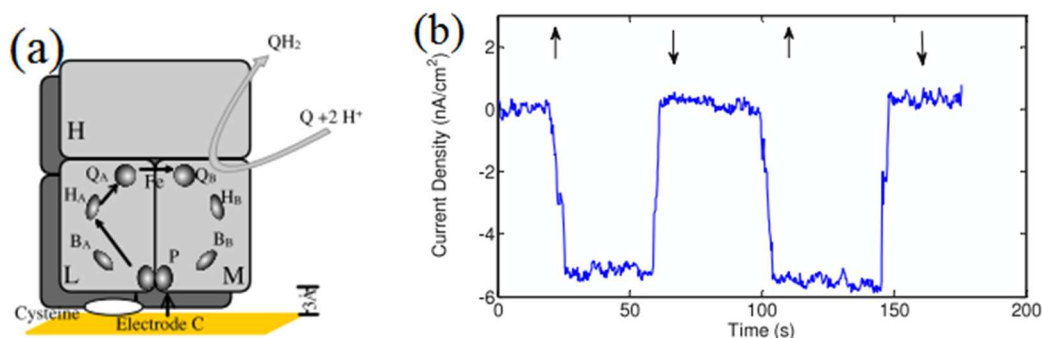
Figure 1.18 (a) A schematic representation of direct attachment of genetically modified RC from primary donor side (P-side) into a Au electrode *via* a cysteine residue. (b) The photocurrent associated with (a) in a three electrode setup using Pt as counter and Ag-AgCl as reference electrode, respectively. (used with permission[71]).

To further improve the photoelectric conversion efficiency of devices with photosynthetic RC complexes, Lebedev *et al.* proposed encapsulation of RCs inside carbon nanotube (CNT) array electrodes.[72] Their approach was to use genetically modified bacterial RC containing a polyHis tag at close proximity to primary donor (P$^+$) with synthesized organic molecular linkers were encapsulated inside carbon nanotubes

and bound to the inner tube walls in unidirectional orientation.[72] Figure 1.19 shows cross sections transmission electron micrograph (TEM) of arrayed CNT membrane without and with RC protein complex.
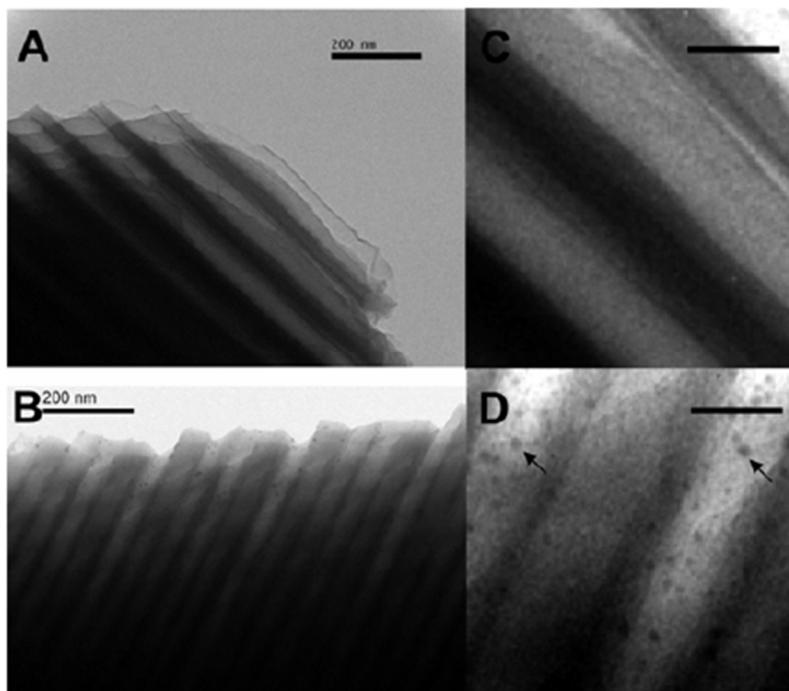
Figure 1.19 TEM of cross section of blank arrayed CNT-Alumina membrane (A) without and (B) with encapsulated RC protein complexes inside. (C) and (D) show enlarged selection from (A) and (B). Arrows point at RC-nanogold conjugates. The 5 nm Au nanoparticles were only used for protein visualization inside CNT (used with permission[72]).

For comparison, Lebedev *et al.* employed another type of carbon electrode, HOPG, for RC immobilization.[72] Immobilization was performed using pyrene as linker molecule. Figure 1.20 shows the photocurrent results for bare HOPG and CNT as well as HOPG and CNT with immobilized RCs. The obtained photocurrent in case of RCs encapsulated in CNT arrays comparing to HOPG was almost 4 time higher.[72]

The photoelectrochemical measurements were performed in a three electrode setup with reduced cyt *c* and ubiquinone-10 as the redox system. It was supposed that cyt *c* molecules would find their way from the pin holes in the RC layer to the interface between CNT and RC complexes and act as a molecular wire, as suggested in their earlier study.[69]
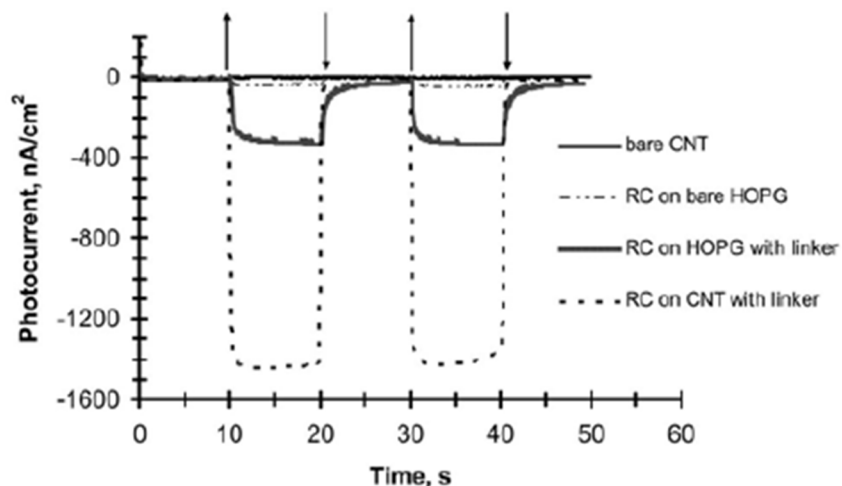
Figure 1.20 Steady-state photocurrent measurement for RC immobilized on CNT and HOPG electrode using an Ni-NTA pyrene linker or at bare electrodes. The arrows indicate light on (↑) and off (↓) (used with permission[72]).

Hence, the tested cell was practically an electrochemical cell with a single diffusible redox mediator in the electrolyte.

Besides the aforementioned techniques, other fabrication methods including electrospray,[50] and Langmuir-Blodgett (LB)[73] were also employed to make photoactive protein-based electrodes. Recently, Mirvakili *et al.* could successfully deposit photosynthetic RCs from purple bacteria onto a HOPG substrate without any linker using the electrospray technique.[50] The obtained photocurrent from such structures indicated that the RC protein complexes show robustness to high voltages (*e.g.* 15 kV used in this study between the syringe needle and the underlying HOPG substrate).[50] Figure 1.21 shows the obtained transient photocurrent along with the morphology of the HOPG substrate before and after the RC electrospray deposition.

The comparison between dip coated and electrosprayed HOPG in Figure 1.21(a) demonstrated that using the electrospray technique can result in higher yield of deposited RC and better surface coverage. This percipience comes from the fact that significantly higher transient (peak) current response was observed for the electrosprayed photoactive HOPG comparing to the dip coated one.
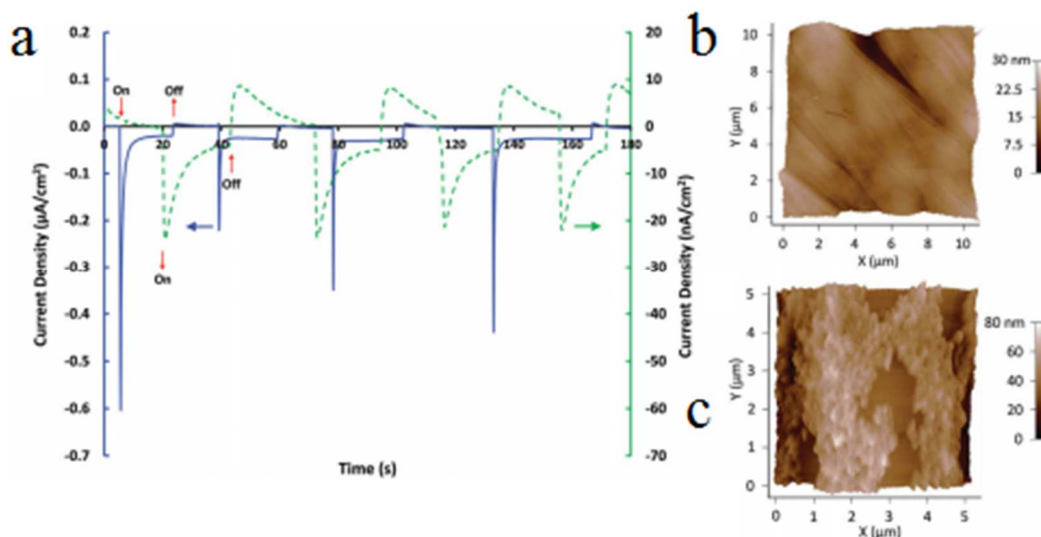
Figure 1.21 (a) Photo-response of the RC treated electrodes: electrosprayed HOPG (blue solid line) and dip-coated HOPG (green dashed-line). Atomic force micrographs: (b) Topography of clean, freshly cleaved HOPG and (c) the corresponding topography of electrosprayed HOPG (used with permission[50]).

In a three electrode setup using a Pt mesh counter electrode, a reference electrode, and ferrocene (Cp$_2$Fe) as the redox mediator, such structure demonstrated a maximum of 0.01% EQE at 804 nm.[50] The comparison between the morphologies of the HOPG surface before and after electrospray deposition confirmed the successful deposition of the complexes on the surface (Figure 1.21(b-c)).

In a most recent study, it was demonstrated that self-organization of RC protein complexes on a Au substrate using LB technology can lead to a densely packed monolayer of the protein with a defined orientation.[73] It is worth mentioning that the LB deposition technique for protein complexes was earlier used in 1992 by Yasuda *et al.* for *Rhodopseudomonas viridis* complexes.[74] The LB method is widely used for the deposition of amphiphilic molecules onto solid substrates.[74] The amphiphilic molecules may preferentially orient using LB as their hydrophilic side can face the water while their hydrophobic side faces air.[73] This potentially results in a highly oriented layer of amphiphilic molecules at the air−water interface. The produced monolayer can be transferred onto a substrate by vertical dipping the substrate into the solution. The reverse dipping would likely reverse the orientation of molecules on the surface.[73] As was explained in this work RC is a complex with a hydrophobic core and two hydrophilic ends. The hypothesis is that the hydrophilic properties of these ends is mostly not the same which eventually helps orientation

these complexes from one end onto a surface. It was stated in an earlier study,[50] that at neutral pH, the RC is a net negative complex with a complicated spatial distribution of charged functional groups while having a high concentration of negative charges at the P side.[24] Figure 1.22 shows the schematic representation of the LB deposition method along with the photocurrent obtained from the samples with layers of the protein coated by forward and reverse dipping (LB method); and direct incubation.
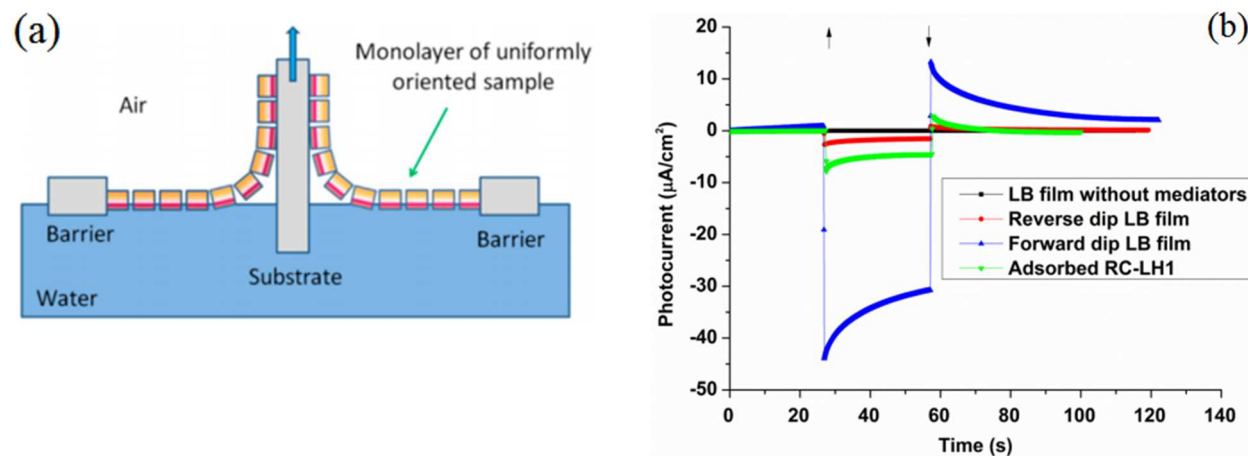
Figure 1.22 (a) Schematic representation of the Langmuir−Blodgett deposition method. (b) Photocurrent produced from samples made with different methods: forward dipping of LB deposition (blue triangles), reverse dipped LB film (red circles), and adsorbed RC-LH1 complexes on gold electrode (green triangles). The arrows indicate when the light was switched on (arrow pointing upward) and when the light was switched off (arrow pointing downward) (used with permission[73]).

The applied potential was −175 mV (*vs* SCE) in all cases, and the light source was an 880 nm LED with 23 mW cm^{-2} of illumination power. Since RCs have the tendency to orient the hydrophilic H subunit toward the water, LB deposition of such complexes would orient the RC with H-subunit facing the electrode.[74] It is worth noting that this interpretation of Kamran *et al.* likely comes from an earlier study in 1992 which was performed using the LB deposition for another type of protein complex, the RCs of *Rhodopseudomonas viridis*.[74] As explained in the earlier studies, the H-subunit of RC impedes the ET from QB to the electrode, due to the 24 A^{o} ET distance.[33] However, in Kamran's study, quinones and cyt *c* both were used as charge carriers in the buffer solution which implies indirect charge transfer between the protein to the electrode as opposed to the direct tunneling approach .[73] It should be pointed out that using a two redox system in the electrolyte has a natural problem of the recombination of the charges in the electrolyte

which results in waste of energy. The results in Figure 1.22(b) shows that LB method is effective for achieving high current densities through deposition of a packed and oriented layer of RCs. Additionally, Kamran *et al.* interpreted that based on the photocurrent results the orientation of complexes on the surface is different using forward or reverse LB deposition.[73] The authors indicated that in forward dipping the RC's primary donor side (P-side) face the electrode while in the reverse dipping the H-subunit is facing the electrode.[73] This potentially could explain why higher level of photocurrents were observed in case of forward dipping as there would be a shorter distance (about 7 A°) between RC's active site and the electrode in this orientation (attachment from P-side) comparing to the other case. However, from the results in Figure 1.22(b), it is not clear to the author of this dissertation why the current direction is similar in both forward and reverse LB deposition. Based on these results it seems LB can be applied as a simple technique to fabricate densely packed RC-LH1 based photoactive monolayers for potential application in solar energy convertors.

The review of the previous studies demonstrates how linking mechanism of photosynthetic RC protein complexes with various orientations and thickness of the linker would affect the conversion efficiency and ET rate. To improve power conversion efficiency of such devices other approaches such as enhancement of light absorption was employed, as well. The following section reviews some of these efforts to enhance the bio-molecular solar energy conversion.

1.3.1.3. Using Photosynthetic plus Light Harvesting Complexes for an Improved Light Absorption

An approach to enhance light absorption in a bio-photovoltaic device is to use a bacterial RC-LH1 core complex, where the RC is encircled by a light-harvesting (LH) complex. The limited optical absorption spectrum and extinction coefficient of the RC complex restricts the photocurrent generated in a cell. Therefore, antenna (LH) complexes may be used to increase light capture—for example, the RC-LH1 core-complex.[43,45,64,75-78]

An LH complex is a complex of subunit proteins which is a part of a larger supercomplex of a photosystem and is utilized by plants and photosynthetic bacteria to absorb more photons from the incoming light than that of RC alone. Through Förster resonance energy transfer, photon energy initially absorbed by

antenna complexes, such as the bacterial LH complexes 1 and 2 (LH1, LH2), is transferred to the RC (with transfer times of about 10^{-10} sec from the edge of the unit to the center), where a charge-separated state is generated with $\sim100\%$ quantum efficiency.[51] Figure 1.23 shows a cartoon of LH complexes and RC in cyanobacteria.[23]
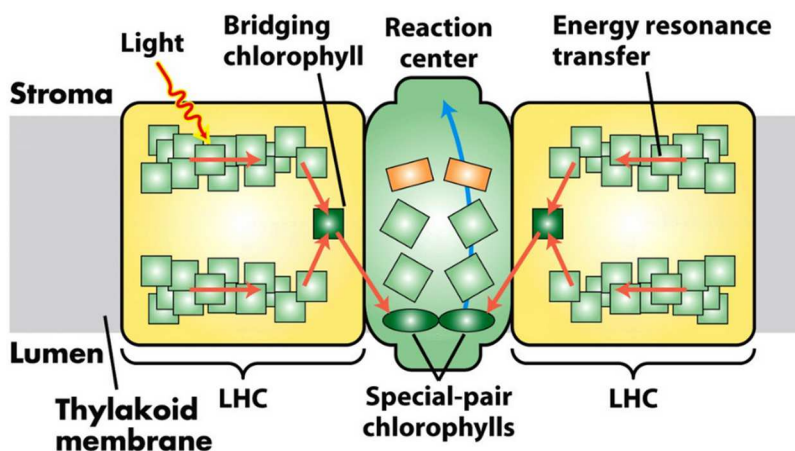
Figure 1.23 A cartoon which shows energy transfer from antenna chlorophyll molecules to RC in cyanobacteria (used with permission[23]).

One of the early studies on incorporating RC-LH1 complexes in bio-photoelectrochemical cells to utilize solar energy goes back to 2006 when Suemori *et al.* self-assembled monolayer of LH core complexes of photosynthetic bacteria on a semiconductor electrode.[79] In that work RC-LH1 complexes were isolated from *Rhodospirillum rubrum* and *Rhodopseudomonas palustris* and self-assembled onto an indium tin oxide (ITO) electrode treated with 3-aminopropyltriethoxysilane (APS).[79] It was shown that such a structure orients RC-LH1s preferentially from P-side onto an ITO surface. The schematic and the energy structure of the immobilized RC-LH1 on an ITO surface are shown in Figure 1.24. The photocurrent measurements were performed in a three electrode setup with APS-ITO electrode incorporating the core complex as a working electrode.[79] The time dependent photocurrent measurement generated from the structure in Figure 1.24(a) is shown in Figure 1.25.
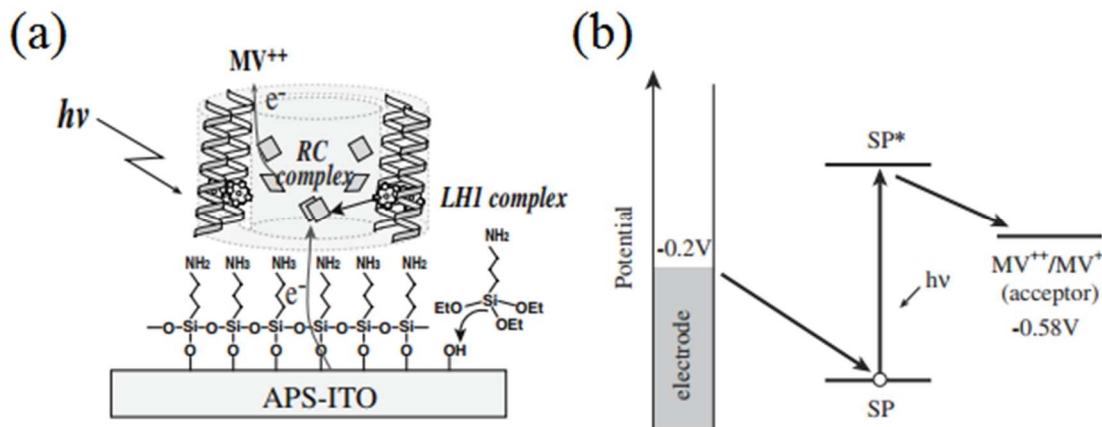
Figure 1.24 (a) Schematic drawing of LH1-RC core complexes on an APS-ITO electrode which shows the electron flow from the complex to MV. (b) Energy diagram for the schematic structure in part (a) (used with permission[79]).

The illumination of the electrode was performed through pulses with λ = 880 nm. The control experiment with only LH1 antenna or the RC core showed negligible photocurrent. Additionally, the photocurrent direction implies one way ET from RC-LH1 core complex to the methyl viologen (MV) redox system.[79]
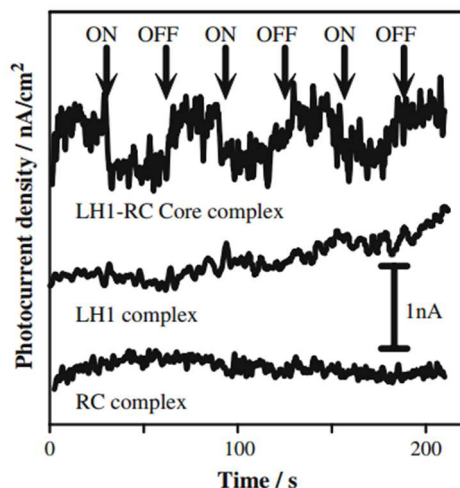
Figure 1.25 Time course of the photocurrent of the LH1-RC core complex, LH1 complex or the RC complex of *R. rubrum* on an APS-ITO electrode when the electrode is illuminated with pulsed light (880 nm) firing continuously for 30 s. The current polarity was set in a fashion that showed cathodic current as negative (used with permission[79]).

A year later, Kondo *et al.*, from Nagoya Institute of Technology in Japan self-assembled monolayer of RC-LH1 core complexes from photosynthetic bacteria on Au electrodes modified with 3 different

27

linkers: alkanethiols: $NH_2(CH_2)_6SH$ (hereafter 6-AHT); $HOOC(CH_2)_7SH$ (hereafter 7-CHT); and $CH_3(CH_2)_7SH$ (hereafter OCT).[64] Their experiments showed that the success rate of core complexes immobilization was depended on the terminating group of the alkanethiols with the following order: amino groups (6-AHT) > carboxylic acid groups (7-CHT) > methyl groups (OCT).[64] Figure 1.26 shows a schematic representation of RC-LH1 assembly on the Au electrode modified with alkanethiol linkers.
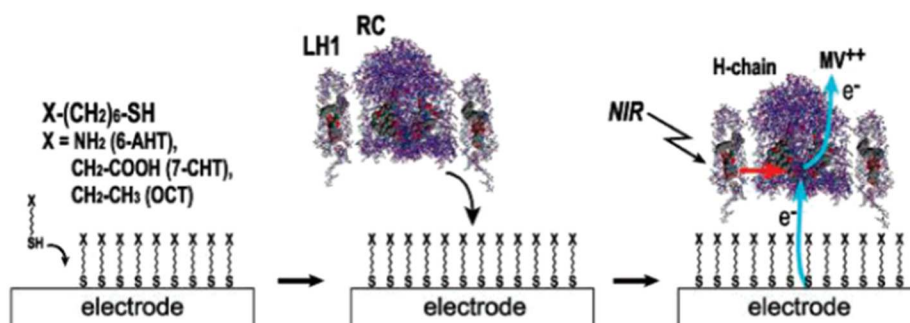
Figure 1.26 Schematic model of assembly of RC-LH1 complex on the electrode modified with alkanethiols. The C-terminus of the LH1 complex and the special pair (SP) side of RC is oriented toward hydrophilic SAMs on the Au substrate and the H-chain is oriented toward the aqueous phase (used with permission[64]).
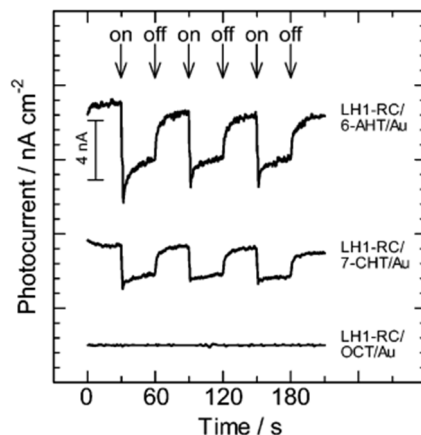
Figure 1.27 Photocurrent response of LH1-RC complex assembled on a gold electrode modified with 6-amino-1-hexanethiol (6-AHT), 7-carboxyl-1-heptanethiol (7-CHT), and 1-octanethiol (OCT) in buffer solution when illuminated at 880 nm (used with permission[64]).

Figure 1.27 shows that the photocurrent response of RC-LH1 complexes on Au electrodes modified with 6-AHT, 7-CHT, and OCT, when these electrodes were illuminated with pulsed light at 880 nm. It was demonstrated that the photocurrent response was sensitive to the surface properties of the SAMs on the

gold electrode. The photocurrent was the highest and the lowest once the Au surface was modified with amino terminated and methyl groups, respectively.[64] Additionally, the observed cathodic photocurrent implied a unidirectional ET from the Au electrodes into RC-LH1 core complexes and accordingly to MV redox system.[64] The above mentioned observations provided useful information about the effect of surface modification of electrodes on the performance of RC-LH1 complexes as solar energy converters.

In 2010 Magis *et al.* studied photostability, photocurrent response, and optical properties of directly adsorbed isolated *Rb. sphaeroides* membranes onto a Au surface.[80] The membrane adsorption were carried out through incubation of protein complexes directly on a gold electrode.[80] Despite the study by Mahmoudzadeh *et al.*,[71] which demonstrated a negligible current for directly adsorbed genetically modified RCs onto a Au surface (Figure 1.18(b)), Magis *et al.'s* study showed a steady state photocurrent of ~10 µA cm^{-2} using RC-LH1s.[80]
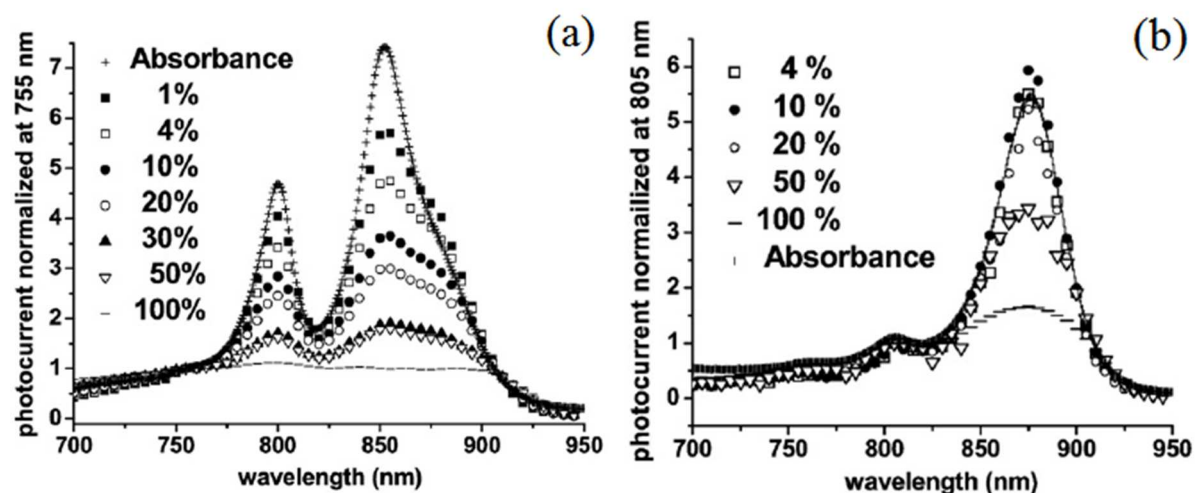
Figure 1.28 a) Light-induced current action and solution absorbance spectra from wild type (WT) RC-LH1 chromatophores. Spectra normalized at 750 nm. (b) Light-induced current action and solution absorbance spectra from RC-LH1 mutant membranes. Spectra normalized at 805 nm. Illumination powers indicated as percentage of maximum (100%) illumination that was 15 mW cm^{-2} (used with permission[80]).

Although based on the presented results it seems that the membranes remain functional while adsorbed onto a gold-electrode, the mechanism of adsorption and the membrane orientation was not clear in the Magis's work. Figure 1.28 shows the wavelength dependent current action spectra of the wild type (WT) and mutant RC-LH1. The photocurrent measurements were performed in a three electrode setup like

the other earlier works in presence of two redox mediators in the electrolyte (*i.e.* cyt and Q0). The absorption peaks of LH2 complexes were presented at 800 and 850 nm. While the LH1 absorption peak appeared as a pronounced shoulder at 870 nm.[80]

In a different work, the same group used direct attachment of RC-LH1 onto Au electrode while using cyt *c* as a molecular relay.[36] RC-LH1 complexes from *Rhodopseudomonas* (*Rps.*) *acidophila* were directly attached onto bare Au electrodes by simply depositing solutions of protein complexes onto the surface and subsequent rinsing.[36] An interesting fact about *Rps. Acidophila* is that this class of complexes are associated with a tetra-heme cyt on the periplasmic side of the membrane.[36,81] The attached cyt *c* can act as the reductant for the photo-oxidized primary electron donor.[36,81]
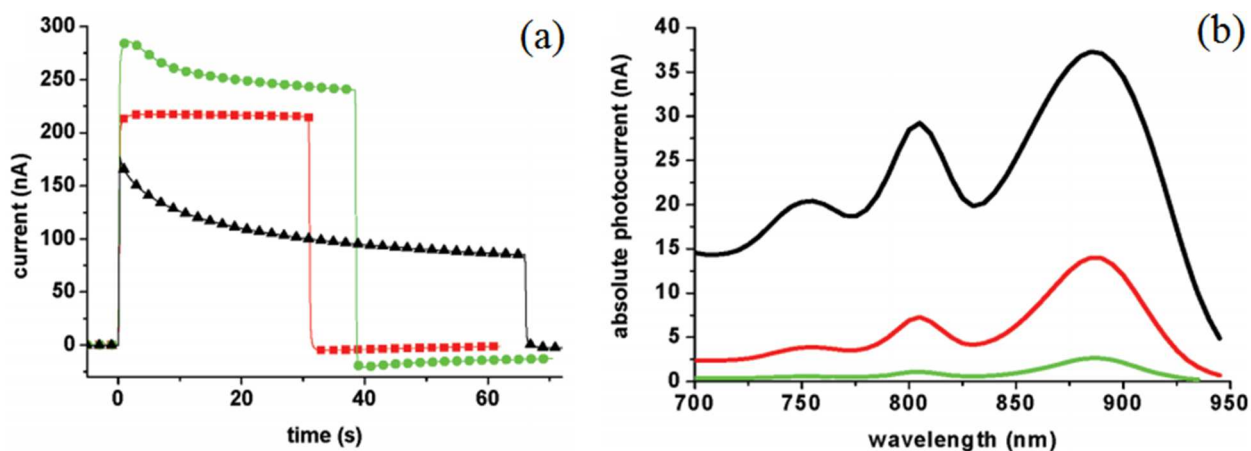
Figure 1.29 (a) The photocurrents response obtained from attached RC-LH1 complexes onto a bare Au in different concentration of Q0 and cyt *c*. The largest photocurrent was obtained for 1000 μM Q0 and 100 μM cyt *c* (circles). (b) Wavelength dependence of RC-LH1 photocurrents (not normalized) at excitation powers of 0.5 (green), 3 (red), and 15 mW cm^{-2} (black). (used with permission[36]).

It was reported in their study that the *Rps. Acidophila* complexes may potentially be attached onto the gold surface *via* the associated cyt *c* through a surface exposed conserved cysteine near the tip of the cyt subunit.[82,83] Figure 1.29(a) shows the photocurrent response from the attached *Rps. Acidophila* complexes onto gold for three different concentration of cyt *c* and quinone (Q0) in the electrolyte. The highest photocurrent (Figure 1.29(a), circle) was observed for 1000 μM Q0 and 100 μM cyt *c* concentrated redox solution. Additionally, increasing the concentration of the redox mediator led to lower decay of current after cessation of light.[36]

The review of the efforts in the area of RC-LH1 complexes shows that the integration of LH antennas for enhancement of photon absorption, can be considered as an effective strategy to increase the photocurrent density and EQE in photosynthetic bio-hybrid devices for solar energy harvesting. Almost all the aforementioned works were concentrated on fabrication of photosynthetic RC-based bio-photoelectrochemical cells through applying a working electrode, with directly attached or linker coupled RCs, in an electrolyte with a reference and counter electrodes. The three electrode measurements can be performed to accurately study the reactions only on the surface of the working electrode (the potential changes of the working electrode are measured independent of changes that may occur at the counter electrode). Also, in the three probe measurement, the surface area of counter electrode would not be a rate-limiting factor. In practice, for solar energy harvesting, a two terminal device has to be designed. Two-probe electrochemical devices using photosynthetic protein complexes and a fabrication approach in which RC complexes and the electrolyte can be injected into the space between working and counter electrodes are discussed in the next section.

1.3.1.4. Two Probes Electrochemical Devices Using Photosynthetic Protein Complexes

In 2012, Tan *et al.* fabricated RC based bio-photoelectrochemical cells, using a similar approach being used for making DSSCs.[62] In their approach, a mixture of the RC protein and the redox mediator was injected into the cavity formed between working (a fluorine-doped tin oxide (FTO) glass) and counter (a Pt-coated rear electrode) electrodes (Figure 1.30).[62] It is worth mentioning that this method of cell construction, using protein complexes, was first employed by Ciesielski *et al.* in 2010 for another type of protein complex, Photosystem I[1] (PSI).[41] Figure 1.30 shows a schematic representation of such structure. In the fabricated cells by Tan *et al.*,[62] N,N,N',N'-tetramethyl-p-phenylenediamine (TMPD) was used as the single diffusible redox mediator in the electrolyte.

---

[1] PSI is an ~500 kDa membrane protein complex that perform oxygenic photosynthesis.
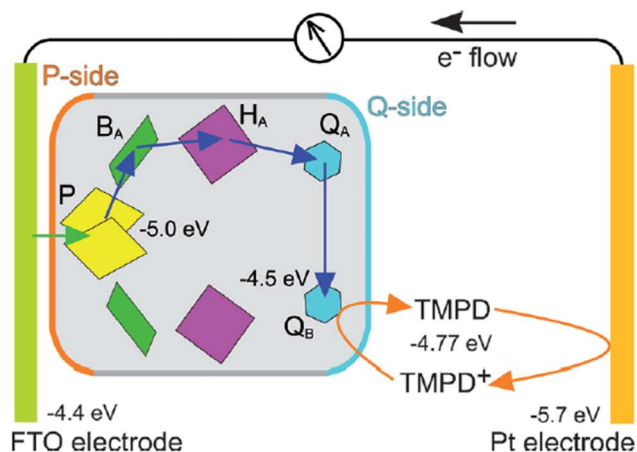
Figure 1.30 Proposed mechanism of operation in the RC and RC–LH1 cells with TMPD as the single redox mediator. Current-supporting RCs (as shown) or RC–LH1 complexes (not shown) are oriented with the P-side close to the FTO-glass electrode. Arrows indicate the route of ET through the RC (blue), through the TMPD/TMPD$^+$ pool to the Pt electrode (orange) and into the P-side of the RC from the FTO-glass electrode (green) (used with permission[62]).

As shown in Figure 1.30 and suggested by the authors, the injected proteins into the cavity between the two electrodes, eventually resulted in attachment of the RC or RC-LH1 complexes with the primary donor (P-side) facing the FTO electrode. Hence a direct ET would occur from the FTO underlying electrode to the complex while TMPD would act as a reductant of P$^+$.[84,85] Accordingly the oxidized mediator--*i.e.* the TMPD$^+$--can act as an oxidant of Q_B^-.[84,85] Figure 1.30(a) shows the short circuit current in a cell with RC-LH1 and TMPD. Figure 1.30(b) shows the action spectrum of external quantum efficiency (EQE) in a sample device.

Figure 1.31(a) shows a 0.15 µA cm^{-2} current density after ~20 s illumination. To confirm the contribution of the protein complexes to the photocurrent generation, control experiments were performed on cells containing TMPD, but lacking any protein component (Figure 1.31(a), linear plot).
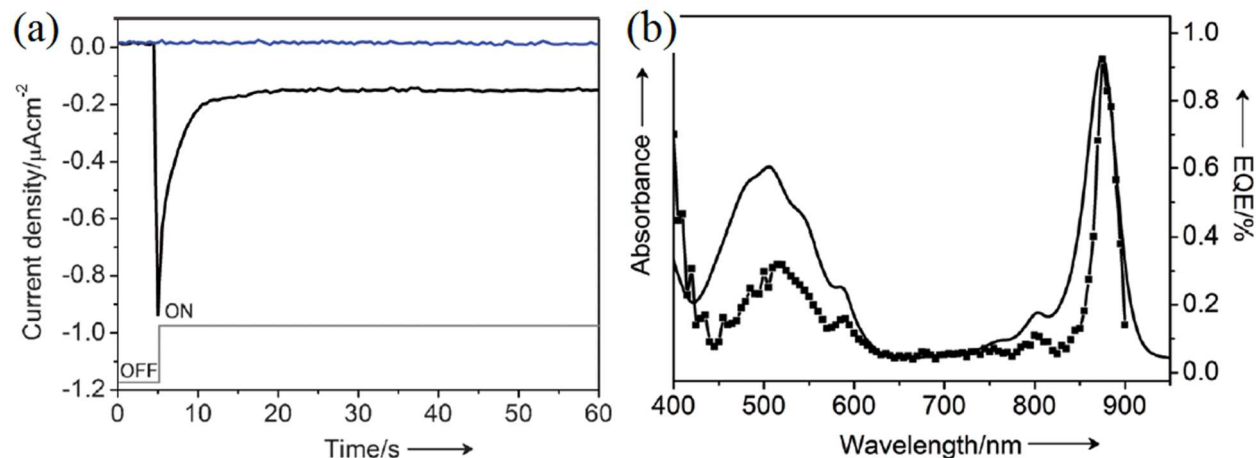
Figure 1.31 (a) J_{SC} output by a cell with RC–LH1 and TMPD (RC–LH1 cell; black) and a control cell with only TMPD (blue) under a pulse illumination, indicated by the gray line. (b) Action spectrum of EQE (squares/lines) compared to the solution absorbance spectrum of the RC–LH1 complex (line). (used with permission[62]).

The negligible photocurrent density supports the interpretation that the photo-response in the RC-LH1-based cells stems from the light harvesting and charge generation in the protein components. Upon switching on the light, the current response showed an initial spike. According to Tan *et al.* the spike could be due to a faster rate of P^+ reduction relative to Q_B^- oxidation, which resulted in a buildup of negative charges within the protein.[62] Upon cessation of illumination, transient positive (reverse) currents (not shown here) were observed for the RC-LH1 photoactive electrodes. The positive current was attributed to the oxidation and reduction reactions at the photoactive working and the counter electrodes, respectively, which helped in dissipating the energy difference between the electrode and the electrolyte to regain a state of equilibrium in the dark.[50,62] Figure 1.31(b) shows a compelling match between the RC-LH1 solution absorption spectrum (line) and EQE across this wavelength range (line-squares) which confirms that the RC-LH1 complexes were functional and intact. The results also indicate the EQE maximum value of 0.95% at ~875 nm.[62]

Recently, Tan *et al.* used various types of counter electrodes including cobalt disilicide ($CoSi_2$), titanium nitride (TiN), multiwall carbon nanotube (MWCNT), and Pt in a two probe protein based solar cell.[61] The hypothesis was that in a structure such as the one schematically shown in Figure 1.30, some of the complexes might eventually detach from the working electrode and be adsorbed on the surface of the

counter electrode. This would reduce the overall generated photocurrent as well as EQE in the cell. Using

a superhydrophobic material such as MWCNT, the adsorption of the protein complexes on the counter

electrode can be prevented. *En route* to fabricate such a structure, the authors observed a variety of reversed

currents in response to discontinuous illumination.[61] In particular, the authors report that the use of

superhydrophobic MWCNT as the counter electrode resulted in a near symmetrical forward and reverse

current upon light on and light off, respectively.[61]
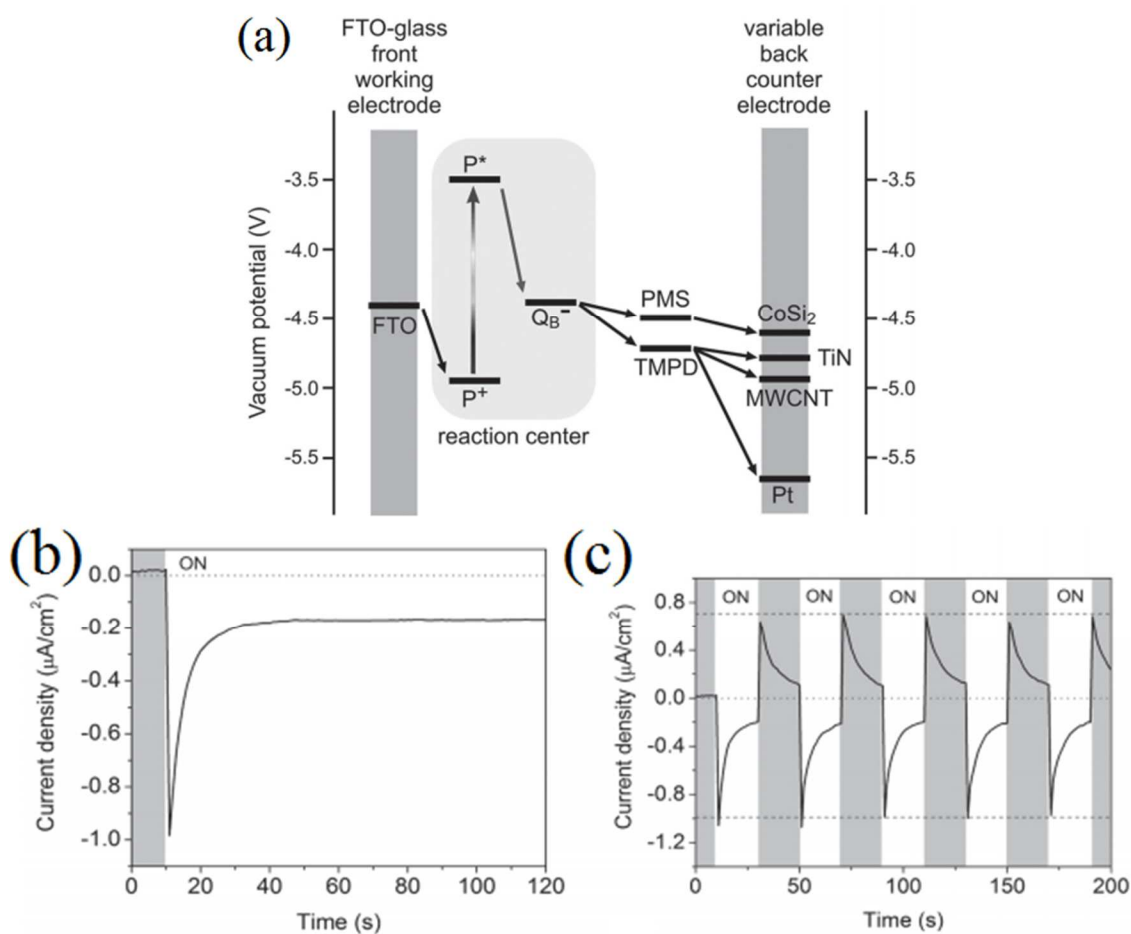
Figure 1.32 (a) Schematic showing the vacuum potentials of key components in a RC-LH1 based bio-photoelectrochemical cells with either TMPD or PMS as the redox electrolyte and different counter electrodes. With TMPD or, for CoSi$_2$, PMS as the mediator, a flow of direct current was observed to the back electrode. (b) Time dependence of J_{SC} produced by a MWCNT/TMPD cell under continuous illumination and (c) exposed to 20 s light-on/light-off cycles (used with permission[61]).

Figure 1.32(a) shows a schematic representation of the energy structure and charge transfer cycle

of a RC-LH1 based bio-photoelectrochemical cell with either TMPD or PMS as redox electrolyte and

various counter electrodes. The photocurrent response of such cells under continuous illumination and discontinuous illumination (light on-off cycles) is shown in Figures 1.372b-c). This study helps fabricating cells capable of different types of direct current (DC) and/or reverse output current using different combinations of photoactive proteins, redox mediators, and synthetic materials.[61]

1.3.2. Hybrid Structures of Semiconductors and Photosynthetic Reaction Centers for Solar Energy Harvesting

Hybrid structures of proteins with synthetic materials can find numerous applications in artificial solar fuel generation, solar energy conversion, and in optoelectronic devices.[22] Several types of protein hybrid structures can be named including semiconductors-RC proteins and quantum dots (QDs)-RCs. Some of the devices explained earlier in this chapter have employed semiconductor materials as the working electrodes.[61,62] However, the author intention here is to explain, the energy levels and the interface structure of such hybrids. Potentially, a semiconducting electrode is more suitable than a metallic one for charge transfer to or from proteins, due to the existence of conduction and valence bands.[22] Using a metallic electrode, a donated electron from an RC can be transferred to the redox electrolyte, before it would be collected at the device terminal (Figure 1.33(a)). This charge recombination at the metallic electrode's surface results in a waste of energy. The ideal scenario is once the working electrode can act only as an electron acceptor or donor. Due to the energy band structure in semiconductors, they potentially can be useful for selective charge transfer in a bio-photoelectrochemical cell using proteins. This approach has previously been used in DSSCs. Also some of the earlier studies in this chapter employed a semiconductor material for the working electrodes.[32,61,62,79] In the following text we review the structure of some devices, other than those already reviewed, in a greater detail, providing a full comprehension on the advantages of hybrid semiconductor-protein arrangements over metal-protein ones. Figure 1.33 demonstrates the energy structure and charge transfer mechanism in a device based on metal-RC electrode *vs* semiconductor-RC electrode.
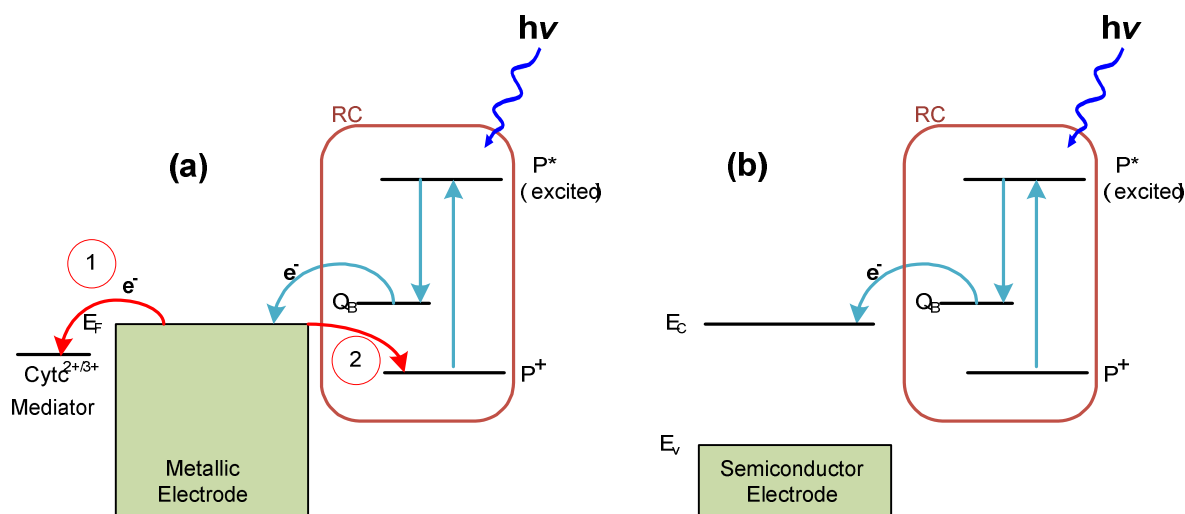
Figure 1.33 Energy level depiction in a device with immobilized RCs at (a) a metallic and (b) a semiconducting electrode. The light blue arrows show the ET from the ground state in P to the electrode via the excited level and Q_B. In (a) the metallic electrode can donate electrons to (1) mediators or (2) P^+ which results in the energy loss (charge recombination). In (b) the electron is transferred from the RC to the E_C. Since E_v is lower than P^+ and cyt $c^{2+/3+}$ the semiconductor is a poor electron donor.

Consider a scenario in which RCs are attached to a semiconductor material as shown in Figure 1.33(b): exposing the hybrid structure to light would induce excitation of the electron at P^+ to its singlet state (P^*) and transferring the electron to Q_B. This electron can either be injected to the semiconductor conduction band or interact with the redox electrolyte.[22] The current direction--*i.e.* generation of either anodic or cathodic current--depends on the energy levels in the semiconductor and the RC; and the redox electrolyte midpoint potential. The hybrid protein-semiconductor electrode would act as a photoanode if E_C (termed as C_B in Figure 1.34) stays lower than RC^*/RC^+ level in the following diagram while the redox reduces RC (Figure 1.34(a)). The hybrid electrode would act as a photocathode if the charge transfer path is similar to the schematic representation in Figure 1.34(b).

One of the early studies in this domain goes back to 1980 when RCs of *Rhodopseudomonas sphaeroides* R-26 were attached to an SnO_2 electrode.[86] The RCs were simply incubated and dried without controlling the adsorption orientation.[86] Figure 1.35 shows a schematic representation of such structure.[87]
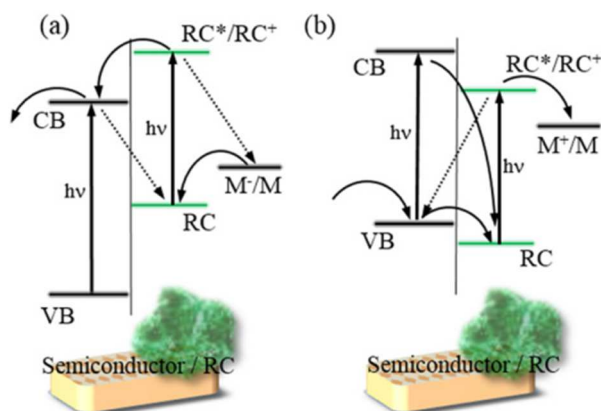
Figure 1.34 Schematic energy diagram in RC/semiconductor electrode. The arrows in the figures represent possible flows of electrons. (a) Anodic ET. The dotted arrows represent possible cathodic ET. (b) Cathodic ET. The dotted arrow represents possible anodic ET (used with permission[22]).
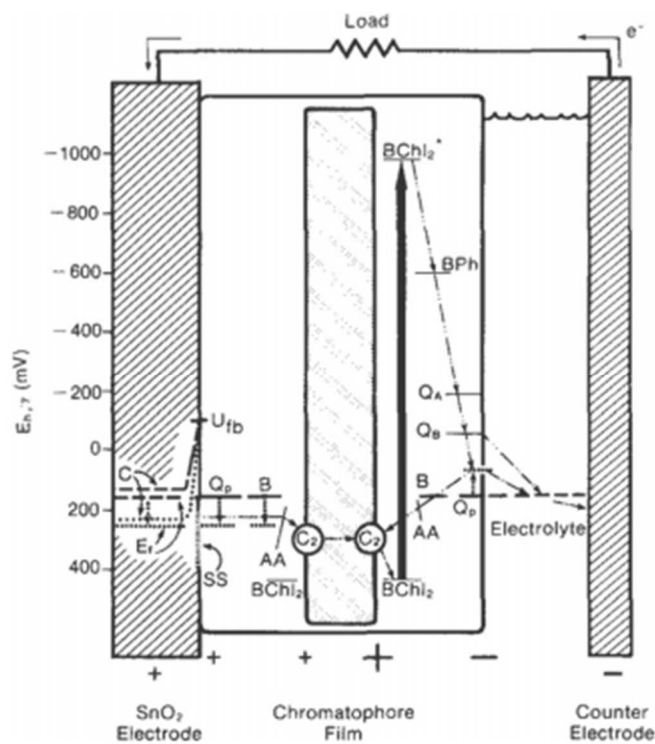
Figure 1.35 Energy level of SnO_2 electrode and bacterial RC. The hybrid electrode exhibits a cathodic photocurrent. (used with permission[87]).

The overall schematic representation of energy structure in Figure 1.35 is similar to the one in Figure 1.34(b), in terms of energy band structure, showing that the hybrid RC-SnO_2 electrode performed as a photocathode. The ET path is likely from SnO_2 to the RC while the charge transfer through electrolyte can happen *via* redox reaction of hydroquinone.[86] The explained structure produced a V_{OC} and I_{SC} of 70 mV

37

and 0.3 μA cm^{-2}, respectively.[86] Using a p-type semiconductor, the photovoltage and photocurrent could potentially be improved.[22]

In 2005, Lu and his coworkers constructed a novel photoactive electrode consisting of the bacterial photosynthetic RC trapped (physical adsorption) on a mesoporous WO$_3$–TiO$_2$ film to facilitate bio-photoelectric conversion by manipulating the excitation relaxation of the proteins.[88] The structure of the semiconductor electrode was a three-dimensional wormlike mesoporous WO$_3$-TiO$_2$ film with tailored pore size of ~7.1 nm.[88] The aforementioned pore size allowed for entrance and entrapment of the bacterial RCs. Figure 1.36 shows the schematic representation of experimental setup for preparation of bio-hybrid device based on tailored mesoporous WO$_3$-TiO$_2$ films with the entrapped RCs.
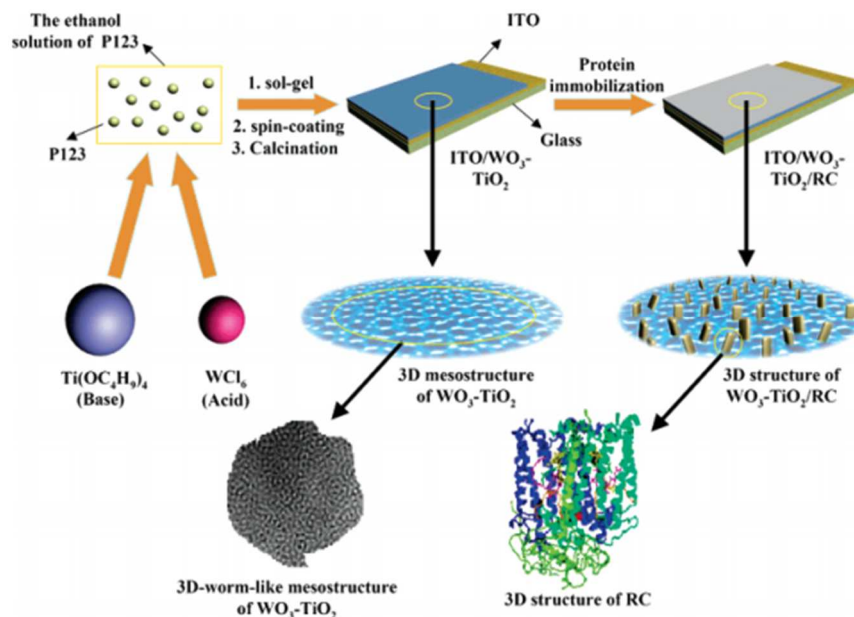
Figure 1.36 Experimental setup for preparation of a bio-photoactive electrodes based on the tailored mesoporous WO$_3$-TiO$_2$ film and RC (used with permission[88]).

To confirm that the RCs were successfully entrapped in the mesoporous electrode, the near infrared (NIR)-visible absorption spectrum of the mesoporous electrode entrapped with RCs was compared to that of RCs in the electrolyte.
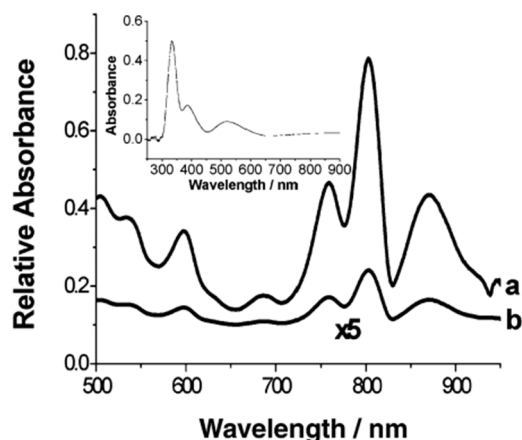
Figure 1.37 NIR-visible absorption spectra of (a) RC (2 µM) in pH 8.0 Tris-HCl buffer and (b) the tailor-made ITO/WO$_3$-TiO$_2$/RC film at 293 K. Absorption of bare ITO/WO$_3$-TiO$_2$ film is subtracted as background. Inset reveals the UV-visible NIR absorption spectrum of the tailor-made ITO/WO$_3$-TiO$_2$ films recorded using blank ITO as background (used with permission[88]).

The results in Figure 1.37 shows that there was a good match between these two which confirmed the interpretation that such structure can successfully be employed for entrapment of bacterial RC and photoactive electrode applications. Both spectra showed three major absorption peaks of RC at 760, ~802, and 870 nm, which correspond predominantly to the Q$_y$ transition for Bphe, Bchl, and P, respectively.[88]

In a comparison to this work, it was shown that a TiO$_2$ structure without WO$_3$ demonstrates several times lower ability in the adsorption of RCs mainly due to the lack of an optimized mesoporous structure for RC effectual entrapment.[88] Additionally WO$_3$-TiO$_2$ structures were synthesized with variable pore size. The summarized results in Table 1.1 suggest that the pore structure (2D hexagonal and 3D wormlike) and size can significantly affect the amount of adsorbed RCs,[88] with 3D mesoporous structures having higher potential for the RC entrapment. The size of pores should be large enough for RC entrapment but not excessively large so the complexes can leave easily.

Table 1.1 Comparison of matrix property with quantity of RC adsorbed (used with permission[88]).

matrix of RC Bio-PEs	pore structure	pore size (nm)	thickness (nm)^a	contact angle (deg)^b	M of RC immobilized (µmol/g)^c
TiO$_2$	intercrystalline voids	4−200	~500	38.6	0.18
WO$_3$−TiO$_2$	2D hexagonal	9.8 ± 0.8	~150	23.4	0.29
WO$_3$-TiO$_2$	3D wormlike	3.4 ± 0.3	~150	24.6	0.31
WO$_3$−TiO$_2$	3D wormlike	7.1 ± 0.6	~150	24.2	0.63

Thickness of WO_3-TiO_2 and TiO_2 films was determined with an average of five measurements. [b] All data for contact angle were measured with an average of four measurements. [c] Molar amount (M) presented here were calculated from the differential absorption spectra of RC solution before and after immobilization (molar extinction coefficient of RC at 802 nm is *ca.* 2.88×105 M^{-1} cm^{-1}) with an average of three measurements.

Figure 1.38 shows the photocurrent measurement results under illumination for a fabricated bio-hybrid photosynthetic solar cell device with the aforementioned photoactive electrode. Such a structure resulted in a 30 µA cm^{-2} current density which is about five times larger than that of RC-free ITO/WO_3-TiO_2 films (~6.4 µA cm^{-2}) and a maximum incident photon-to-current conversion efficiency (IPCE) of ~11% (around 800 nm).[88] This confirms the contribution of RCs in photoelectric effect of such a device.
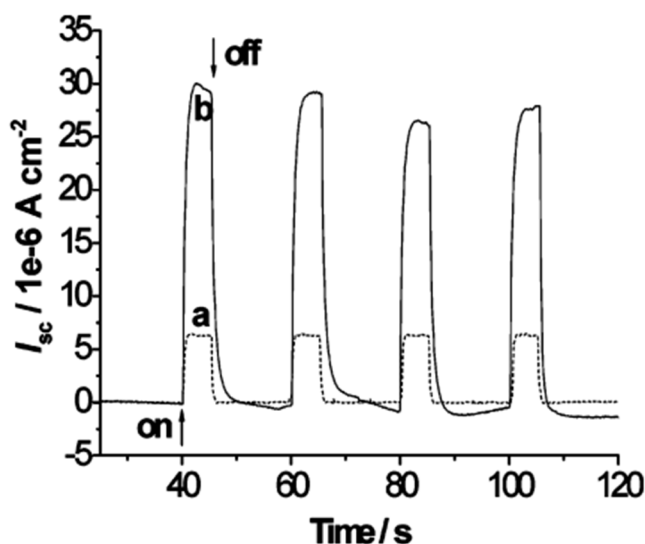
Figure 1.38 I_{SC} responses of RC-free ITO/WO_3-TiO_2 film (a, dot line) and ITO/WO_3-TiO_2/RC film (b, solid line) in pH 8.0 Tris-HCl buffer containing 8 mM sodium dithionite illuminated with a 20 W incandescent lamp (5 mW cm^{-2}). The electrode bias is set at the V_{OC} (~-0.1 V *vs* SHE) (used with permission[88]).

In 2011, Takshi *et al.* used a solution of suspended RCs with mediators in an electrochemical device and studied the effect of various metallic and wide bandgap semiconducting materials, including carbon, Au, ITO, SnO_2, and WO_3 as the working electrode, on the photocurrent density.[35] It was shown that in contrast to the common knowledge that believes RCs should be coupled to an electrode for current generation, free floating suspended RCs can generate noticeable photocurrent and photovoltage in lack of

any linking mechanism.[35] This percipience comes also from an earlier work by the same author,[89] which later was confirmed by other groups as well.[34,36] However, it is worth mentioning that the recombination of the mediators in the bulk of electrolyte and\or oxidation and reduction at the surface of electrode leads to a waste of energy in systems with two redox mediators.[35] The main finding of this study though is not the use of solubilized RCs but rather to show how the electrode materials can affect the rates of the reactions in a similar cell. It was demonstrated that selection an appropriate material for the electrode, the charge transfer between the mediators and the electrode can potentially be rectified to achieve larger photocurrents.[35] Figure 1.39 shows the obtained photocurrents in bio-photovoltaic cells with (a) metallic and (b) semiconducting electrodes.
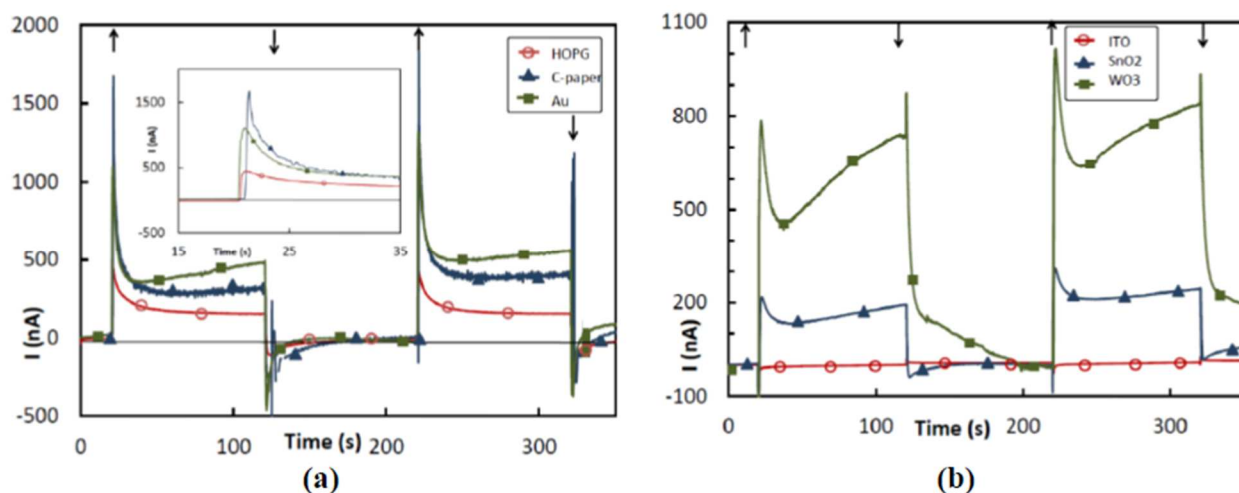
Figure 1.39 Photocurrent in the bio-PV cells with (a) metallic and (b) semiconducting electrodes. The inset plot is the transient current with a quick rise and slow decline. Light: ON (↑), OFF (↓).The electrolyte was composed of Cp_2Fe and MV with RCs. The electrolyte was applied in a three probe setup. The electrode surface area was 0.2 cm^2. The illumination was performed with a beam of white light with an incident intensity of 2.8 mW cm^{-2}. (used with permission[35]).

Figure 1.39(a) inset shows two regimes for the transition: (1) a quick rise in the magnitude of the current followed by (2) a gradual decline.[35] It was suggested that the fast response came likely from the reduction of Cp_2Fe^+ while the graduate decline was due to a slow oxidation of MV^+.[35] Additionally, Figure 1.39(a) demonstrates that using a similar material such as carbon with different morphology and surface area (c-paper vs HOPG), the current can be different. Using a C-paper as working electrode, the cell indicated almost two times current density comparing to that of HOPG.[35] Furthermore, the author explains

that another potential reason for the difference in the photocurrents might be the difference between the energy structures of carbon in HOPG and carbon fibers.[35] In case of using Au, higher level of currents were obtained which might be a result of complexes adsorption through cysteine residues on the Au's surface which can increase the kinetics of charge transfer.[35] The low level of currents in case of using ITO indicates similar rates of Cp_2Fe^+ reduction and MV^+ oxidation at the electrode's surface.[35] Among all metallic and semiconductor materials in this work, WO_3 demonstrated the largest photocurrent density ($\sim$5.1 μA cm^{-2}) which could be due to position of WO_3's E_C which is close to the energy level at Q_B in the RC. Hence, WO_3 would behave as a poor electron acceptor from MV^+ and responds to the reactions more selectively than the rest of the materials.[35]

The use of semiconductor electrodes in bio-PV devices for selective charge transfer and larger photocurrent was studied in a greater detail by Usgaocar et $al.$[90,91] In their study, Fluorine doped Tin Oxide (F:SnO$_2$), Copper(II) Oxide (CuO) and Nickel Oxide (NiO) electrodes were investigated as a mean for achieving selective redox reactions.[90,91] The reactions of MV, ferricyanide/ferrocyanide and ferric/ferrous couples on the three semiconducting electrodes were studied using cyclic voltammetry and sampled current voltammetry.[90,91] Figure 1.40 shows the semiconductor-electrolyte interface energy alignment.
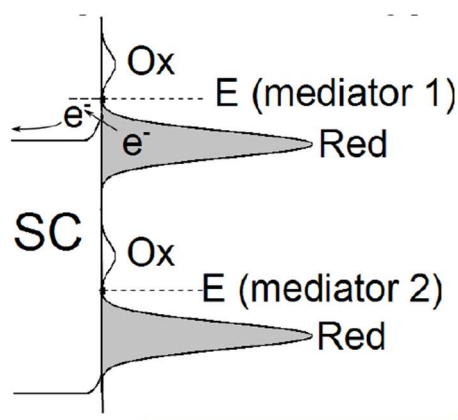
Figure 1.40 Semiconductor-electrolyte interface energy alignment. Larger conduction band and redox potential separation should lead to slower reaction rates (used with permission[91]).

It was suggested in this study that semiconductor and redox couple reactions rates are ruled by the overlap between energy levels in both systems.[90] As shown in Figure 1.40, a redox couple with a large E_C overlap, should have higher redox reaction rates compared to one that overlaps the semiconductor

42

bandgap.[90] It was indicated that the rate of ET between the electrodes and the redox couples depends on the

difference between the semiconductor majority carrier band edge and the standard redox potential of the

redox couple. The authors applied cyclic voltammetry (CV) to measure the standard redox potential of the

mediators. Figure 1.41(a) demonstrates CV curves with $F:SnO_2$ and aqueous MV, $Fe(CN)_6$ and Fe^{3+}/Fe^{2+}

solutions. The relative peak magnitudes and separations show a preferential reaction between $F:SnO_2$ and

MV.[90,91] Figure 1.41(b) shows sampled current voltammetry between SnO_2 and multiple mediators.
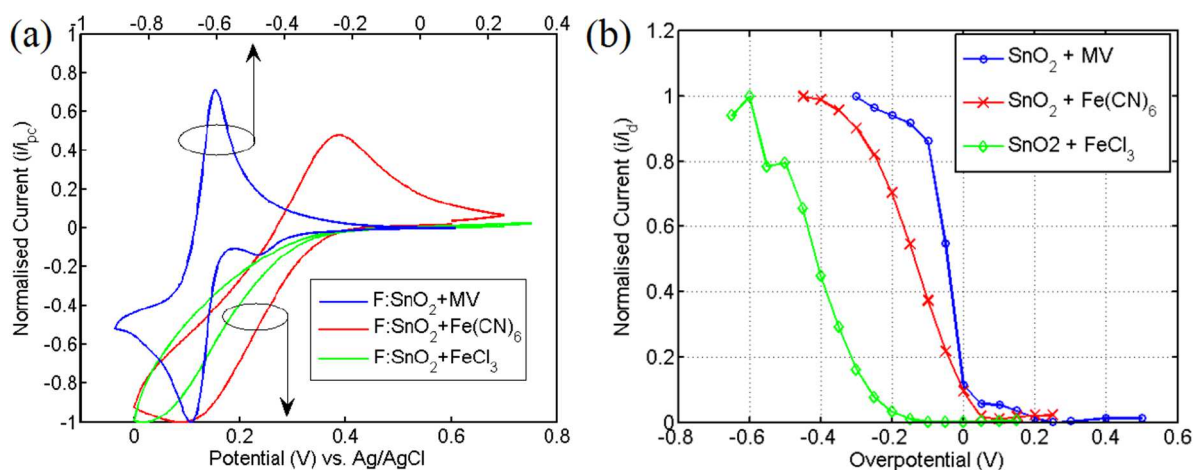
Figure 1.41 (a) CVs of SnO_2 in presence of various mediators at a scan rate of 10 mV s^{-1}. Current axis is common and potential axes are as marked. Currents are normalized to the cathodic peak current. (b) Sampled current Voltammetry between SnO_2 and multiple mediators. Currents are normalized to the diffusion current (used with permission[91]).

The sampled current voltammetry data in Figure 1.41(b) indicated that MV reaches the mass

transport limitation at significantly lower overpotential than $Fe(CN)_6$ and Fe^{3+}/Fe^{2+}. Table 1.2 summarizes

the results of Figure 1.41 which includes the electrochemical midpoint potentials of mediators as well as

reaction rates which were estimated from the plots.

Table 1.2 Rates of reaction of mediators with $F:SnO_2$ electrode. E_{CB} is the $F:SnO_2$ C_B edge *vs* the vacuum level (used with permission[91]).

Mediator	E_0 (vs Vac.) (eV)	E_{cb} - E_o (eV)	k_o (cm/s)
MV	4.1	~0	1.1×10^{-4}
$Fe(CN)_6$	4.7	0.6	6.0×10^{-6}
Fe^{3+}/Fe^{2+}	5.2	1.1	2.0×10^{-7}

The results suggested that the rate constant of MV on $F:SnO_2$ was two orders of magnitude higher

than that for the ferric/ferrous ion.[90,91] Therefore, Usgaocar's studies reported selectivity using a $F:SnO_2$

electrode with MV compared to Ferricyanide/Ferrocyanide ($Fe(CN)_6$) and Ferric/Ferrous (Fe^{3+}/Fe^{2+}) redox couples.[90] Similar results were obtained using the NiO electrode while the electrochemical instability hampered the tests of the CuO electrode.[90] Additionally, the rate of reaction varied inversely with the difference between $F:SnO_2$ E_C and the mediator redox potential.[90,91] As Table 1.2 suggests this difference can be up to several order of magnitudes. It is reasonable to assume that choosing an appropriate semiconductor and a redox couple, higher selectivity towards one redox couple can be achieved.[90]

1.3.3. Hybrid Structures of Quantum Dots and Photosynthetic Reaction Centers

Quantum dots (QDs) are small nanocrystals of semiconductors that show quantum mechanical characteristics. Nabiev and his coworkers showed that coupling a CdTe QD to an RC using electrostatic assembly, a nearly threefold increase in the rate of generation of excitons in the RC can be achieved.[92]
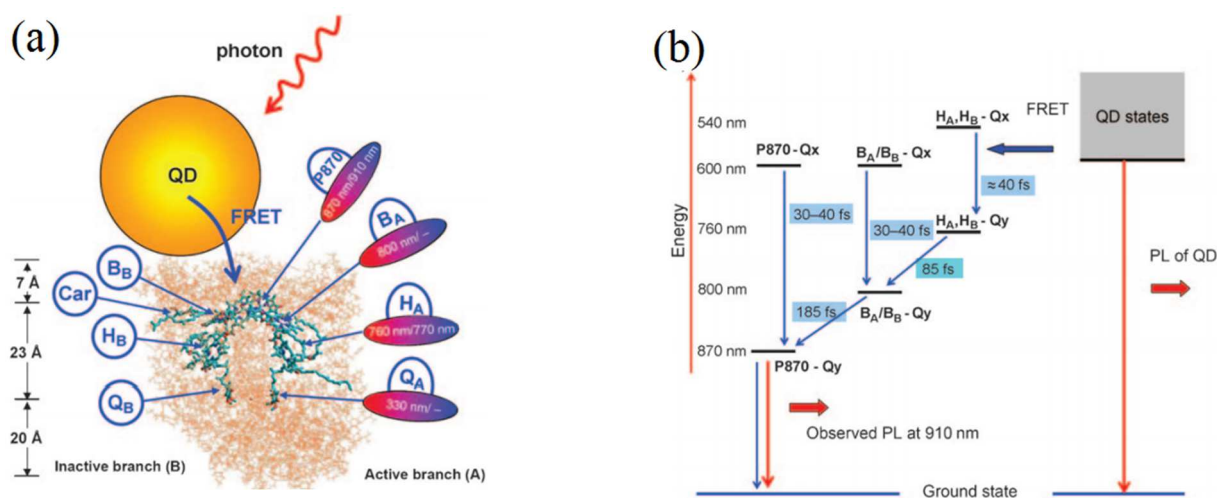
Figure 1.42 (a) Organization and functionality of a complex composed of the RC (from *Rb. sphaeroides*) and a QD; the diagram is given to scale. Active (A) and inactive (B) branches in the electron-transfer cofactor are shown. The positions of the absorption/photoluminescence maxima for the BChl special pair (P870), BChl monomer (B), bacteriopheophytine (H), and quinone (Q) are indicated for the active branch (A) only. Photons are absorbed by both the RC and the QD. An exciton from the QD is transferred to the RC by FRET. Car=carotenoid. The FRET shows the Forster resonance energy transfer from QD to the RC. (b) The energy-level diagram for the states of the reaction center. QD supplies excitation to the RC by means of FRET. Excitation quickly relaxes to the P870–Q_y level. The continuous blue arrows designate the non-radiative energy transfer (FRET) between the levels, while dashed red arrows stand for relaxation to the ground state with de-excitation of light quanta (used with permission[92]).

The QDs act as artificial antenna that absorb light efficiently in a wide range of energies within the solar spectrum and accordingly transfer the harvested energy to optical enhancement of RC.[92] Figure 1.42(a)

shows a model of the system composed of the *Rb. sphaeroides* RC assembled with photoluminscent QDs. Figure 1.42(b) shows the diagram of energy relaxation inside the RC. The results of this work shows an enhancement in the photoluminescence emission of the special pair in the RC (at 910 nm).[22]
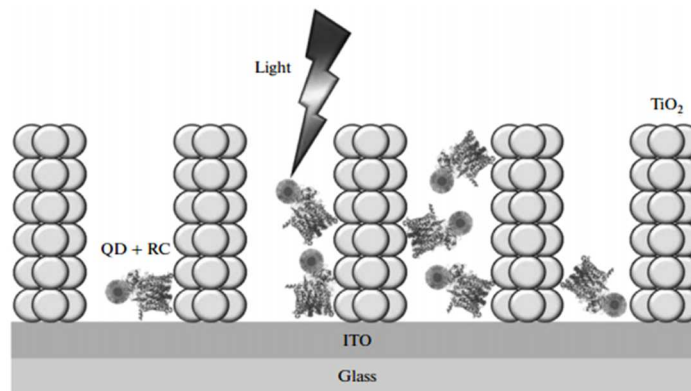
Figure 1.43 Schematic representation of crystalline mesoporous films TiO_2 with adsorbed hybrid structures QDs + RCs (used with permission[93]).

In 2013, complexes of CdSe/ZnS and CdTe QDs with *Rb. sphaeroides* RCs were developed which demonstrated an efficient ET from the electron donor (QD) to the acceptor (RC) both in the solution and in the films of crystalline mesoporous TiO_2.[93] Figure 1.43 shows a schematic representation of crystalline mesoporous films of TiO_2 with adsorbed hybrid structures QDs + RCs. Such structures have applications in solid state photovoltaic cells composed of interacting natural organic and inorganic elements.

1.3.4. Solid State Solar Cells using Photosynthetic Reaction Center Complexes

To the best of author's knowledge the only solid state solar cell device using photosynthetic reaction center complexes made so far is the one by Das *et al.*[60] Other efforts on making solid state devices using proteins mainly employed other types of complexes. In this work, oriented monolayer of photosynthetic complexes were self-assembled on a surface of an electrode, stabilized with surfactant peptides, and coated with a protective organic semiconductor.[60] Figure 1.44(a) shows the energy structure of an RC photovoltaic cell with the photocurrent spectrum of the device shown in Figure 1.44(b).
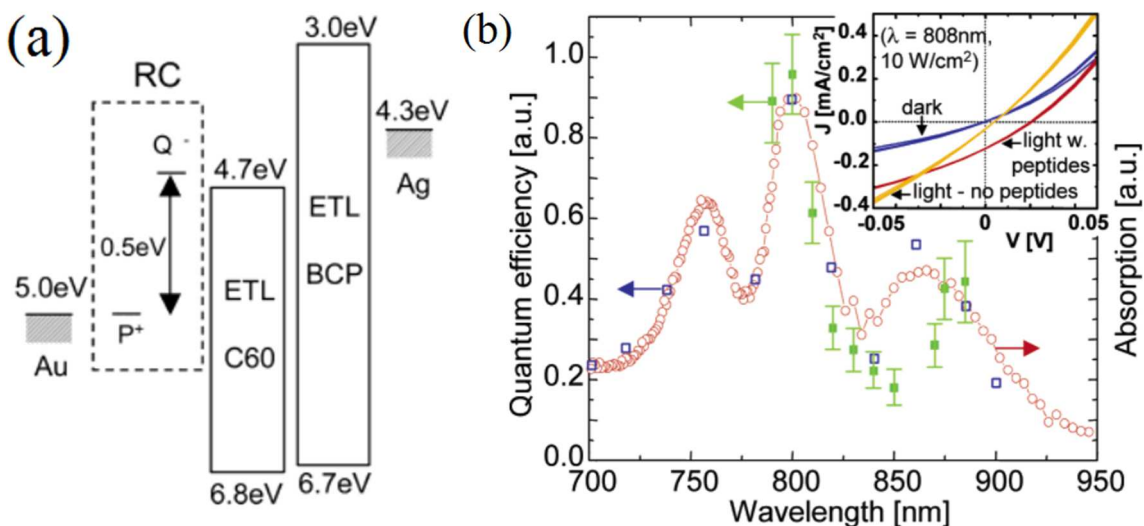
Figure 1.44 (a) Energy level diagram of an RC photovoltaic cell. LUMO energies are estimated from the HOMO and the optical energy gap. It is assumed that no charge transfer occurs at the material interfaces. (b) Photocurrent spectrum of photovoltaic devices employing bacterial reaction centers. A comparison between the photocurrent spectrum of solid-state (■) and wet electrochemical cell devices (□) and the solution absorption spectrum of the bacterial reaction centers (O), demonstrates that the observed photocurrent originates in the RCs. (Inset) stabilization of RC complexes with A6K/V6D peptides improves the internal quantum efficiency of the devices to 12% under short circuit conditions (used with permission[60]).

This study in 2004 by Das *et al.* on a sealed solid state device, using RCs stabilized with two cationic and anionic peptide surfactants, reports on a short circuit current density of ~0.12 mA cm^{-2} under an excitation intensity of 10 W cm^{-2} at $\lambda = 808$ nm.[60] It came to the attention of the author of this dissertation that using the EQE equation in the manuscript, the EQE in Das *et al.*'s work should be calculated 0.00185%. Hence, their reported efficiency of 0.9% is a calculation error.

1.3.5. Other Chlorophyll and Carotenoid Based Proteins for Solar Energy Harvesting

In addition to RC and RC-LH1 complexes, other chlorophyll-based proteins such as Photosystem I (PSI) and PSII have also been explored for solar energy conversion application.[40,41,94,95] A recent review summarizes some of these efforts in applications of RC, PSI, and PSII in biological-driven solar power production.[31] Several studies have focused on the assembly of PSI onto various substrates such as P-dope silicon and graphene oxide, which resulted in enhanced current densities over 100 µA cm^{-2}.[40,94] A most recent study successfully incorporated large photosynthetic complex trimers into solid-state plastic solar cells that were exclusively prepared by solution processing which resulted in a significant change in the

open-circuit voltage.[96] Other applications of light harvesting proteins could be in production of solar fuels such as H_2.[97] Beside carotenoid-based photosystems, bacteriorhodopsin as a robust light-driven proton pump has found various applications in solar energy conversion,[47,48,98] optoelectronics,[99] and organic field effect transistors.[100] A recent study on fabricating a photovoltaic cell using aqueous bacteriorhodopsin generated a photoelectric response of ~33 $\mu A\ cm^{-2}$.[46] Overall, the tendency toward biomimetic devices and the need for the production of clean energy by mimicking nature brings the light-capturing proteins applications in bioelectronic devices to the forefront of cutting-edge research. The fast-paced activities in exploring new configurations and attaining higher efficiencies of biological solar energy conversion using various photosynthetic proteins,[30,101,102] fuel the idea that mimicking nature is a promising approach for developing a sustainable energy technology. The overall effort will advance the application of biological materials in electronic devices with a far reaching impact in the fields of solar cells, biosensors, and bionanotechnology.

In conclusion, chapter 1 gave an overview of the various type of strategies to integrate photosynthetic protein complexes in electrochemical and electronic devices for applications in solar energy harvesting. In summery the presented approached were included: immobilization of proteins of various surfaces directly or using linkers, using LH antenna complexes along with RC cores to increase in light absorption, and making two probe and hybrid structures. In continuation, chapter 2 will explain the various materials and methods used in this work.

CHAPTER 2 : MATERIALS AND METHODS

2.1. Materials

In the experiments with isolated wild type RCs, N,N-Dimethyldodecylamine N-oxide solution (LDAO), was used as detergent which was purchased from sigma Aldrich. Ubiquinone-10 coenzyme Q2 (2,3-dimethoxy-5-methyl-6-geranyl-1,4-benzoquinone, ≥90%), 2-amino-2-hydroxymethyl-propane-1, 3-diol (Tris buffer), cytochrome *c* (cyt *c*) from equine heart, and 98% ferrocene (Cp$_2$Fe) were purchased from Sigma-Aldrich, as well. For preferential immobilization of the RC protein on the HOPG electrode from H-subunit side (N-(1-pyrene) iodoacetamide) linker molecules were used which was purchased from Invitrogen. Cyt *c* was reduced (cyt *c*$^{2+}$) by the addition of excess Na$_2$S$_2$O$_4$ to 72 mg of protein dissolved in 6 mL of 0.1 M Tris−HCl buffer (pH 8.0).[33] To remove the excess Na$_2$S$_2$O$_4$, the protein sample was run through a Sephadex G-50 column and an orange/red fraction was collected and analyzed by UV−vis spectrophotometry.[33] The concentration of the reduced form of the protein was calculated using the absorption band at 550 nm ($\varepsilon = 27.7$ mM^{-1} cm^{-1}).[103]
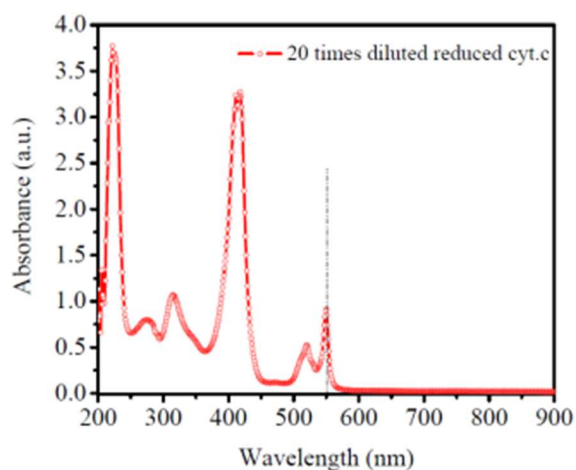
Figure 2.1 Absorption spectrum of reduced cyt *c* at room temperature. The peak intensity is monitored spectroscopically and the concentration is determined from Beer's law (used with permission[33]).

2.2. Protein Purification and Isolation

The isolation and purification of photosynthetic proteins in this work was performed at Dr. J. Thomas Beatty's Lab in the Department of Microbiology and Immunology at the University of British Columbia (UBC). The purified RC/RC-LH1 proteins were shipped from UBC in form of frozen samples in special packages containing ice. Upon arrival, the proteins were stored in a -80℃ freezer at USF. The samples were used for fabricating various devices without any further purification of the proteins. The preparation and purification process of the proteins (carried out in Dr. Beatty's lab) is explained here. Wild type RCs from *Rb. sphaeroides* were isolated using a modified version of the method of Goldsmith and Boxer.[33,71,104] Briefly, cells were centrifuged at 9000g and resuspended in 10 mM Tris (pH 8), 150 mM NaCl, and 2 mM $MgCl_2$.[33] A few crystals of DNase A were added to the suspension, and the cells were broken by two passages through a French press.[33] Broken cells were centrifuged at 9000g to pellet unbroken cells and the supernatant centrifuged overnight at 30000 rpm in a Beckman Coulter Type 70 Ti rotor to pellet membranes.[33] Membranes were resuspended in 10 mM Tris (pH 8) and 150 mM NaCl and solubilized with 1.5% N,N dimethyldodecylamine N-oxide (LDAO).[33] Solubilized membranes were ultracentrifuged at 541000g, and six His-tagged RCs were purified from the supernatant using affinity chromatography.[105] The concentration of RCs after purification was determined by their absorption at 804 nm, as described by Goldsmith and Boxer.[104] Figure 2.2 shows the absorption spectrum of RCs of *Rb. sphaeroides* at room temperature.

Figure 2.2 Absorption spectrum of RCs of *Rb. sphaeroides* at room temperature (used with permission[33]).

The complete view of the RC protein with all five cysteine residues has been shown in Figure 2.3.
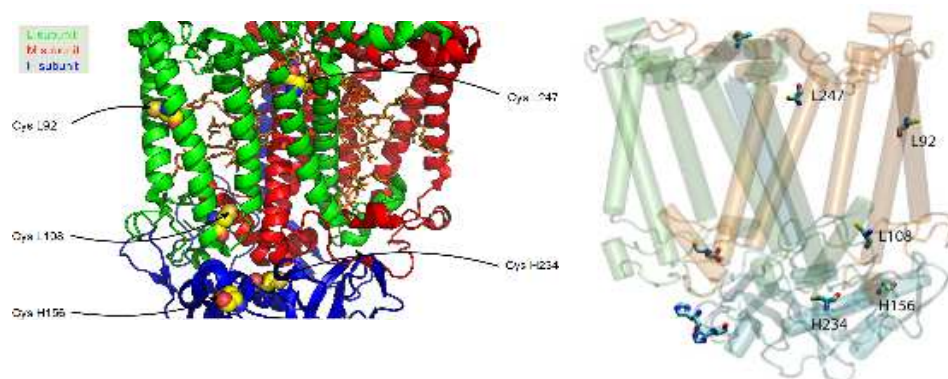
Figure 2.3 The complete view of the RC protein with all five cysteine residues (used with permission[33]).
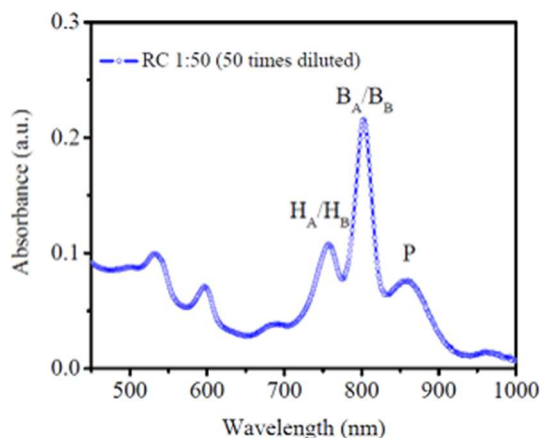
The solvent accessibility of cysteines in the RC at pH 8 (using PDB 2J8C) can be explained by the following values, obtained by using the DSSP algorithm; L92: 6, L108: 0, L247: 4, H156: 3 and H234: 6.[33] The DSSP algorithm is the standard method for assigning secondary structure to the amino acids of a protein, given the atomic-resolution coordinates of the protein.[106] The DSSP program also defines the geometrical features and solvent exposure of proteins, given atomic coordinates in Protein Data Bank format. These numbers are in Angstroms (A°) squared (*i.e.* area). The numbers are generated by calculating the surface area of a particular residue by simulating a water molecule of radius 1.4 A° rolling around that residue.[33] So L92 has a cysteine with 6 A°^{2} in contact with a water molecule.[33] However, these numbers do not predict which residues are the main contributors to binding since for instance H234 has twice the area has H156 exposed, but considering the crystal structure (PDB 2J8C), H156's side chain points away from the protein towards the solvent, unlike H234, which is exposed more to internal space than the exterior (Figure 1.20, Chapter 1).

The production and purification of the RC-LH1 dimer in *Rb. sphaeroides* were similar to the description by Abresch *et al*.[107] All protein solutions utilized a buffer of 10 mM Tris-HCl, pH 8, and 25 mM NaCl. Membranes were solubilized with 0.5 % sodium cholate combined with 4% *n*-octyl-*β*-D-glucopyranoside (BOG), and the six-histidine-tagged proteins bound to a Ni^{2+}/NTA column. The detergent

was then changed to a combination of 0.2 % sodium cholate and 0.06% *n*-dodecyl-*β*-D-maltopyranoside (DDM) in all the following steps.
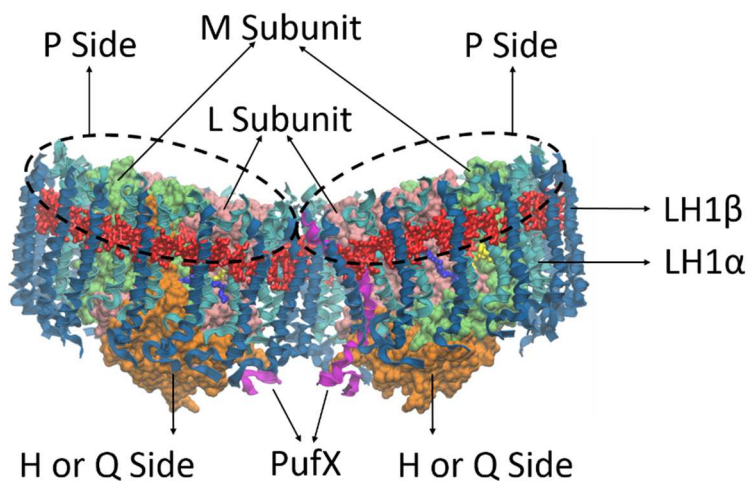
Figure 2.4 The schematic of dimeric RC-LH1-PufX complex used in our work, showing the L, M, H subunits, the LH1 shell\cylinder (LH1α and LH1β), the Pufx opening in the shell, and P and Q sides.[108] The LH1 α-chain is shown in teal and the β-chain in light blue. The RC H, L, and M subunits are colored orange, pink, and green, respectively. The BChls are in red, BPhes in yellow, the quinones in dark blue. The structures are based on the coordinates in the PDB files 4JC9 and 4JCB (http://www.rcsb.org/pdb/results/results.do?qrid=9F17A9BF&tabtoshow=Current) (used with permission[108]).

The column was washed with 10 column volumes of buffer solution containing 5 mM imidazole, and the protein eluted from the column by raising the concentration of imidazole to 150 mM. The column eluate was layered onto a sucrose gradient (15% to 35%) and centrifuged in a Beckman SW41 swinging bucket rotor at 4° C for 44 h at 30000 rpm. The bottom (dimer) of two bands was collected, and the sucrose removed by dialysis. Figure 2.4 shows the schematic of dimeric RC-LH1-PufX complex used in our work.

The presence of antenna (light-harvesting) complexes increases the limited optical absorption spectrum of the RC.[45,75,76,78,109] Similarly to the RC, under illumination and through Förster resonance energy transfer, photon energy initially absorbed by antenna complexes, such as the bacterial light-harvesting complexes 1 and 2 (LH1, LH2), is transferred to the RC, where a charge-separated state is generated with ∼100% quantum efficiency.[51] Figure 2.5 shows the proposed structural models of the RC-LH dimer and RC studied in our work.

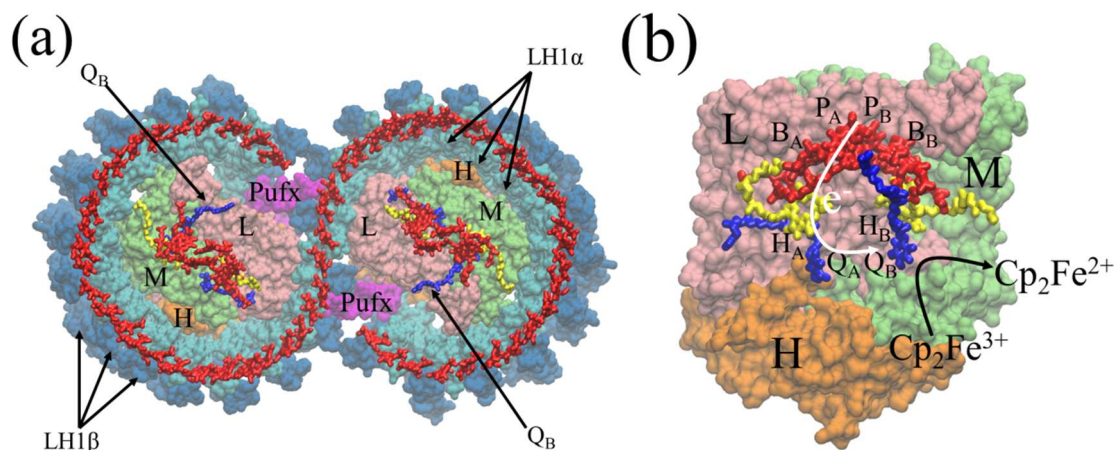Figure 2.5 Proposed structural models of the RC-LH dimer and RC studied in our work. (a) Dimeric RC-LH1-PufX complex (view from the periplasmic side of the membrane) of Rb. sphaeroides. Direct excitation with light or indirect excitation by resonance energy transfer from the LH1 initiates electron flow in the RC and between the Q_B and the Cp_2Fe electron acceptor. The LH1 α-chain is shown in teal and the β-chain in light blue. (b): Structure and mechanism of the *Rb. sphaeroides* RC, showing the light-induced ET pathway (white arrow). L, M and H refer to the three proteins of the RC. In both panels the RC H, L, and M subunits are colored orange, pink, and green, respectively. The BChls are in red, BPhes in yellow, the quinones in dark blue, and the cofactors are superimposed on top of the protein surface. The structures are based on the coordinates in the PDB files 4JC9 and 4JCB (http://www.rcsb.org/pdb/results/results.do?qrid=9F17A9BF&tabtoshow=Current) (used with permission[108]).

2.3. Preparation of Working Electrodes

In experiments which planar Au was used as working electrode, the electrode was fabricated by evaporating an adhesion layer of 20 nm of Cr (at a deposition rate of 2 A°/s) followed by 400 to 500 nm gold (at a deposition rate of ~1-2 A°/s) onto glass substrates using Varian e-beam evaporator which resulted in electrodes with RMS roughness < 2 nm.[33] The Au electrodes were cleaned by rinsing sequentially with acetone, methanol, isopropanol, deionized water, and dried completely under a N_2 stream prior to performing experiments.[3] In the experiments that highly ordered pyrolytic graphite (HOPG) was used as the working electrode, the electrode was prepared by gluing a gold coated substrate to the back of a fresh-cleaved HOPG piece (from SPI).[34] Different methods of making photoactive electrodes have been used in this dissertation which will be explained in detail in the following chapters.

2.4. Electrochemical Setup

The Au and HOPG working electrodes (either photoactive one treated with protein or the non-treated ones) were used in an electrochemical cell. A 13 cm length of Pt wire of 0.25 mm diameter was

shaped to a coil and used as the counter electrode. In some experiments a solution of coenzyme Q2 was used as the electrolyte.[3] In some experiments, a Cp$_2$Fe redox solution was prepared by dissolving Cp$_2$Fe in 0.1 M Tris buffer and ultra-sonication for 48 hrs and used as the redox electrolyte. In some other experiments two mediators were used such as Q2 and cyt *c*.[33,34] For the three probe experiments in which a reference electrode was needed, a Ag/AgCl electrode was used. All the experiments were carried out at room temperature using 0.1 M Tris−HCl at pH 8 as the background electrolyte. The current polarity convention in all experiments was set in a fashion that defined cathodic current as negative. Each cell was kept in the dark until the open-circuit potential (OCP) stabilized. For the photocurrent measurements, the same potential was applied to the cell by the potentiostat such that the current in the dark was zero.[3,33,41] All fabricated cells were illuminated with a commercial solar simulator (RST300S (AM 1.0), Radiant Source Technology) at an incident light intensity of 80 mW cm^{-2} at the electrode's surface.[3,33] The solar light source uses a XL3000 PerkinElmer Fiber Optic Illumination (FOI) system that employs a 300 W Cermax Xenon light. Photocurrents and photovoltages were recorded using a VersaSTAT 4 (Princeton Applied Research) potentiostat in either three or two electrode setups. The three electrode measurements were performed to accurately study the reactions only on the surface of the working electrode (the potential changes of the working electrode are measured independent of changes that may occur at the counter electrode).[3] Hence, the surface area of Pt counter electrode would not be a rate-limiting factor.

2.5. External Quantum Efficiency

For EQE measurements two different light sources were used. I some experiments Light from a Xenon arc lamp (Newport 300-Watt) was dispersed by a monochromator (Cornerstone 260 ¼M) and focused on the sample using a lens. I some experiments, light from a Tungsten Halogen lamp (Oriel 6334NS 24 V250W) was focused onto the entrance slit of a monochromator (Cornerstone 260 1/4M) using a pair of parabolic mirrors. The dispersed light passing through the exit slit (slit width: 5 nm) was subsequently focused onto the device using a convex lens. The photocurrent was measured in the three-electrode cell. At each wavelength step, the photocurrent was monitored for two complete cycles consisting of illumination

followed by the dark, where the light was blocked by a computer controlled shutter at the exit slit of the monochromator. The incident power was measured by a thermopile detector (Oriel 71945) connected to a multimeter (Keithley2000).

2.6. Characterization

2.6.1. Photochronoamperometry

Photochronoamperometry is an electrochemical technique in which an electrochemical cell is biased at a certain potential and the current is measured over time in periods of darkness and illumination. The photochronoamperometry tests can be performed in a three electrode system or a two electrode setup (without any reference electrode), using a potentiostat along with a light source such as a solar simulator. Figure 2.6 shows the setup used in this work for performing photochronoamperometry tests.
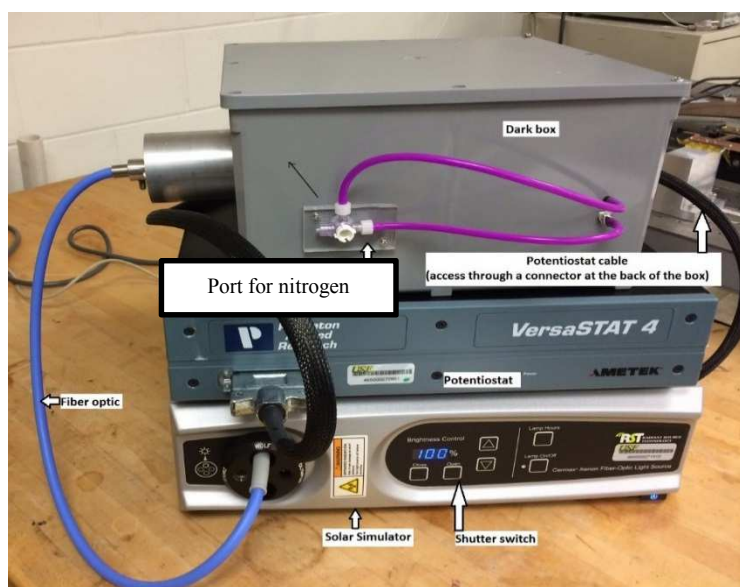

Figure 2.6 The setup for performing electrochemical tests.[110] The sample can be placed inside the dark box and the illumination can be controlled by turning on and off the shutter switch on the simulator. The output light from the simulator is conducted to the box through the fiber optic cable and is pointed at the sample inside the box. The potentiostat cable is also connected to the sample through a socket at the back of the dark box (used with permission[110]).

2.6.2. Cyclic Voltammetry

Cyclic voltammetry (CV) is a potentiodynamic electrochemical measurement in which the potential of a working electrode is ramped linearly as a function of time. The main difference between linear sweep voltammetry and CV is that, in CV after reaching the set potential, the electrode's potential is ramped around

54

to return to the initial value. It is possible to perform this test for one cycle or more. All CV tests in the current dissertation, were performed in a three electrode setup. In such a system, the potential is applied between the working and the reference electrodes while the current is measured between the working and the counter electrodes. The CV results will demonstrate the current at the working electrode *vs* the applied voltage and it can potentially be used for estimating the electrochemical midpoint potentials of a redox electrolyte, capacitance of a surface, and surface coverage of an electrode with an entity. Additionally, CV can provide information about electrochemical reaction rates. The capacitive current or the background ground in cyclic voltammetry is produced by the double layer charges on the surface of the electrode (Figure 2.7). In a CV test as an increasingly reducing potential is applied over the initial forward scan, the cathodic current will increase and reach its apex at E_{pc} (Figure 2.7).
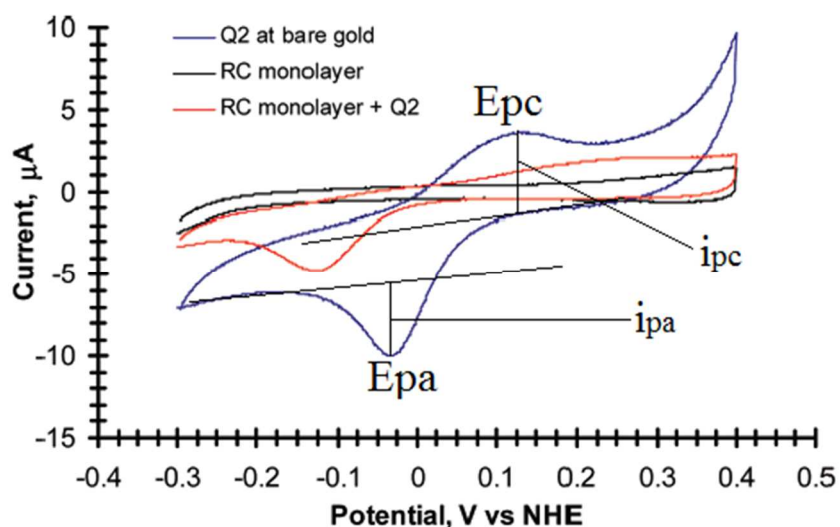

Figure 2.7 CVs of 40 μM Q2 in solution measured with a bare gold electrode (blue trace) or gold electrode covered with RC protein (red trace). CVs of gold electrode covered with RC protein but without Q2 (black trace). The protein was attached to the electrode through linker 1. Experiments were performed in 100 mM Tris buffer at pH 8 in the dark. Scan rate = 20 mV s⁻¹ (used with permission[81]).

Reaching the reduction potential of the redox electrolyte, the cathodic current decreases since the concentration of reducible analyte is depleted. In a reversible reaction, over the reverse scan the reduced analyte will be re-oxidized, giving rise to a current with opposite direction (anodic current) which will reach to its apex at E_{pa}. Figure 2.7 shows an example of CVs for Q2 redox electrolyte at a bare Au surface as well as at a treated Au surface with a monolayer of RCs.

55

In a quasi-reversible reaction, as the potential scan rate increases, the separation of the peak potentials becomes larger and the full-width-at-half-maximum (FWHM) for both cathodic and anodic peaks becomes broader.[111,112] In comparison, in a completely reversible system, there is a linear relationship between the peak current and the scan rate, and $\Delta E_p = E_{pa} - E_{pc}$ is 0 at low scan rates.[113] For a redox couple that is immobilized on the electrode surface, the peak current is given by:[112,114]

$$i_p = \frac{n^2 F^2}{4RT} v A \Gamma$$

Eq. 2.1

where n is the number of electrons transferred, F is the Faraday constant ($\sim$96485 C mole^{-1}), v is the scan rate, A is the electrode active area, and Γ is the electroactive surface density of the redox material immobilized in the surface. Additionally, the electrochemical midpoint potential of a redox species can be determined as the average of cathodic and anodic electrochemical potentials.[3,33]

2.6.3. Electrochemical Impedance Spectroscopy

Electrochemical Impedance Spectroscopy (EIS) is an electrochemical experimental technique which can be applied to separate and quantify sources of polarization, and is typically measured by applying an AC potential to an electrochemical cell while monitoring the current through the cell. Since the measurements are performed at various AC frequencies, the name impedance spectroscopy was chosen. EIS can also be applied to characterize processes and complex interfaces. EIS data are often represented in form of Nyquist and Bode plots as shown in Figure 2.8 as an example. Bode plots refer to demonstration of the impedance magnitude (or the real or imaginary components of the impedance) and phase angle as a function of frequency and show the frequency-dependence of the impedance of the cell under test. A complex plane or Nyquist plot depicts the imaginary impedance, which is indicative of the capacitive and inductive character of the cell, *vs* the real impedance of the cell. Because both data formats have their advantages, it is usually best to present both Bode and Nyquist plots. Additionally, the electrode reaction mechanisms of the electroactive species at the surface of an electrode can be determined using EIS.
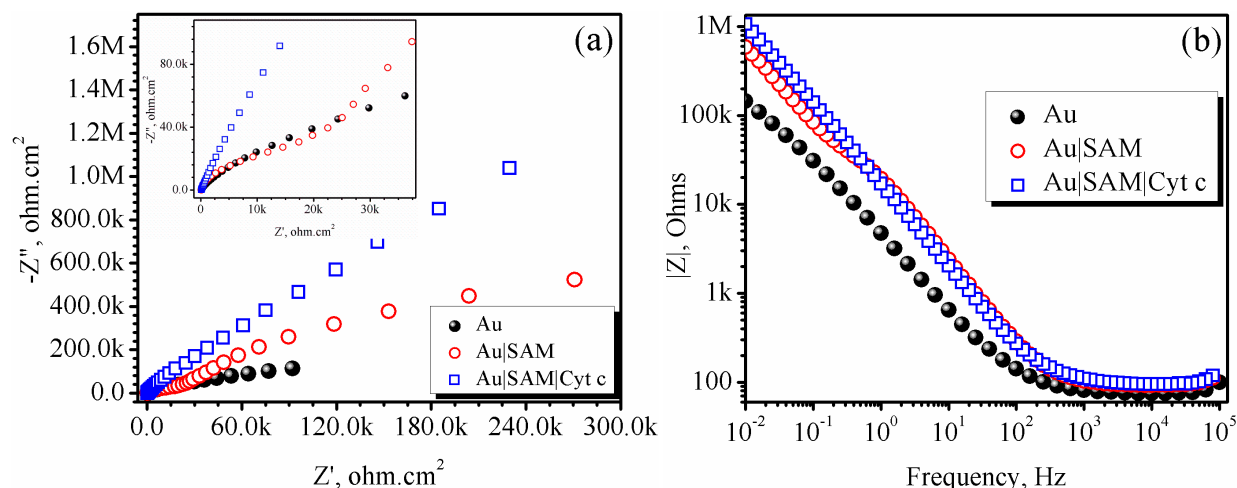
Figure 2.8 EIS results of bare Au, Au|SAM, and Au|SAM|cyt c structures. (a) Nyquist plots for Au, Au|SAM, and Au|SAM|cyt c structures. (b) Bode plots in the range of 0.01 Hz to 100 kHz for Au, Au|SAM, and Au|SAM|cyt c structures. Electrode area = 1.0 cm^2.

The analysis of EIS data for SAMs of various materials on an electrode's surface, can also provide comparative results by developing the appropriate equivalent circuits as well as estimating the double layer capacitance (C_{dl}) and polarization resistance (R_p) of each layer. EIS experiments can be quite useful as they allow several different parameters to be measured in one experiment. However, problems may arise due to the non-ideal behavior of the system under study. Non-ideal behavior can dramatically alter the values obtained from analysis based on the simple models such as a Randles circuit model (the basic equivalent Randles model consists of three components; the electrolyte resistance (R_s), charge-transfer resistance or polarization resistance (R_p), and double-layer capacitance (C_{dl}). The non-idealities can be addressed through the incorporation a constant phase element (CPE) into the circuit in place of one or more of the elements in the Randles circuit, as has been described elsewhere.[113] The CPE is commonly used for modeling frequency-dependent resistive or capacitive behavior.

2.6.4. Ellipsometry

The ellipsometry technique is an optical technique used for analysis and metrology to measure accurately and with high reproducibility the thickness and complex dielectric function of a given material. We applied spectroscopic ellipsometry to measure the thickness of the various layers of SAM, cyt c, and RC in the current study. The thickness measurements were performed using a Rudolf Research Type

ellipsometer AutoEL (wavelength of 6328 Å (He−Ne laser)) at an incident angle of 70° for carboxylic acid-terminated SAMs; a Sopra spectroscopic ellipsometer ES 4G (multilayer optical spectrometric scanner) at an incident angle of 70.1° was used for cyt *c* and RC layers. The refractive index and the coefficient of absorption values for the Au substrates were measured to be 0.1508 and 3.3280, respectively. The ellipsometric data were analyzed assuming an index of refraction of 1.4846 for the SAM monolayer, as suggested by the supplier (Sigma-Aldrich).[3]

2.6.5. Photoemission Spectroscopy

In the current study X-ray photoelectron spectroscopy (XPS) and low intensity XPS (LIXPS) were applied to provide further evidence for the successful attachment of the desired molecules and estimation the electrode's work function (WF), respectively.

2.6.5.1. X-ray Photoelectron Spectroscopy (XPS)

Different types of photoemission spectroscopy (PES) technics can be categorized based on the type of particles that hit the samples and those coming out. If the hitting particle is a photon and the particles coming out from the sample is an electron, the technic would be called XPS which can provide useful information about the filled core states. The core electrons are local close to the nucleus and have binding energies characteristic of their particular element. XPS is usually being used for elemental and chemical state quantification. XPS is a very surface sensitive technic which gives information about the depth of 10 nm of a sample's surface, which is about 30 atomic layers. XPS technique is based on Einstein's idea about the photoelectric effect, developed around 1905 that describes the ejection of electrons from a surface when photons were impinged upon it. During the mid-1960's Dr. Siegbahn and his research group developed the XPS technique. In 1981, Dr. Siegbahn was awarded the Nobel Prize in Physics for the development of the XPS technic. Figure 2.9 shows the working principles of XPS.
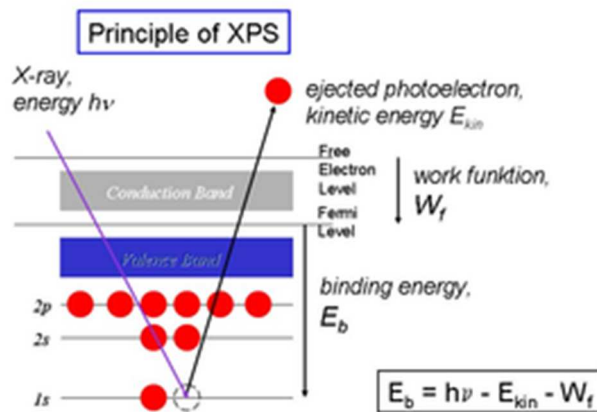
Figure 2.9 The working principles of XPS.

In an XPS test, the excitation of electrons happens with medium energy X-rays (Al or Mg-K$_\alpha$), or He-UV-radiation. The analysis of only elastically scattered electrons would be performed using a hemispherical energy analyzer. The analysis takes place at ultra-high vacuum (UHV)-conditions with a base typically pressure of $\sim 10^{-10}$ mbar. As Figure 2.9 demonstrates, the binding energy of a core electron (E_b) can be calculated using the energy of the X-ray source (hv), the ejected photoelectron energy (E_{kin}), and the WF of the material. The WF is the energy difference between the Fermi and the vacuum levels. Fermi level is the highest energy level occupied by an electron in a neutral solid at absolute 0 temperature.

In the current work, for photoemission spectroscopy analyses, all samples were prepared in a glovebox which was outfitted to the fast load lock of a multi-functional characterization system.[115] This commercial multi-chamber system (SPECS, Berlin, Germany) consists of two preparation chambers and one analysis chamber outfitted for XPS. The base vacuum level of this system was 2×10^{-10} mbar. An Mg Kα X-ray emission source with incident energy of 1253.6 eV and 20 mA emission current was used.

2.6.5.2. Low Intensity XPS (LIXPS)

The WF of a material can be measured both using PES and Kelvin probe (KP). While PES allows the measurement of the absolute WF, KP only gives the contact potential difference (CPD) between the actual probe and the sample surface. Figure 2.10 shows a typical UPS spectrum of a Au sample.
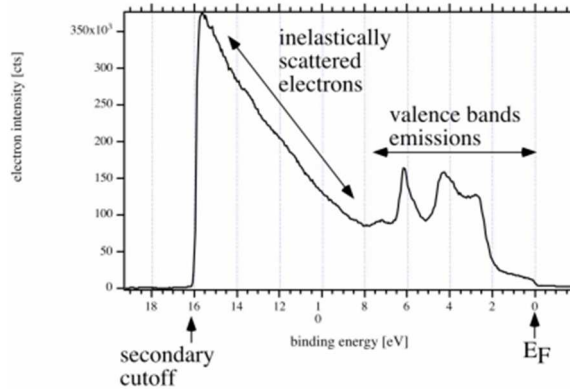
Figure 2.10 UP-spectrum of Au surface.

The spectrum consists of three features of interest: The spectrum is calibrated in a way that the Fermi level is located at 0 eV binding energy. The Fermi level (or "edge") manifests itself as a step, since it separates occupied and empty states (PES works only with occupied states, since there need to be electrons that can be photoemitted, *i.e.* states above the Fermi level do not emit electrons). Further to the left at low binding energies (0-10 eV) the valence bands structures of Au are visible. The strong peaks correspond to the d-bands of Au, which have a high density of states and are fairly narrow. Then there is the high binding energy cutoff (or "secondary edge"), where the spectrum ends. Electrons close to the edge are the slowest electrons of the spectrum (right at the edge they have a kinetic energy of zero after leaving the sample surface, *i.e.* they had barely enough energy to overcome the work function of the material). The electrons responsible for the secondary edge and the sloping up tail before the edge are inelastically scattered electrons, which were initially emitted from the valence bands states, but lost energy through scattering processes on their way to the sample surface. Since we know the binding energy of the electrons right at the secondary edge, we can determine the work function, which is just the difference between the energy of the UV photons (21.21 eV for He I radiation) and the binding energy of the secondary edge (15.9 eV in the case of Au). From Figure 2.10 it follows that the investigated Au surface has a WF of $\Phi_{Au} = 21.21$ eV – 15.9 eV=5.3 eV. In the current study, LIXPS measurements were performed prior to the XPS in a standby mode with 0.1 mA emission current. The corresponding significantly low amount of photon flux was generated and used to measure the sample work function (WF) free of charging artifacts.[116]

60

2.6.5.3. Ultraviolet Photoemission Spectroscopy

The ultraviolet photoemission spectroscopy (UPS) measurement gives useful information about the band structure and work function of a material. The main difference between UPS and XPS is that, UPS provides information about the filled valance states while XPS generate information on filled core states. Additionally, UPS uses UV He lamp. The UPS experiments in the current study were carried out with a SPECS UVS10/35 UV source by discharging highly pure helium gas (99.99%). The He I line was generated by controlling the discharging voltage in a range of 600 V to 750 V.

In the following chapters, various methods of fabricating an original bio-photoelectrochemical cell have been explained aiming at presenting methods and strategies to maximize the external quantum efficiency of such devices.

2.6.6. Atomic Force Microscopy

In some experiments, the morphology of the electrodes before and after exposure to RC solution and subsequent rinsing was studied with tapping mode AFM (Digital Instruments) in air. The Au electrode samples for the AFM experiments were prepared using e-beam evaporated gold on Si wafers. The substrates were exposed to the diluted RC solution (~0.03 μM) at 4 °C for 1 h, rinsed with buffer and DI water, and then dried under N_2 gas flow. NanoSensors SuperSharpSilicon™ probes with a typical tip radius of 2 nm, a spring force constant of 1.3 N/m, and resonant frequency of ~61 kHz were employed in the measurements.

CHAPTER 3 : THE APPLICATIONS OF DIRECTLY AND INDIRECTLY ATTACHED PHOTOSYNTHETIC COMPLEXES IN SOLAR ENERGY HARVESTING

3.1. The Role of Gold-Adsorbed Photosynthetic Reaction Centers and Redox Mediators in the Charge Transfer and Photocurrent Generation in a Bio-Photoelectrochemical Cell[2,3]

3.1.1. Abstract

Bacterial photosynthetic reaction centers (RCs) are promising materials for solar energy harvesting, due to their high quantum efficiency. A simple approach for making a photovoltaic device is to apply solubilized RCs and charge carrier mediators to the electrolyte of an electrochemical cell. However, the adsorption of analytes on the electrodes can affect the charge transfer from RCs to the electrodes. In this work, photovoltaic devices were fabricated incorporating RCs from purple bacteria, ubiquinone-10 (Q2) and cytochrome c (cyt c) (the latter two species acting as redox mediators). The adsorption of each of these three species on the gold working electrode was investigated, and the roles of adsorbed species in the photocurrent generation and the cycle of charge transfer were studied by a series of photochronoamperometric, X-ray photoelectron spectroscopy (XPS), Atomic Force Microscopy (AFM), and cyclic voltammetry (CV) tests. It was shown that both redox mediators were required for photocurrent generation; hence, the RC itself is likely unable to inject electrons into the gold electrode directly. The reverse redox reactions of mediators at the electrodes generates electrical current. Cyclic voltammograms for the RC-exposed gold electrode revealed a redox couple due to the adsorbed RC at ∼+0.5 V (*vs* NHE), which confirmed that the RC was still redox active, upon adsorption to the gold. Photochronoamperometric

---

studies also indicated that RCs absorb, and are strongly bound to the surface of the gold, retaining functionality and contributing significantly to the process of photocurrent generation. Similar experiments showed the adsorption of Q2 and cyt *c* on unmodified gold surfaces. It was indicated by the photochronoamperometric tests that the photocurrent derives from Q2-mediated charge transfer between the RCs and the gold electrode, while solubilized cyt *c* mediates charge transfer between the P-side of adsorbed RC and the Pt counter electrode. Also, the stability of the adsorbed RCs and mediators was evaluated by measuring the photocurrent response over a period of one week. It is found that ~46% of the adsorbed RCs remain active after a week in aerobic conditions. Significantly extended lifetime is expected by removing oxygen from the electrolyte and sealing the device.

3.1.2. Introduction

The reaction center (RC) protein complex in photosynthetic bacteria harvests photons and generates spatially separated positive and negative charges with a quantum yield of nearly 100%.[60,117] This property of RCs can be exploited to fabricate bio-photoelectrochemical solar cells.[57,60,117,118] One approach is to immobilize RCs on an electrode using linker molecules.[38] Trammell *et al.* have developed methods for attaching RCs to a conductive electrode with diverse orientations by using appropriate linker molecules.[44,63,65] The electrochemical properties of protein complexes attached to modified electrodes have also been extensively reported.[119-126] We have previously demonstrated a diffusion model to explain charge transport between attached RCs and a modified carbon electrode.[127] In another approach, the proteins are directly coupled to the electrode (without any linker) to improve the charge transfer by reducing the distance to the electrode. Interesting electronic properties can arise from a direct coupling between proteins and metal surfaces; several studies have investigated charge transfer in RCs directly coupled to a gold surface.[36,53,80] Our team has demonstrated the attachment of a mutant RC, with a single surface-accessible cysteine group, to a gold electrode, in which electrons can tunnel from the gold surface to the immobilized proteins.[71] Hollander *et al.* adhered *Rhodobacter Sphaeroides* RCs by incubating them onto a bare gold surface, which resulted in stable structure, showing that the gold surface functionalization is not required for the stable binding and the protein functionality.[36] The direct adsorption of protein has been shown

elsewhere to be only partially reversible because many protein segments may be simultaneously adsorbed onto a solid surface and the protein may undergo structural changes due to the adsorption.[128,129] On the other hand, there may be also electrostatic repulsion forces between the proteins and the solid surface, which oppose the adsorption process.[130] However, protein conformational changes, which can occur during the adsorption process, greatly contribute to the driving force for the adsorption.[131,132] Changes in conformation may occur immediately during adsorption or slowly over time after the protein has attached to the surface. Recently Frolov *et al.* reported the fabrication of a photoelectronic device by direct chemical binding of the photosystem I (PS I) RCs to a gold surface through surface exposed cysteines.[133]

Ciesielski *et al.* have found that a simple bio-photoelectrochemical solar cell may be constructed by a single-step injection of an electrolyte containing protein complexes (from photosystem I, (PS I)) and charge transfer mediators between a gold cathode and an ITO anode.[41] The results of chronoamperometric study indicated a multilayer assembly of PS I complexes on gold over several days.[41] The kinetics of the photocurrent production by an electrode modified with a PS I monolayer in the presence of electrochemical mediators is also reported in another work.[134]

Here, inspired by Ciesielski *et al.*'s work,[41] a bio-photoelectrochemical cell was made by injecting wild type RCs from *Rhodobacter Sphaeroides* and charge carrier mediators (Q2 and cyt *c*) into a cell with gold and Pt electrodes. This was intended as a simple method to build a bio-photoelectrochemical cell without the need for any extensive protein incubation. However, the RCs would likely attach to the gold surface due to the cysteine tags on the protein. This would form an RC layer which could be permeable to the mediators. Hence, the formation of an adsorbed layer consisting of RCs and both mediators on the gold surface is expected in such systems. The focus of the present study is to discern the role of adsorbed entities in the charge transfer and photocurrent generation processes. A series of photochronoamperometric, XPS analysis, cyclic voltammetry, and AFM tests were performed for this study.

3.1.3. Background

In purple photosynthetic bacteria, photochemical energy conversion initiates in a pigment-protein complex spanning the cytoplasmic membrane: the RC.[49] The RC of *Rhodobacter sphaeroides* is comprised

of three proteins called L, M and H. The L and M subunits ligate the pigment and other cofactors that make up the RC. The cofactors, which constitute an ET pathway, include a bacteriochlorophyll (BChl) dimer (termed as P, the primary donor), two monomer bacteriochlorophylls ($BChl_A$ and $BChl_B$), two bacteriopheophytins ($BPhe_A$ and $BPhe_B$), two quinones (Q_A and Q_B) known as electron acceptors, and one non-heme iron are symmetrically arranged in the L and M subunits.[53-55] All cofactors are non-covalently bound to the polypeptides. Figure 3.1(a) shows a RC schematic with the protein subunits and cofactors, and the approximate location of surface-exposed cysteine residues. The C156, on the H-subunit, is the most surface-exposed cysteine, and therefore holds the greatest potential for bonding to gold surfaces (see Figure 2.3 for a complete view of RC complex and all five cysteine residues).[38,65,135]

The x-ray crystallographic structures of photosynthetic RCs have contributed significantly to the understanding of the kinetics of ET, and biological ET processes in general.[57-59] Upon absorption of a photon, P is raised to an excited singlet state (P^*) followed by ET from the primary donor to the primary quinone (Q_A) along the L branch, forming the charge separated state $P^+Q_A^-$ (Figure 3.1(b)). Afterwards, the electron is transferred from Q_A to Q_B.
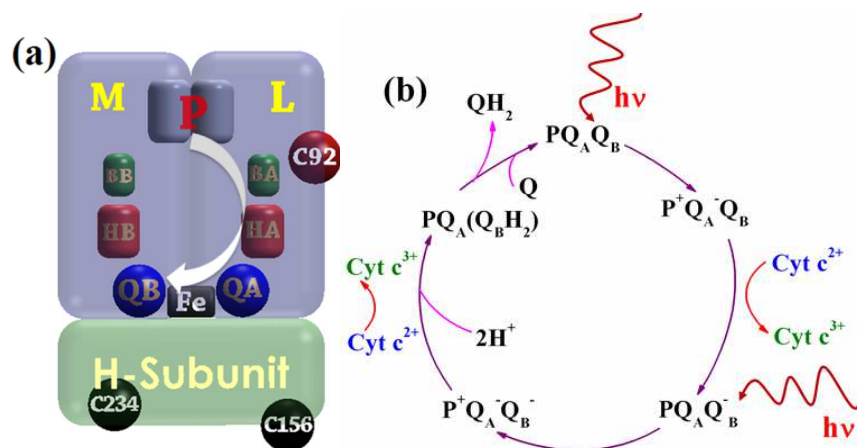
Figure 3.1 (a) Representation of the RC, protein subunits and cofactors, and approximate location of solvent-exposed cysteine groups, of which C156 is the most externally exposed. White arrow shows the ET path from P to QB. (b) Charge transfer cycle in the RC.

In vivo, cyt *c* acts as a diffusible ET mediator to reach to the P-side of RC and donate an electron to P. Therefore, oxidized cyt *c* is the mediator, carrying the positive charge. After absorption of two photons and receiving two protons, a quinol (QH_2) is produced at the Q_B site. QH_2 diffuses out from the protein and

acts as an electron carrier mediator. The photosynthetic cycle repeats after the Q_B vacancy is filled with a fresh quinone (*i.e.* Q2) (Figure 3.1(b)).

3.1.4. Results

3.1.4.1. Photochronoamperometric Study

Three bio-photoelectrochemical cells were fabricated with electrolytes containing; (i) RC, cyt c^{2+}, and Q2; (ii) RC and Q2; (iii) RC and cyt c^{2+}. The concentration of Q2, cyt c^{2+}, and RC was 60, 80, and 0.03 µM, respectively. Figure 3.2 shows the photocurrent densities for these cells measured in a three-probe configuration. The photocurrent density was negligible for electrolytes containing RCs and only one mediator (Figure 3.2(ii) & (iii)). After adding the second mediator (Q2 or cyt c^{2+}), the photocurrent significantly increased, suggesting that both the photogenerated charges are transferred from RCs to the electrodes *via* the mediators (indirect charge transfer). The photocurrent is anodic, meaning that electrons are predominantly transferred from the RC into the gold electrode *via* mediator interactions.
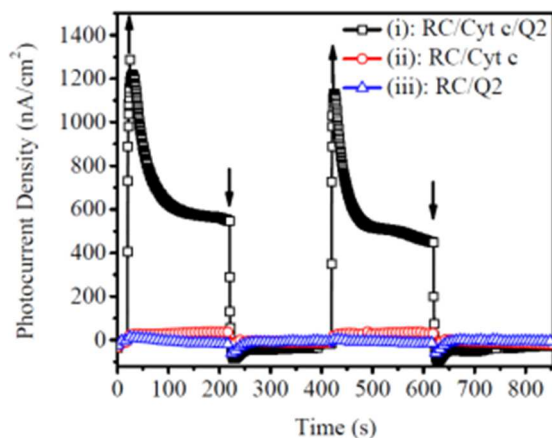
Figure 3.2 Photochronoamperometric measurements (3-probe configuration) of the bio-photoelectrochemical cells containing RC and either cyt *c*, Q2 or both mediators. The potential was set to the value of the open circuit potential in dark. In this case, the open circuit potential was ~0.195 V *vs* NHE in presence of both mediators in the system. The arrows indicate light ON (↑) and OFF (↓).

A systematic series of experiments was conducted to elucidate whether each analyte (*i.e.:* RC, Q2, and cyt *c*) adsorbed on the working electrode, as well as the role of these adsorbed species in the process of photocurrent generation and charge transfer.
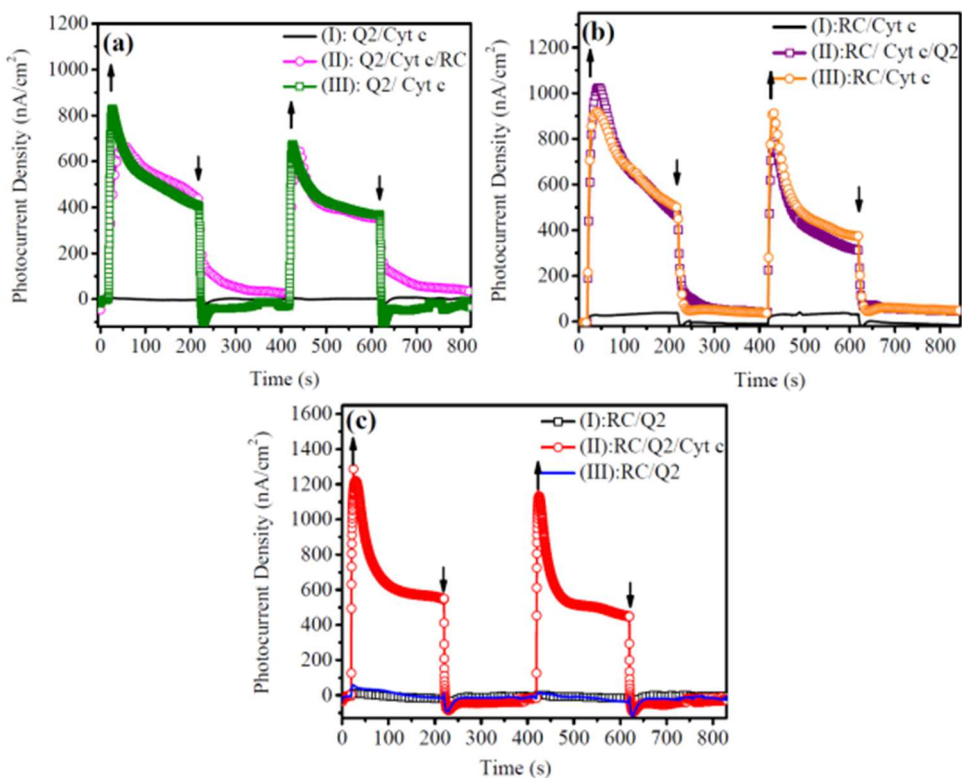
Figure 3.3 Photochronoamperometric measurements to identify the contribution of adsorbed: (a) RCs, (b) Q2, and (c) cyt *c* onto the gold electrode surface in the produced photocurrent. The insets in each figure describe the electrolyte at each step. The testing potential was the open circuit potential in dark. The arrows indicate light ON (↑) and OFF (↓).

The gold electrode was exposed to all three analytes in turn. After measuring the photocurrent, the electrodes were washed thoroughly several times with the buffer, then transferred to a cell containing fresh electrolyte lacking the analyte of interest. If an analyte is significantly adsorbed, the photocurrent likely would be preserved in an electrolyte that lacks the analyte in question. To test the attachment of RCs to the gold electrode, the photocurrent was first measured in a cell containing both Q2 and cyt c^{2+} redox mediators but no RCs. As expected, no photocurrent was observed (Figure 3.2(a), step I). In step II, the photocurrent was measured ~1 hour after RC was added to the electrolyte. By adding RC (step II), a photocurrent was produced, which increased sharply and dropped gradually to ~375 nA cm^{-2}. After step II, the electrode was removed from the cell and rinsed thoroughly several times with the buffer in a way that presumably left only the strongly bound RC attached to the gold surface.

The RCs' attachment to the gold electrode was tested by measuring their ability to generate a photocurrent. In step III, the electrode was applied in a new cell with a clean counter electrode and a fresh electrolyte lacking RC and containing both mediators. Similar photocurrents to the one in step II were obtained, indicating that a reasonably stable adsorption of RCs to the gold surface had occurred. RC protein complex is thought to adsorb *via* the C156, near the cytoplasmic surface on the H-subunit, which resulted in the stable binding between RC and the gold surface.

Furthermore, it is indicated that RCs bound to the gold surface were functionally active and significantly contributed to the photocurrent generation. Magis *et al.* have previously shown that adsorbed photosynthetic membranes onto a gold surface maintain their energy and electron transferring functionality.[80] Our results also have shown no indication of RC denaturation due to the adsorption, as in other reports demonstrating that redox proteins, deposited directly on a gold electrode, can retain full functionality.[36,133]

To test the adsorption of Q2 on the gold electrode surface and its contribution to the produced photocurrent, photochronoamperometric measurements were first carried out in a cell containing RCs and cyt c^{2+} (Figure 3.3(b), step I). Subsequently, in step II, Q2 was added to the electrolyte; after which, the electrode was rinsed and placed in a new cuvette with an electrolyte lacking Q2 (step III). Washing out unbounded Q2s and changing the electrolyte did not reduce the photocurrent, indicating that Q2 was strongly adsorbed at the electrode surface (Figure 3.3(b) steps II and III). It has also been reported that quinol (QH_2) may possibly be adsorbed on a gold surface causing a reversible electrochemical oxidation which results in the quinone.[136]

The adsorption of cyt c on the gold surface and its role in the production of photocurrent was investigated using the same approach as for RCs and Q2. The photocurrent was first measured in a cell having only Q2 (60 µM) and RC (0.03 µM). As expected, the photocurrent was negligible (Figure 3.3(c), step I). In step II, cyt c^{2+} was added to the electrolyte in a concentration of 80 µM, which resulted in an increased photocurrent (Figure 3.3(c), step II). The electrode was then removed from the cell and rinsed with the buffer before transferring to a new cuvette with fresh electrolyte lacking cyt c^{2+}. An almost zero

photocurrent in the cell lacking cyt *c* (step III) indicates cyt *c* redox mediators is needed in the bulk of an electrolyte to carry charges to the counter electrode.

For stability study, the photocurrent amplitude was measured over a period of seven days and the results are reported in Figure 3.4.
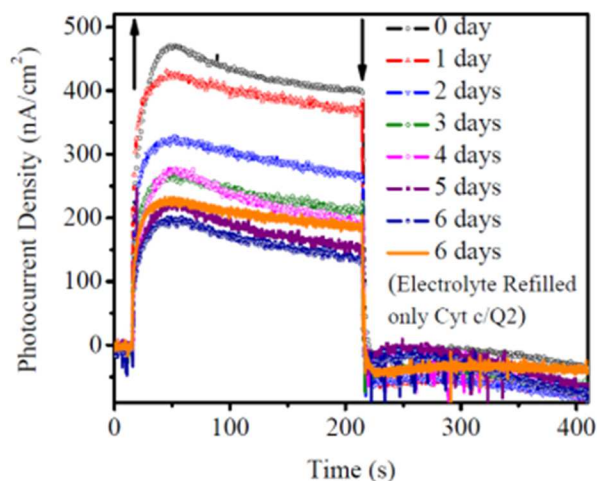
Figure 3.4 Photocurrent plots for the cell stability study: the photocurrent amplitude was measured over a period of seven days; the arrows indicate light ON (↑) and OFF (↓).

3.1.4.2. Photocurrent Spectrum of the RC Protein Complex on the Gold Electrode

To determine whether the origin of the photocurrent was indeed the RC absorption and charge carrier generation, a photocurrent spectrum was obtained across the range of wavelengths where a distinctive triplet of RC cofactor absorptions are known to occur (bacteriopheophytin at 760 nm, monomeric bacteriochlorophyl at 802 nm and the Bacteriochlorophyl "special pair" at 870 nm).[51] The 3-electrode cell, including RC and both mediators, was illuminated with monochromatic light between 650 nm and 950 nm in 6 nm steps, and the resulting photocurrents are presented in terms of incident photon to generated electron quantum efficiency. Figure 3.5 shows the complete trace for the monitored cell current continuously (5 points per second) over alternating periods of darkness (60 seconds) and illumination (60 seconds), while the wavelength was increased incrementally (6 nm steps) between illumination periods. The photocurrent at each wavelength was estimated as the average of the last ten current readings before the cessation of illumination. Quantum efficiencies were calculated from these photocurrents, taking into account the

efficiency of the monochromator (and resulting inconsistency of illumination intensities) at each wavelength.
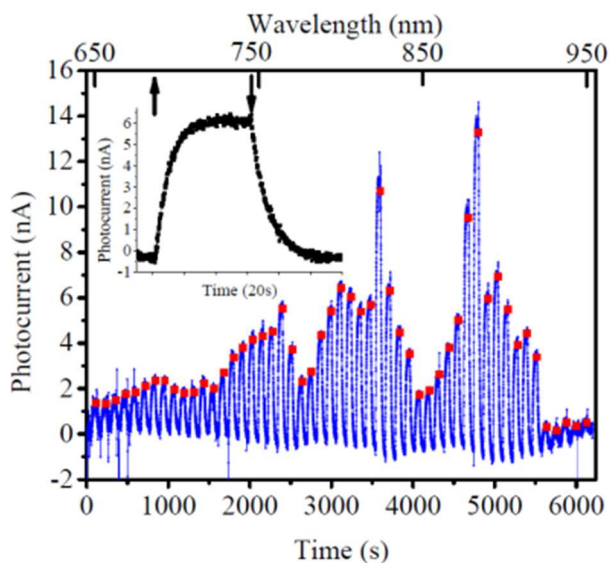
Figure 3.5 Photocurrent action spectrum obtained for the cell containing RC, cyt *c* and Q2 in the electrolyte. The continuous raw data is shown in blue, with estimated photocurrents at the end of illumination in red. An example of an individual "on/off" trace is shown in the inset, with the start and cessation of illumination indicated with arrows. The arrows indicate light ON (↑) and OFF (↓).
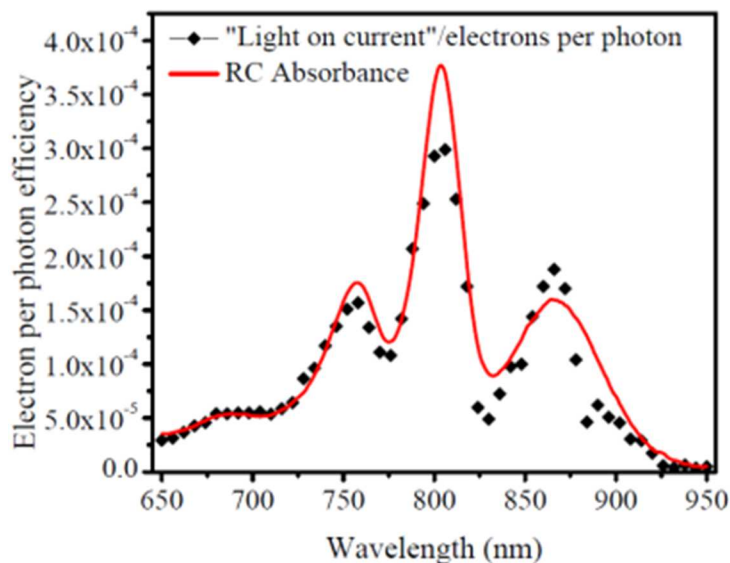
Figure 3.6 Electron per photon efficiency spectrum for the 3-electrode cell containing RC and both mediators (black symbols), compared with the absorbance spectrum of RC in 0.1 M tris buffer (red line).

A convincing match between the RC absorption spectrum and the efficiency of photocurrent generation across this wavelength range strongly supports the conclusion that the photocurrent stems from

70

the light harvesting and charge generation of the RCs (Figure 3.6). The photocurrent was only generated when the monochromator illumination was focused directly onto the gold electrode, and not just into the surrounding electrolyte. This suggests that the Au-bound RCs constitute the active material.

3.1.4.3. X-ray Photoelectron Spectroscopy

Valuable reports have indicated the usefulness of XPS in providing some robust qualitative estimation of the presence and electronic properties of biological materials on different surfaces.[115,121] Also, efforts including presenting XPS analysis have been performed by Bourg *et al.* to provide a detailed insight into the actual nature of Au-S bonding by comparison of the high resolution XPS spectra of 2D and 3D self-assembled monolayers (SAMs) and reference Au (I) complexes,[137] which can be used for explaining the bond between protein complexes and a gold surface.
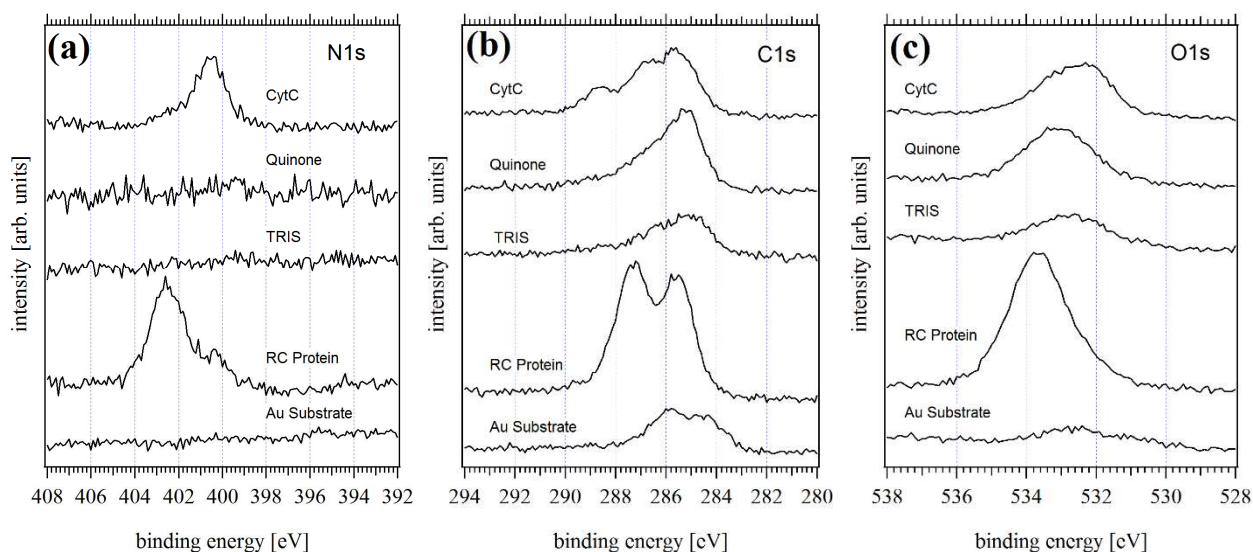
Figure 3.7 N1s (a), C1s (b), and O1s (c) core level XP spectra measured on e-beam evaporated gold before and after exposing to either RC, pure buffer, Q2 or cyt *c*, and subsequent rinsing.

Here, XPS was used to monitor the adsorption of all analytes *i.e.* RC complex protein, Q2, and cyt *c*. To further validate the strong adsorption of RCs to the gold surface, an XPS measurement of samples was performed after they were exposed to a solution of buffer and 0.03 μM RC. Figure 3.7(a-c) shows N1s, C1s, and O1s core spectra for the bare gold, electrodes exposed to only buffer, and electrodes exposed to

the RC and mediators dissolved in the buffer. The RC adsorption to the gold electrode after buffer rinsing is illustrated by Figure 3.7(a).

The N1s core level emissions from bare gold surface and buffer treated surface are similar. However, strong N1s emission peaks appear after treatment with a solution containing RC protein complex and buffer. The advent of these peaks confirms the adsorption of RC on the gold surface. The RC is a complex of several proteins and therefore contains N as a part of the polypeptide backbone and in some amino acid side chains, which is evident from the appearance of the N1s emission peak consisting of two components representing different bonding types.

The adsorption of Q2 on the gold electrode was further validated by a XPS test in which rinsed bare gold surface was exposed to a 60 μM solution of Q2. Since Q2 lacks N, the C1s and O1s core level emissions needed to be studied to verify Q2 adsorption. Figure 3.7(b) indicates that a small C1s emission peak from surface contamination can be seen on the gold substrate (one observes that by exposing gold to the environment, there will always be C and O emissions). After gold surface treatment in a buffer containing Q2, a strong C1s emission peak was observed, which can be assigned to the adsorption of Q2. The O1s peak from the Q2 treated sample consists of two components.

To validate if cyt c binds to gold surface, XPS analysis was carried out for a fresh gold electrode surface, which was exposed to a buffer solution containing cyt c^{2+} (80 μM). XPS has been shown to be a useful instrument for detection of a small heme protein (*e.g.* cyt c) due to the sensitivity of the spectroscopy method to N and C atoms.[121,138] XPS results on cyt c exposed electrodes are shown in Figure 3.6. Figure 3.7(b) shows 285.4 eV peak which likely arises primarily from aliphatic R groups of the polypeptide chain backbone of cyt c, while carbons bound to oxygen and nitrogen are responsible for the asymmetry observed on higher binding energy side.[121] It is not unexpected that proteins may adsorb on the conductive electrode surface.[122] The XPS data confirmed cyt c adsorption on the electrode surface (Figure 3.7(a)). As shown in Figure 3.7(a), adventitious nitrogen is notably absent from bare gold and buffer rinsed gold surface. After treating gold surface with solution containing cyt c, a N1s peak (~400.8 eV) is obtained from gold surface. Cyt c protein is rich in lysine amino acid residues,[139] therefore N1s signal can be assigned to the nitrogen-

containing side chains of cyt *c* such as lysine and histidine.[121] Earlier results by photochronoamperometric tests showed the adsorbed cyt *c* does not contribute to the cycle of charge transfer.

3.1.4.4. UV-Vis Spectrophotometry

To estimate the amount of RC adsorbed on the gold electrode, the absorption spectrum of the electrolyte containing RC before and after insertion of gold electrode was obtained by a UV-Vis spectrophotometer. The results are shown in Figure 3.8.
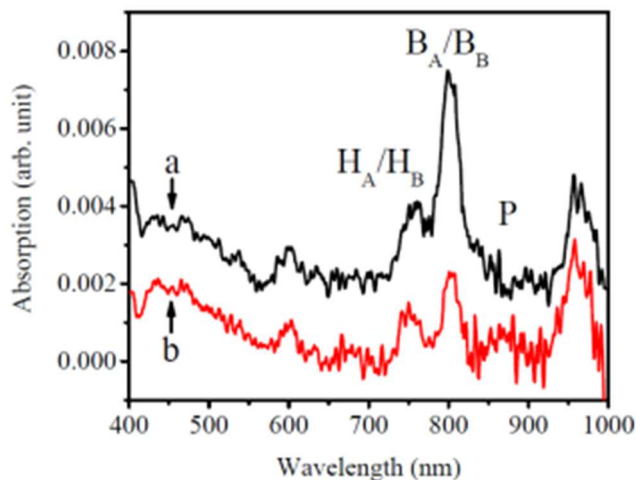
Figure 3.8 Absorption spectra of the electrolyte containing RC (a) before and (b) after insertion and removal of a gold electrode. The original concentration of RC before exposing to the gold electrode (curve a) was ~0.03 µM. The concentration dropped to ~0.0066 µM in (b).

The gold electrode was taken out from the electrochemical cell in less than 30 minutes. The concentration of RCs in the bulk of electrolyte before and after insertion and removal of the gold electrode was estimated by their absorption peak at 804 nm. Figure 3.8 clearly demonstrates that a significant amount of solubilized RC in the electrolyte were attached to the gold electrode during the aforementioned period, which resulted in a major decrease in the concentration of RCs in the bulk of electrolyte. The concentration dropped from ~0.03 µM to ~0.0066 after exposing the electrolyte to the gold surface. Hence, almost 78% of the solubilized RCs in the bulk of electrolyte were directly adhered to the gold electrode's surface.

3.1.4.5. Atomic Force Microscopy

In order to characterize the adsorbed RC, the morphology of the gold electrode surface was studied using Atomic Force Microscopy (AFM) before and after exposure to 0.03 µM RC solution. The bare gold

shows a smooth microstructure with (RMS) roughness of ~2.0 nm and no visible features, while after

exposure to the RCs and subsequent rinsing an increased roughness of ~3.4 nm is exhibited (Figure 3.9(a)).

This more distinctive surface texture most likely corresponds to the adsorbed protein on the surface of the

gold. The topographic image of the surface (Figure 3.9(b)) suggests areas of RCs aggregation as well as

particles with height of ~6-7 nm (red markers), which could relate to individual RC protein complexes. As

suggested by Trammell *et al.*, the broadening of single proteins in the AFM image may be caused by the

finite size of the apex of the cantilever.[63] In general, the apparent lateral dimensions of all AFM-imaged

proteins are overestimated when the geometry of the probe tip is comparable to the size of a protein

molecule.[140]
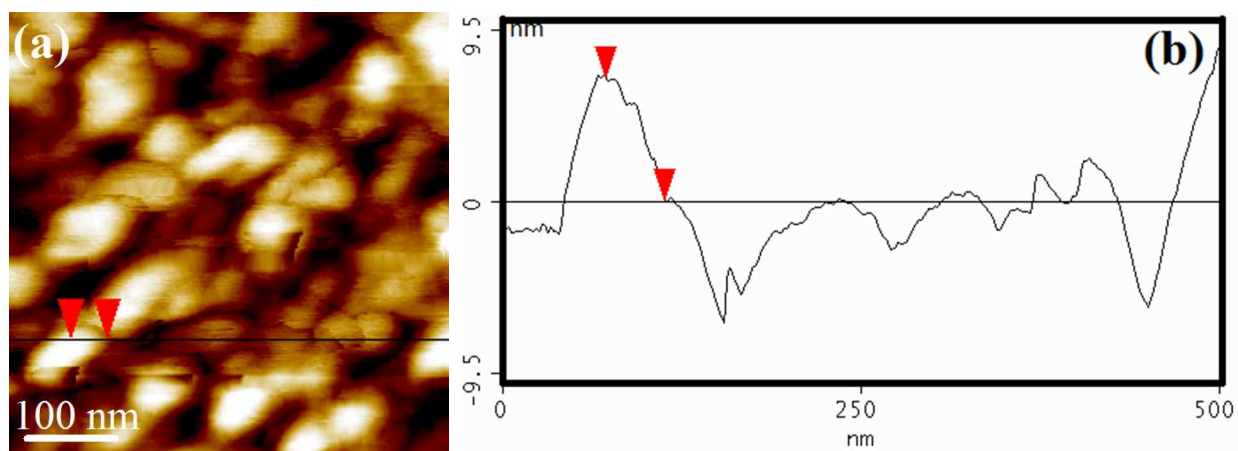
Figure 3.9 (a) An AFM topographic image of directly adsorbed RCs on a gold surface and (b) a section analysis along the black solid line in (a) showing the heights of the protein particles. The images were obtained in air using noncontact tapping mode.

The topographic image of a surface formed with 0.03 µM diluted RC after an hour demonstrates

particles with lower height (~4.7 nm), which is lower than one might expect for a RC protein complex

(Figure 3.10). This might be due to protein flattening (denaturing due to the absence of water) on the

electrode as it already was suggested by Trammell *et al.* as one of the possible reasons for observing proteins

with lower thicknesses on a gold surface.[63]
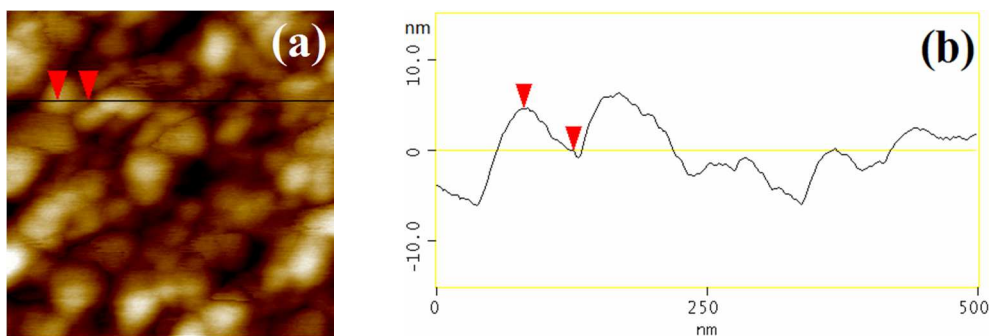
Figure 3.10 (a) An AFM topographic image of directly adsorbed RCs on a gold surface (after rinsing and drying under N2 stream) and a RC protein particle after one hour exposure to aerobic conditions and (b) a section analysis along the black solid line in (a) showing the heights (~4.7 nm) of the flattened/denatured protein particles. The images were obtained in air using noncontact tapping mode.

Similar studies were recently performed by Mukherjee *et al.* on the morphology of PS I from aqueous buffer suspensions onto alkanethiolate SAM/Au substrates, which showed the formation of complex columnar structures rather than a uniform monolayer formation due to solution phase protein aggregations.[126,141] In our studies, additional AFM tests were also performed with higher concentration of RC (~0.8 µM and ~14.5 µM) to show the effect of RC concentration on surface morphology and roughness. The results are shown in supplementary Figure 3.11.
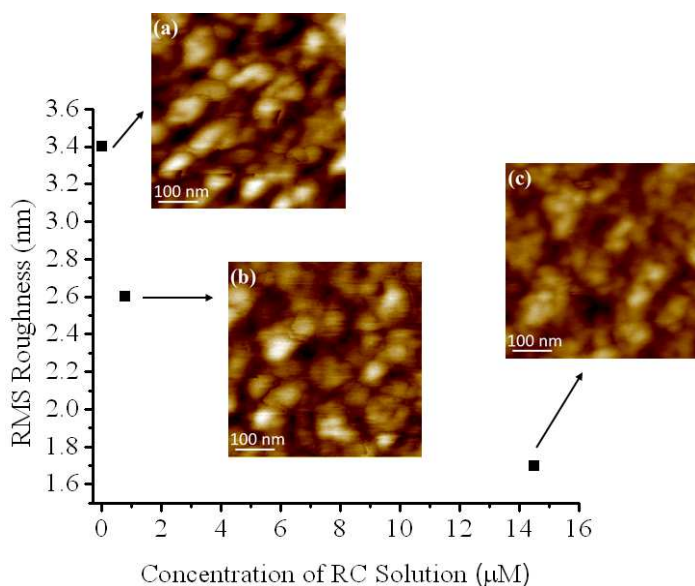
Figure 3.11 Changes in RMS roughness of the adsorbed RC film on the gold as a result of increasing the concentration of RC solution, a) 0.03 µM RC stock, b) 0.8 µM RC stock, and c) 14.5 µM RC stock. RCs were incubated on a cleaned gold surface at 4 ºC for 1 hour and subsequently rinsed with DI water and dried under N2 stream. The images were obtained in air using noncontact tapping mode.

As Figure 3.11 demonstrates by increasing the concentration of RC solution from 0.03 μM to 0.8 μM and finally to 14.5 μM the RMS roughness of the adsorbed RC film would be decreased from 3.4 nm to ~2.6 nm and ~1.7 nm, respectively. This can be explained with respect to the 3D images shown in Figure 3.12. As it can be seen, at lower concentrations there are noticeable gaps between the adsorbed proteins aggregates on the surface; however, one notes that by increasing the RC concentration these gaps can be filled with extra RC particles, which results in development of a smoother adsorbed layer.
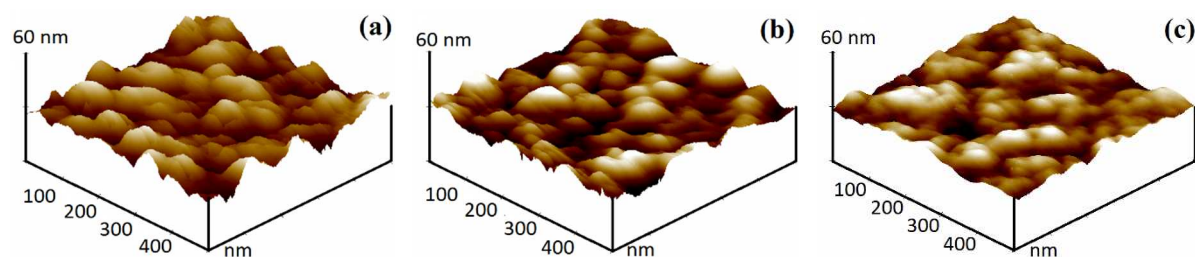
Figure 3.12 3D AFM topographic images of the adsorbed RC film on a gold surface from: (a) 0.03 μM RC stock, (b) 0.8 μM RC stock, and (c) 14.5 μM RC stock. RCs were incubated on a cleaned gold surface at 4 oC for 1 hour and subsequently rinsed with DI water and dried under N_2 stream. The images were obtained in air using noncontact tapping mode.

3.1.4.6. Stability

The arrival of the RC protein complex at the gold electrode surface could be driven by diffusion,[142] and the adsorption likely occurs through a cysteine residue on the protein. For device applications, the stability of the adsorbed RCs is crucial. Naturally, RCs may desorb or denaturize with time. Baszkin and Norde have suggested different techniques to study protein adsorption/desorption phenomena as well as structural changes.[143] In our work, photocurrent amplitude and UV-Vis spectroscopy of the electrolyte were applied for studying the bound protein stability. The stability of the fabricated bio-photoelectrochemical cells can be evaluated by measuring the photocurrent in the cells over a period of time. Ciesielski *et al.* employed a similar method to study the stability of bio-photoelectrochemical cells.[41]
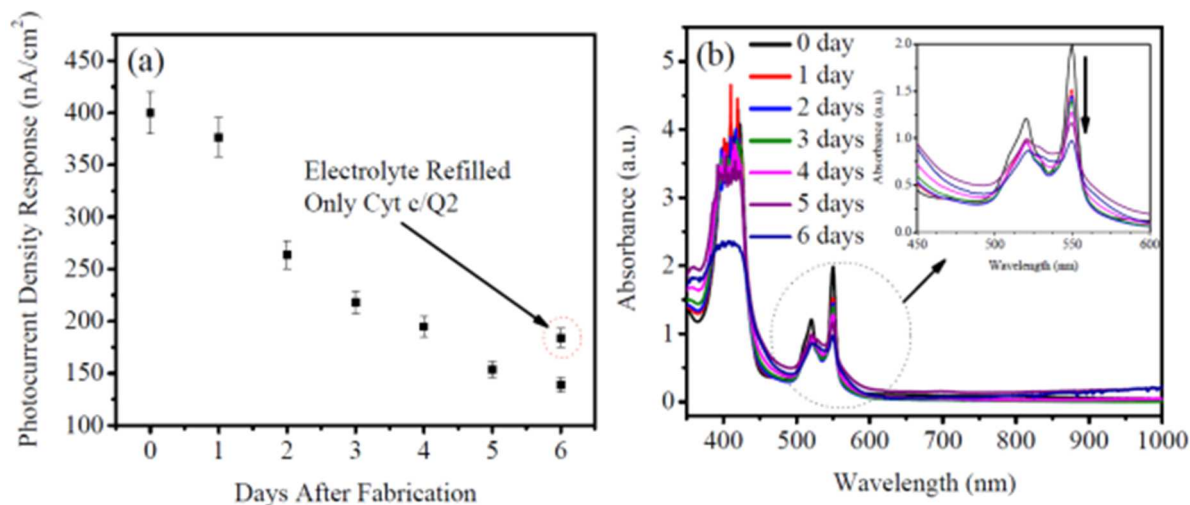
Figure 3.13 Bio-photoelectrochemical cell stability. a) Photocurrent density response over a period of seven days. Peak photocurrent production occurred on the fabrication day, after which it decreased, due to the adsorbed RCs denaturation as well as redox mediators' degradation/adsorption. In this particular study the cell was refilled with a new electrolyte after seven days. b) Absorption spectra of the electrolyte over a period of seven days; the inset shows cyt c degradation/adsorption during this time. The black arrow in the inset shows the decreasing trend of a cyt c absorption peak (550 nm) from a maximum (0 day) to minimum (after 6 days).

In our work the photocurrent response was monitored for one week, during which time the cell was stored at 4-6 °C in aerobic conditions. The possibility of release of RCs from the gold electrode's surface was investigated by UV-Vis absorption spectroscopy of the electrolyte, as was the denaturation/adsorption of redox mediators.

For the stability study, a bio-photoelectrochemical cell was fabricated with an electrolyte containing RC, cyt c^{2+}, and Q2 with the aforementioned concentrations. The gold electrode was kept in the fabricated cell at room temperature for almost an hour. During this period, RC protein complexes assembled at the gold surface. The electrode then was removed from the cell, rinsed several times with the buffer, and finally was applied in a new cell with a clean reference and counter electrode, a fresh electrolyte lacking RC, and containing both mediators. A photocurrent density of ~398 nA cm^{-2} was measured. The electrode was removed and the absorption spectrum of the electrolyte was measured to monitor the potential amount of RCs released from the gold electrode's surface. The measurements were repeated over a period of seven days and the results are reported in Figure 3.13.

As shown in Figure 3.13(a), the photocurrent density decreased from ~398 nAcm^{-2} to ~139 nA cm^{-2} over the period of a week. In our system three different reasons might be considered for the reduction in photocurrent response over time: 1) release of RCs from the gold electrode's surface; 2) structural/conformational changes of the adsorbed RC protein complex on the gold surface; 3) denaturation/adsorption of the redox mediators. The absorption spectra of the electrolyte imply the existence of a strong bond between the adsorbed RCs and the gold's surface because the major absorption peak of native RCs (804 nm) was not observed (Figure 3.13(b)).
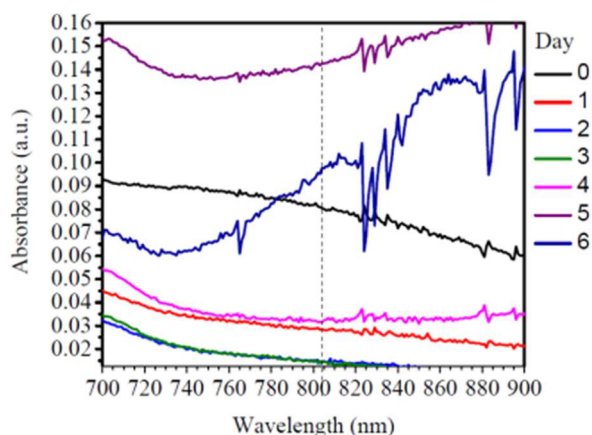
Figure 3.14 Absorption spectra of the electrolyte for the detail around 804 nm to demonstrate that no absorption peak of the native RCs (804 nm) in the electrolyte was observed. This implies the existence of a strong bond between the adsorbed RCs and the gold's surface.

Figure 3.14 shows the detail of the plots around 804 nm. The bond strength between adsorbed RCs and the surface of the gold was tested by monitoring the absorption peak of native RCs (804 nm) in the electrolyte. The absorption spectra of the electrolyte imply the existence of a strong bond between the adsorbed RCs and the gold's surface since no absorption peak of native RCs (804 nm) in the electrolyte was observed. The detail of the plots around 804 nm is presented below.

Therefore, the decrease in photocurrent over time may be attributed to the denaturation of some of the RCs and/or degradation/adsorption of the redox mediators, particularly cyt *c*. Since cyt *c* is required in the bulk of electrolyte, either adsorption or degradation of cyt *c* also would affect the photocurrent. To evaluate the effect of mediators' degradation/adsorption, the cell was refilled with a fresh electrolyte containing only cyt *c* and Q2 on the 7th day after the fabrication. The photocurrent density response

increased to ~184 nA (~46% of the initial value), which indicated that the decrease in photocurrent over time was partially due to redox mediators' (cyt *c*) denaturation and/or adsorption. Also, the change in the peak at 550 nm in the absorption spectrum (Figure 3.13(b)), which corresponds to the concentration of cyt *c*, is consistent with the degradation or adsorption of the mediator. However, the photocurrent production did not return to its initial value after refilling the cell with the fresh electrolyte containing only redox mediators, which shows that the denaturation of a number of RCs adsorbed on the gold's surface is likely due to conformational/structural changes. Comparison of the photocurrents suggested that ~46% of the RCs remained active after a week in aerobic conditions. As shown by Ciesielski *et al.*, the device lifetime should be extended significantly by removing oxygen from the cell (anaerobic condition) and sealing.[41]

3.1.4.7. Estimation of the Midpoint Potential of ET Cofactors at the RC-Gold Electrode in the Dark

Due to the direct interaction of the mediators with the gold electrode, the midpoint potential values of redox mediators (Q2 and cyt *c*) and redox active parts of the RC protein complexes were assessed by CV. CV data were recorded for various combinations of cofactors with and without adsorbed RC in dark conditions. Similar CV tests were performed under illumination to show the effect of light on the electrochemical potential values. Figure 3.15 depicts voltammograms for 60 µM Q2 in the electrolyte at a freshly cleaned bare gold electrode and at a gold electrode with directly adsorbed RC. The CV for the RC-adsorbed electrode without Q2 in solution is also shown for comparison.[63] The CV data for Q2 in Figure 3.15 indicates that the midpoint potential of Q2 at pH 8 is ~0.042 V vs NHE at the bare gold. The results are consistent with values reported by other groups.[65,136,144] As shown previously, cyclic voltammograms for Q2 at the RC-adsorbed gold electrode illustrate anodic and cathodic currents. Also, the adsorbed RCs considerably block the background current between Q2 and electrode, which suggest the RCs have adsorbed to the gold electrode.[63]
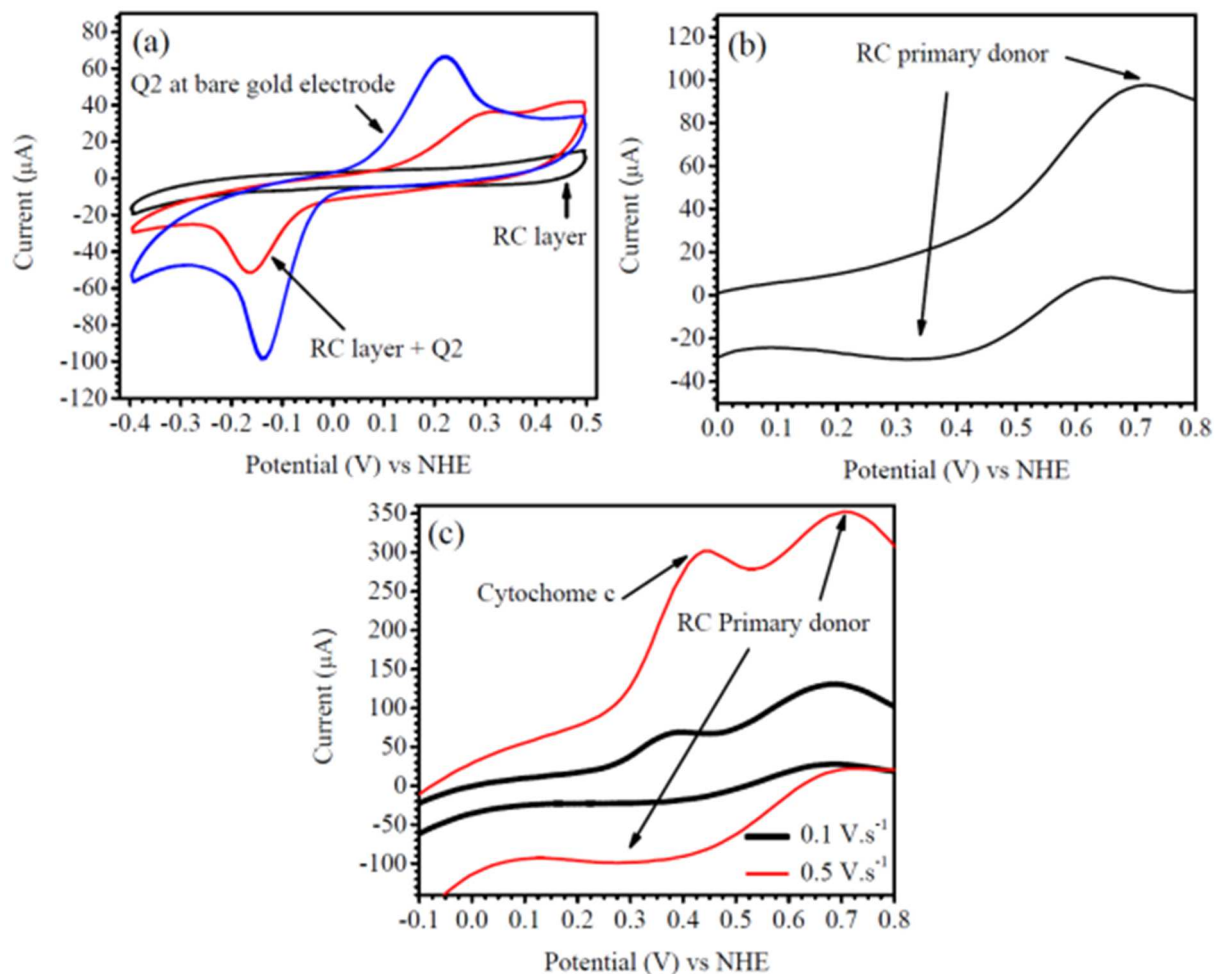
Figure 3.15 CVs of (a) 60 μM Q2 in solution measure with a clean bare gold electrode (blue trace) or gold electrode with adsorbed RC (red trace). CVs of gold electrode with adsorbed RC protein complex but without Q2 (black trace). (b) CV of a RC-modified electrode, and (c) CV of the RC-modified electrode (after addition of 80 μM cyt c to the electrolyte) with different scan rates; 0.1 V s^{-1} (bold black line) and 0.5 V s^{-1} (narrow red line).

As we show in Figure 3.15(a), the adsorbed RC is electroinactive in this range. Cyclic voltammograms over a more oxidizing voltage region for the RC-exposed gold electrode revealed a redox couple due to the adsorbed RC. Figure 3.15(b) demonstrates a redox couple at ~+0.5 V (*vs* NHE), which is similar to that reported by Trammell *et al.*[63] This confirms that the RC is still redox active, upon directly coupling to the gold. We note that the CV tests were performed after RC incubation and keeping the electrochemical cell in dark for half an hour. Figure 3.1(c) depicts voltammograms for a RC-adsorbed gold electrode after addition of 80 μM cyt c to the electrolyte, with 0.1 V s^{-1} and 0.5 V s^{-1} scan rates. As shown in Figure 3.15(c), upon cyt c addition to the electrolyte, a new peak was introduced, which we assign to cyt

c (Figure 3.16 CVs of RC-adsorbed electrode without and with cyt *c* in solution side by side). The results are consistent with previous reports by Trammell *et al.*[63] The voltammogram indicates that cyt *c* is electroactive at the RC-modified electrode. The CV of cyt *c* at bare gold surface indicates midpoint potential of ~+0.2 V (data not shown).[63] Millo *et al.* reported 0.244 V midpoint potential for cyt *c* immobilized on smooth gold surfaces chemically modified with 11-mercaptounodecanoic acid.[145] Arrows in Figure 3.15(c) show the redox couple of the primary donor and cyt *c*. The slight shift in the RC primary donor peak position after cyt *c* addition is attributed to the formation of the super-molecular complex between RC and cyt *c*.[63] The peak cathodic current of RC primary donor in Figure 3.15(c) was decreased significantly after keeping the cell in dark for 9 hours (following text).

Figure 3.16 shows the recorded CV data for various combinations of Q2 with and without adsorbed RC in light and dark conditions. CV measurements in light were performed to show the effect of cell illumination on the electrochemical potential values. Figure 3.16(a-c) depicts voltammograms for 60 μM Q2 in the electrolyte at a freshly cleaned bare gold electrode and at gold electrode with directly adsorbed RC in the dark and in light. As it is indicated Q2 is electroavtive with midpoint potential of 0.042 V *vs* NHE in the dark and RC is electroinactive without Q2. Hence, as it is indicated below, illumination of the cell influences the reduction and oxidation potential values of Q2 at bare gold and Q2 at RC-adsorbed gold. However, there is no noticeable difference between the RC's voltammograms in dark and light as it was shown to be electroinactive without Q2. Upon addition of cyt *c* to the cell including only RC and the gold electrode, new peak will be introduced, which can be assigned to cyt *c*. Figure 3.17(a) shows a clear difference between CVs of RC-adsorbed electrode without and with cyt *c* in solution. The results are consistent with previous reports by Trammell *et al.*[63] As shown below, the peak cathodic current of RCs' primary donor was decreased after keeping the cell in dark for 9 hours in aerobic conditions.
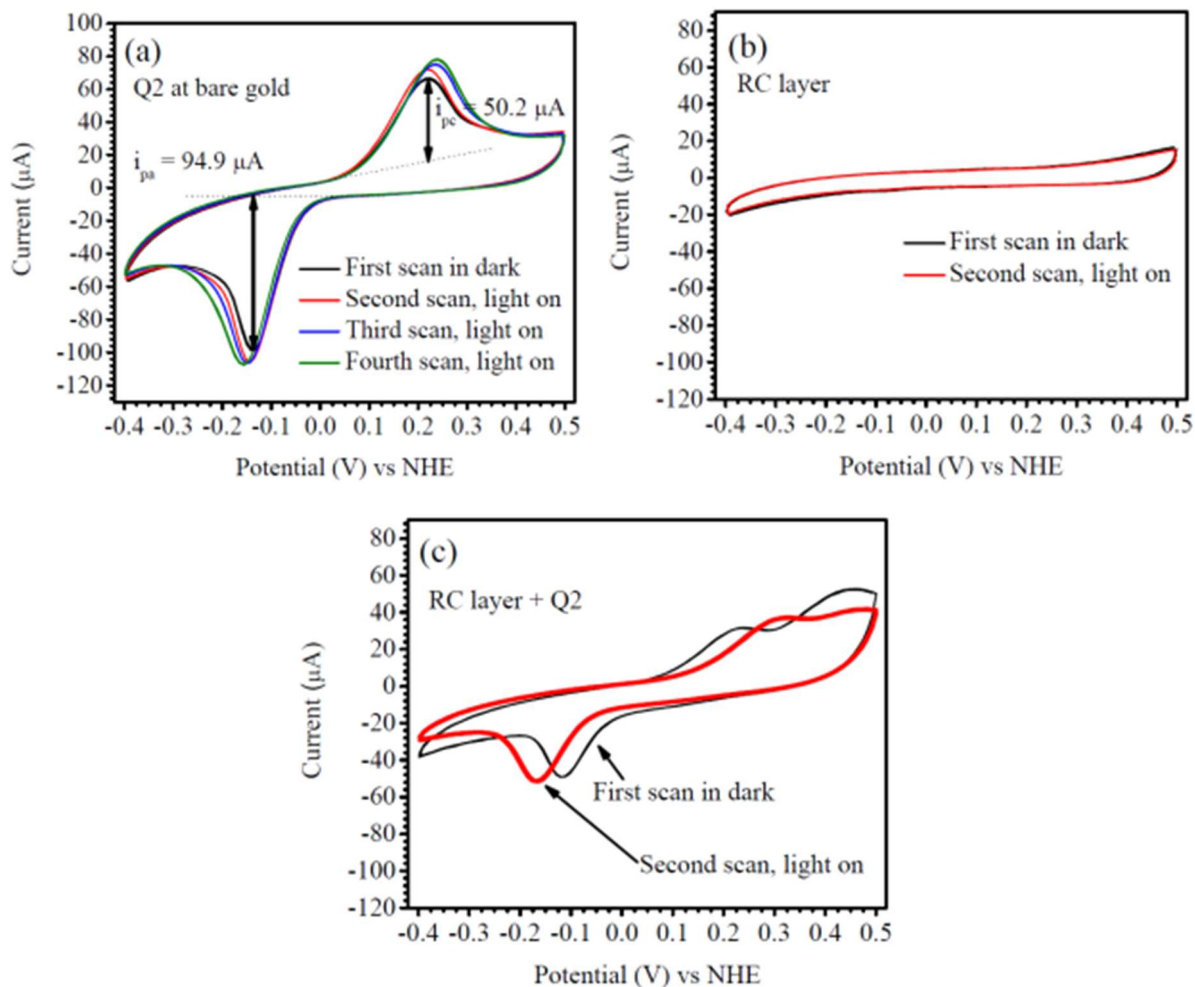
Figure 3.16 The influence of cell illumination on successive cyclic voltammograms at 10 mV s^{-1} for: (a) Q2 at bare gold, (b) adsorbed *Rb. sphaeroides* RC pH 8 buffer, and (c) Q2 at adsorbed-RC gold electrode.
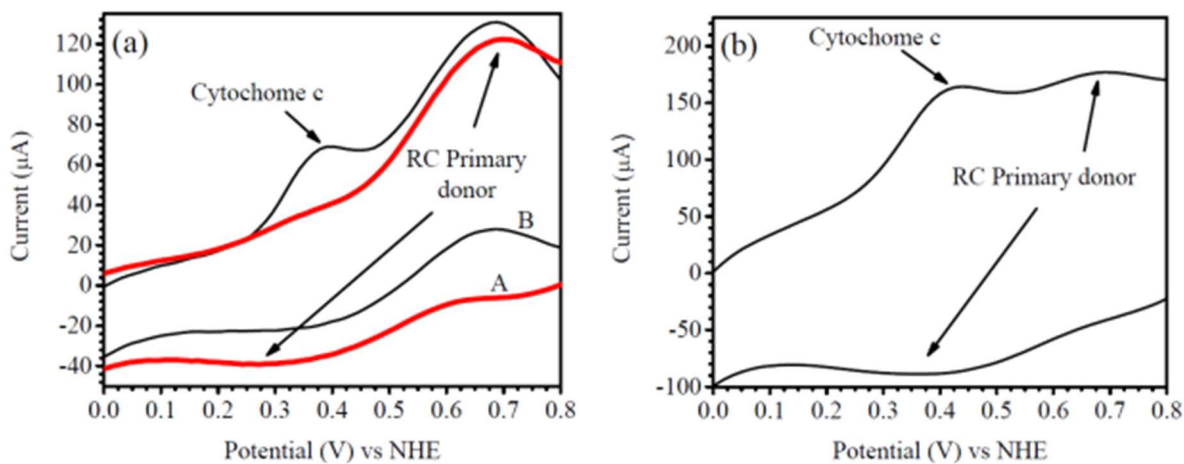
Figure 3.17 CVs of RC-adsorbed electrode (A) without cyt *c* and (B) with cyt *c* in solution (scan rate: 0.1 V s^{-1}) and (b) decrease in the peak cathodic current of RCs' primary donor after keeping the cell in dark for 9 hours.

3.1.5. Discussion

The UV-Vis spectrophotometry study (Figure 3.8) showed that about 78% of the RCs in the electrolyte adsorb on the gold surface. Also, the results from both XPS (Figure 3.7) and AFM (Figure 3.9) studies indicate that the adsorbed RC layer is fairly stable with a strong adhesion to the gold. Due to the presence of the cysteine C156 on the surface of the H-subunit, it is likely that RCs would be attached to the gold electrode from the H-subunit side (see Figure 3.18) with a preferential orientation.[38,135] The rest of the RCs (~22%) would be adsorbed at the counter electrode (Pt) and be free floated in the electrolyte. However, the small differences between the amount of photocurrents in steps II and III of Figure 3.3(a) indicates that the contribution of the RCs in the electrolyte and adsorbed on the counter electrode in generating photocurrent at the gold electrode (working electrode) is negligible.

Despite the adsorption of RCs on the gold electrode, the measurements in Figure 3.2 suggest that the photogenerated charges in the RCs are not able to transfer to the electrode directly. Hence, both types of mediators are required for the photocurrent generation. As explained, cyt c^{3+} and QH_2 act as the positive and negative charge transfer mediators, respectively (see Figure 3.1(b)). In an electrochemical cell containing two mediators in the electrolyte, the photocurrent would be the superposition of anodic ($QH_2 \rightarrow Q+2e^-+2H^+$) and cathodic (cyt $c^{3+}+e^- \rightarrow$ cyt c^{2+}) reactions at the electrode surfaces.[127,146] Since in this work the current polarity convention was set in a fashion that defined anodic current as positive; the observed anodic currents imply domination of ET from the RCs to the gold electrode *via* QH_2/Q reaction. The shape of the photocurrent with a rapid increase and gradual drop suggests concurrency of both anodic and cathodic reactions again with domination of anodic reaction from the conversion of QH_2 to Q. Similar shapes of the photocurrent also were observed in another work when using two electrochemical mediators.[89] The kinetics of the reactions in a different bio-photoelectrochemical cell with one mobile mediator has been studied by Ciesielski *et al*.[41,134] However, studying the kinetics in a system with more than one redox reaction is complicated and may require additional experiments to measure the reaction rates separately. Furthermore, previous studies indicated that the anodic current in the cell may be limited by the diffusion of QH_2 but not the kinetics of the redox reaction.[127] Therefore, before analyzing the thermodynamics of the

system, an appropriate model for the reactions in the device must be developed, which is not in the scope of this work. Nevertheless, the net anodic current in all the photochronoamperometric measurements indicates the domination of QH_2/Q reaction at the gold electrode.

The XPS results indicate the capability of gold to adsorb Q2. Also, the results in Figure 3.3(b) suggest that the charge transfer is mediated mainly by the quinone adjacent to the electrode, while the contribution of dissolved Q2 in the ET between the attached RCs and gold is negligible. This implies that Q2s shuttle back and forth between the RCs and the electrode (Figure 3.18).[36,127]

Although XPS results show that cyt *c* can be adsorbed on gold, the photocurrent measurements in Figure 3.3(c) indicate that only dissolved cyt *c* contributes to the photocurrent cycling toward counter electrode. A solubilized redox mediator (*i.e.* cyt *c*) is required in the electrolyte to complete the charge transfer pathway. As long as there is ample cyt *c* in the solution, current cycling is enabled *via* cyt *c* in the bulk of electrolyte toward the Pt counter electrode. In this system, solubilized cyt *c* interacts with the P-side of the RC protein complex, taking the positive charges and diffusing toward the Pt electrode surface to be reduced again. Therefore, the adsorbed cyt *c* on the gold electrode surface does not contribute to the current cycling. However, adsorbed cyt *c* can significantly contribute to the photocurrent cycling when modified RCs are attached to the gold surface from the P-side as it was shown by Lebedev *et al.*[69] In that case, the use of chemical coupling agents may possibly allow for a covalent attachment of metalloproteins to electrode surfaces, which can be of prime importance in the construction of biosensors,[147] optoelectronic devices,[148] and other applications.[27,149,150] Figure 3.18 shows a summary of the discussion in the form of a cartoon of ET events between RCs, electrochemical mediators, and the electrodes surface. It should be stated that since both mediators are required to sustain the photocurrent, the electrode can interact with both mediators to donate and accept electrons, which is inefficient for photocurrent generation. However, we expect significant improvements will be made by employing semiconducting electrode materials with suitable energy levels for selective charge transfer.[35]
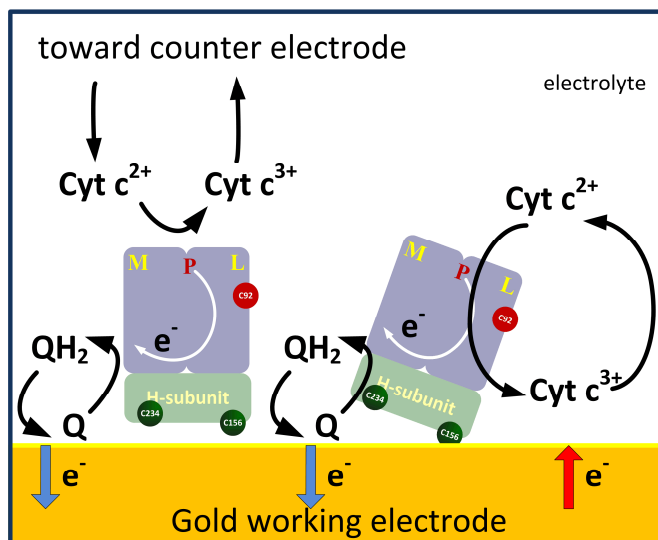
Figure 3.18 The ET events between RCs, electrochemical mediators, and the gold electrode. RCs are most likely attached to the gold surface through C156 cysteine. The path of ET inside RCs is shown by with arrows. The observed anodic photocurrent is generated by dominated electron carrier mediators (QH$_2$/Q) which shuttle back and forth between the RCs and the gold electrode. The positive charge at the P-site is transferred to the counter electrode by cyt c in the bulk of the electrolyte. Interaction of cyt c with the gold electrode limits the photocurrent.

A detailed study of the structure and electrochemical properties of such protein based photovoltaic devices when using wide band gap semiconductors to increase the photocurrent is underway in our group and will be reported in forthcoming papers.

3.1.6. Conclusion

A bio-photoelectrochemical cell has been constructed by injection of RCs suspension, Q2, and cyt c between gold and Pt electrodes. Here, we described formation of an adsorbed layer containing RCs and both mediators on the surface of the gold electrode. Cysteine C156 on the surface of H-subunit facilitated the expected preferential orientation of RCs on the gold surface. Photochronoamperometric results suggested Q2-mediated charge transfer on gold electrodes from RCs toward gold, while current cycling is enabled *via* solubilized cyt c in the bulk of the electrolyte toward the Pt counter electrode. In the absence of either one of the mediators (Q2 or cyt c^{2+}), the photocurrent was almost zero. Hence, it appears that indirect charge transfer dominates in these experimental bio-photoelectrochemical cells. The attachment of RCs and mediators to the gold surface was strong enough and was further approved by XPS, AFM, and stability analysis. The stability of the adsorbed RCs and mediators was evaluated by measuring the

85

photocurrent response produced by the same cell over a period of time. Monitoring the stability of the photocurrent showed that ~46% of the adsorbed RCs remained active after a week in aerobic conditions. Further stability may be achieved by applying anaerobic conditions and sealing the device. The RC-adsorbed gold electrode revealed a redox couple due to adsorbed RC at ~+0.5 V (*vs* NHE), which confirms that the RC does not change its redox properties upon directly coupling to the gold. The voltammogram indicated that both Q2 and cyt *c* were electroactive at the RC-modified electrode. AFM micrographs of the adsorbed RC film, formed from a 0.03 µM RC solution, reveals the presence of large particles, which resulted from RCs aggregation on the gold surface as well as RC particles with height of ~6-7 nm, which is the known dimension of a *Rb. sphaeroides* protein.

3.2. Free-floating Reaction Centers (RCs) *vs* Attached Monolayer of RCs in Bio-photoelectrochemical Cells

3.2.1. Abstract

The high quantum efficiency (~100%) in the bacterial photosynthetic reaction center (RC) has inspired research on the application of RCs to build protein based solar cells. Conventionally, applying RCs as the photosensitive layer on the surface of a carbon electrode has shown poor photocurrents in the cells. The low photocurrent is partly due to the weak absorption of light in the monolayer of RCs. Also, an Atomic Force Microscopy image of the electrode shows lots of defects on the immobilized RCs at the electrode surface. In this work, we have built a bio-photoelectrochemical cell in which the RCs are floating in the electrolyte instead of being attached to the surface of an electrode. Despite the simple structure of the cell, the photocurrent is significantly higher in the new cell compared to when RCs are attached to an electrode. The amplitude of current reached to ~40 nA for free floating RCs, about five times larger than that in the cell with attached RCs. The aging effect was studied in both cells in a course of a week. The lifetime of attached RCs on electrode surface was slightly better than solubilized RCs in the electrolyte. Also, it is found that the mechanism which governs the charge transfer from RCs to the electrodes is the same in both bio-photoelectrochemical cells.

3.2.2. Introduction

Photosynthetic reaction centers (RCs) are capable of producing separated positive and negative charges by absorbing photons.[60] This property of RCs can be exploited to fabricate solar cells.[44,63,65,69,72] Employing RCs in a bio-photoelectrochemical cell to harvest solar energy, the charges must be transferred to the electrodes either directly or through charge carrier mediators.[127] Two approaches dominate the techniques to fabricate cells; (I) using an electrode with immobilized RCs by linker molecules,[44,63,65,71] and (II) using solubilized RCs in the electrolyte with mediators.[89] In the first approach, RCs are immobilized on the electrode surface with a specific orientation to have a short distance between negative (or positive) charge in the RC and the electrode for direct charge transfer. The opposite charge in the RC is transferred to the counter electrode through a mediator, as shown in Figure 3.19(a). In the second approach, RCs are directly deployed in the electrolyte and both negative and positive charges are carried through the mediators. Figure 3.19(b) shows quinone (Q) as a diffusible mediator which takes the negative charge from a RC protein and diffuses to both working and counter electrode surfaces, while the positive charge is transferred *via* cytochrome *c* (cyt *c*). The schematics of both structures and charge transfer mechanism are shown in Figure 3.19. In this work, we have compared the structure and photocurrent of a bio-photoelectrochemical cell with immobilized RCs with those in a cell with solubilized RCs.
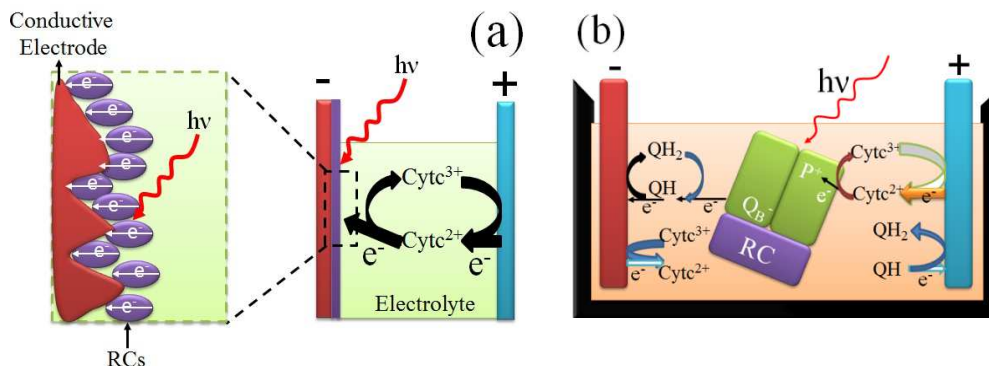
Figure 3.19 Schematics of a bio-photoelectrochemical cell based on (a) immobilized RCs on a surface of a conductive electrode and (b) solubilized RCs in an electrolyte.

The photosynthetic RC is a protein complex which converts the energy of absorbed photons to electrochemical energy. The main components of the RC protein are L, M and H subunits. Cofactors are

the parts of RC protein where the energy conversion takes place and include a closely interacting dimer P

(P/P*) of bacteriochlorophyll (BChl) molecules, two BChl monomers (B_A, B_B), two bacteriopheophytins

(H_A, H_B) and two quinones (Q_A and Q_B). Between the Qs, there is an iron atom which stabilizes the complex.

All these elements are bound together by transmembrane helices that introduce some asymmetry into the

structure (see Figure 3.20(a)).
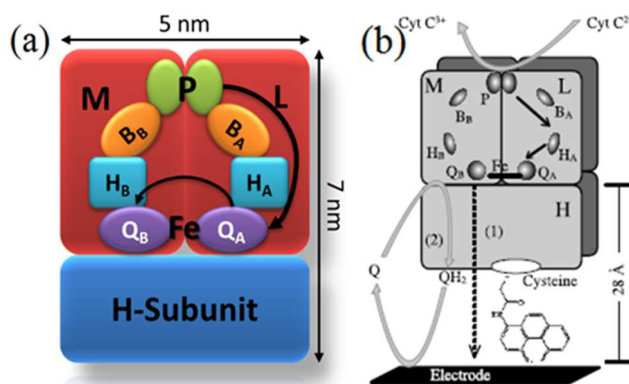
Figure 3.20 (a) Schematic of a photosynthetic RC protein, which indicated M, L, H subunits, and cofactors. Arrows inside the RC protein show the ET path from dimer P to QA and to QB (the size of RC proteins was estimated by crystallographic analysis elsewhere[170]) and (b) schematic of an immobilized RC from H-subunit on HOPG surface by pyrene linker molecules (used with permissions from Ref. 90).

ET within RC starts from the special-pair (dimer P), which acts as the primary electron donor. ET

proceeds *via* B_A to H_A, subsequently to the primary quinone (Q_A), and finally to the secondary quinone (Q_B)

(Figure 3.20(a)). Hence, the RC molecule act as a dipole structure with the negative charge (e⁻) at Q_B and

positive charge at P. Charge transfer mediators can take the positive and negative charges and diffuse to the

electrodes surface. This ET is in the base of the photosynthetic processes in the bacteria.

Valuable efforts have been performed so far to enhance the device photocurrent by RCs

immobilization on different electrodes' surface with specific orientation. Correspondingly construction of

oriented and aligned monolayers of RCs protein on gold electrodes was tried by forming self-assembled

monolayers (SAMs) of linkers on the electrode surface.[44,63,65] An appropriately functionalized SAM of

linker molecules can serve to orient the RC at the electrode surface to achieve high photocurrents.[44] Binding

RCs from the primary donor (P) or the opposite site side (H-subunit), to the carbon electrodes was tried by

using bi-functional linkers and genetically engineered proteins.[65,71] Figure 3.20(b) shows schematics of an immobilized RC protein from H-subunit on the surface of a HOPG electrode, by using pyrene linker.

Lebedev *et al.* has also found that the efficiency of the bio-photoelectrochemical devices can be improved by encapsulating RC proteins inside Carbon nanotube arrayed electrodes.[72] It also has been shown that using cyt *c* as a conductive wiring between immobilized RC protein and an electrode surface, ET is significantly improved.[69] Yet the overall photocurrent in a bio-photoelectrochemical cell is low, when a monolayer of RCs is immobilized from H-subunit on the surface of a carbon electrode, which is partly due to the weak absorption of light in the monolayer of RCs and poor quality of the RC layer. In addition linkers are insulating materials between RCs and the electrode, which affect the rate of the charge transfer to the electrode.[36] Unlike conventional immobilization of proteins on the electrode surface, direct RCs utilization in the electrolyte of the bio-photoelectrochemical cell offers a substantial simplification in fabrication.[41] Also, the choice of the electrode would not be limited to the availability of a linker in a photoelectrochemical cell with solubilized RCs.

In contrast to numerous efforts on protein immobilization, there are only a few reports on direct application of proteins in the electrolyte of a cell.[36,41,89] The reason might be due to concern about proteins denaturation by direct contact with a surface of an unmodified electrode.[117,151] However, the recent results indicate good stability of the RCs in the absence of the insulating layer on the electrodes.[36,89] In this work, the photocurrent response and the lifetime of a bio-photoelectrochemical cell with immobilized RCs from H-subunit on a carbon electrode has been compared with another cell with solubilized RCs in the electrolyte. The scope of this work is limited to RCs immobilized from the H-subunit side (Figure 3.20(b)) and comparing the photocurrents.

3.2.3. Discussion

Two different bio-photoelectrochemical cells were fabricated; in one cell the proteins were immobilized on the HOPG surface from H-subunit (Figure 3.20(b)) by employing SAM of N-(1-pyrene) as linkers on the surface, while in the other one RC proteins were dissolved in the electrolyte (0.03 μM). The electrodes surface area (16.3 mm^2), the counter electrode, and the concentration of analytes were similar in

both cells. In both approaches initially the same amount of RCs was used. For the cell with solubilized RCs, the concentration of floating RCs in the electrolyte after adding the buffer was reduced to ~0.03 µM. In both cases, the photocurrent experiments first were performed in an electrolyte containing 0.1 M Tris buffer (HCl, pH 8.0) and RCs while, mediators were added subsequently one by one. The final concentration of mediators was similar in both cells; 60 µM and 80 µM for Q and cyt c^{2+}, respectively. We studied the differences in photocurrent and aging between the two described cells. Figure 3.21 shows the photocurrent *vs* time for both cells in periods of 200 s in the dark and in the light. In presence of RCs, the photocurrents in both cells were negligible for electrolytes without any mediator. By adding only one mediator the current slightly increased. However, significant improvement in the photocurrent was only observed when both mediators (cyt *c* and Q) were present, suggesting indirect charge transfer between RCs and electrodes *via* mediators.[89,127] In principle if tunneling was effective, only one mediator (cyt *c*) would be enough for the cell with immobilized RCs. The results suggest that despite immobilized RCs in one of the cells the mechanism of charge transfer in both cells is dominated by indirect charge transfer *via* mediators. Therefore, there is no advantage for immobilized RCs from H-subunit over free-floated RCs in terms of charge transfer mechanism.

Interestingly, the cell containing dissolved proteins in the electrolyte (Figure 3.21(b)) showed almost five times higher photocurrent than the cell with immobilized RCs (Figure 3.21(a)). Considering the same mechanism of charge transfer in both cells, the photocurrent difference is likely due to the amounts of RCs in each cell. Although the initial amounts of RCs were the same, a part of the applied RCs was washed away during preparation of the electrode for the immobilized approach. Although the intention of immobilizing RCs was to enhance direct charge transfer, further study showed a poor quality of multilayer proteins on the HOPG.
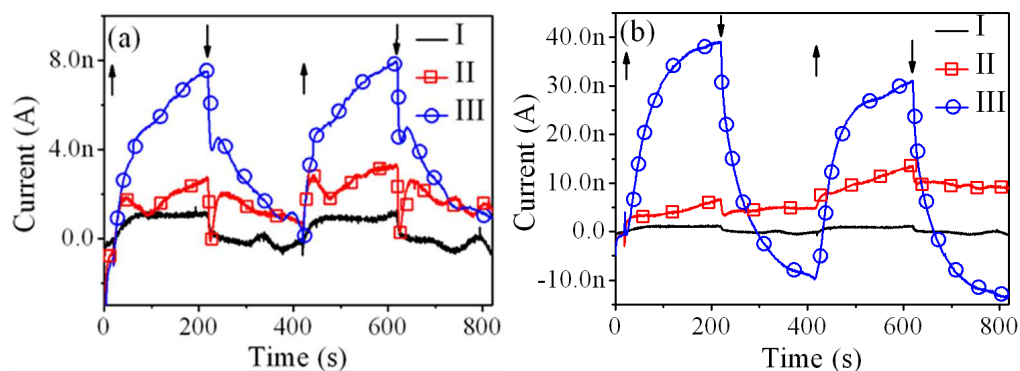
Figure 3.21 The measured photocurrents for: (a) proteins immobilized on the HOPG surface and (b) solubilized proteins. The electrolyte in each step had: (I) no mediator, (II) only cyt *c*, and (III) both cyt *c* and Q. The arrows indicate light ON (↑) and OFF (↓).

Atomic force microscopy (AFM) was used to study the surface image of the immobilized RCs on the HOPG surface. The key element for successfully mapping out the surface topography of a protein layer is the tip which touches the sample surface. The force constant of the employed AFM probe spans the gap between contact and non-contact mode and is tailored for the force modulation mode. AFM micrographs for the bare HOPG electrode and immobilized RCs on the HOPG electrode (3 μm × 3 μm), obtained in tapping mode. The HOPG electrode exhibited a smooth surface, while the immobilized RCs on the HOPG showed a granular morphology. As Figure 3.22(a) demonstrates, immobilizing RCs on the electrode surface increased the roughness of the surface. The root mean square (rms) roughness for immobilized RCs on the surface was about 120-140 nm, which was extremely higher than ~1 nm obtained for the HOPG. Apparently, the RCs on the electrode were formed a multilayer structure. Further surface study by two-dimensional section analysis (Figure 3.22(b)) showed protein-protein association which formed protein (RCs) clusters.[118] The vertical distance between the lowest point and highest point of the image, estimated by section analysis (Figure 3.22(b)), was ~498 nm. Additionally, AFM image of the electrode showed lots of defects on the RC layer at the surface of the electrode.
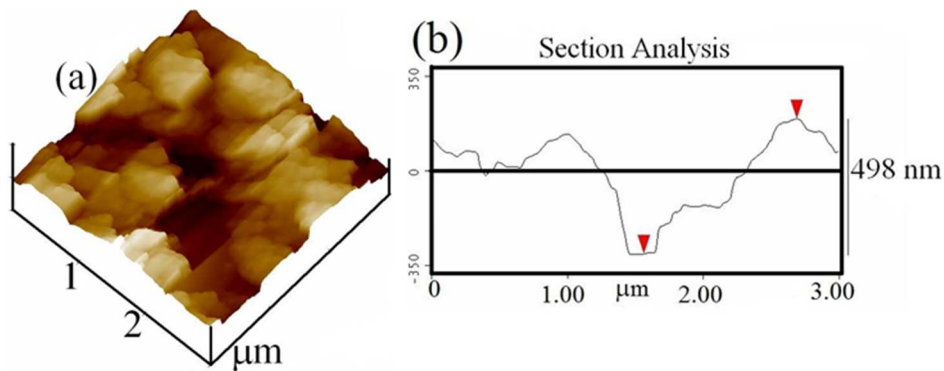
Figure 3.22 (a) Surface morphology of immobilized RCs on the HOPG surface and (b) section analysis showing the vertical distance between the lowest point and highest point of the image.

The photoelectrochemical results indicated that the charge transfer mechanism in immobilized approach was through the mediators similar to the cell with solubilized RCs. Furthermore, AFM morphology of the immobilized RCs from H-subunit on the HOPG electrode, showed a poor quality of a multilayer structure. Considering the efforts required for protein immobilization, it seems that deploying RCs directly in the electrolyte would be a more practical approach. However, a concern about the cell with solubilized RCs is the aging effect. Previous results show that proteins denature more quickly when they are adsorbed to unmodified HOPG electrodes.[117] We have studied the aging effect in both cells in a course of a week. The results in Figure 3.23 shows 50% of the reduction in the photocurrent in the cell with immobilized RCs whereas; the photocurrent reduction was about 61% in the other cell. Although the reduction in the photocurrent was larger for the cell with solubilized RC, the amount of the photocurrent after a week was still larger than the one in the cell with immobilized RC.
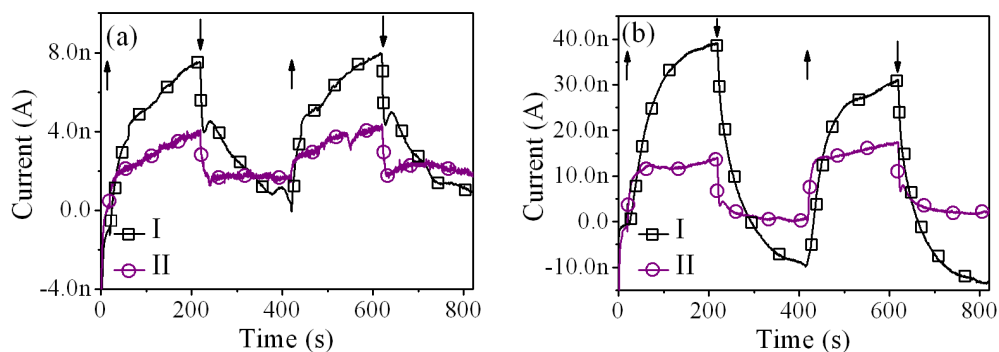
Figure 3.23 The study of aging effect for the bio-photoelectrochemical cells with: (a) immobilized proteins and (b) solubilized RCs. The results from (I) fresh cells and (II) one week after fabrication are demonstrated. The arrows indicate light ON (↑) and OFF (↓).

3.2.4. Conclusions

We studied the 3-probe photocurrent behavior in two bio-photoelectrochemical cells; in one of them, the proteins were immobilized on the surface of a HOPG electrode from H-subunit side by using linker molecules, while in the other, RC proteins were dissolved in the electrolyte. The concentration of mediators and the surface area of electrodes were similar. Obtained results showed solubilized RCs can generate significantly higher photocurrents up to five times larger. AFM study of the surface indicated that a multilayer structure of RCs with poor quality was formed when the proteins were immobilized. Lots of defects were observed in the AFM image of immobilized RCs on the surface which could be one of the potential drawbacks of the immobilization approach along with tedious procedure of RCs incubation on the surface. Additionally, employing linker molecules to immobilize proteins on the surface did not provide any advantages in terms of direct charge transfer from immobilized RCs from H-subunit to the electrode. However, the lifetime of RCs was slightly better in the immobilized approach.

CHAPTER 4 : HYBRID WIRING OF THE RHODOBACTER SPHAEROIDES REACTION CENTER FOR APPLICATIONS IN BIO-PHOTOELECTROCHEMICAL CELL[4]

4.1. Abstract

The growing demand for non-fossil fuel-based energy production has drawn attention to the utilization of natural proteins such as photosynthetic reaction center (RC) protein complexes to harvest solar energy. The current study reports on an immobilization method to bind the wild type *Rhodobacter sphaeroides* RC from the primary donor side onto a Au electrode using an immobilized cytochrome *c* (cyt *c*) protein *via* a docking mechanism. The new structure has been assembled on a Au electrode by layer-by-layer deposition of a carboxylic acid-terminated alkanethiol (HOOC (CH$_2$)$_5$S) self-assembled monolayer (SAM), and layers of cyt *c* and RC. The Au|SAM|cyt *c*|RC working electrode was applied in a three probe electrochemical cell where a peak cathodic photocurrent density of 0.5 μA cm^{-2} was achieved. Further electrochemical study of the Au|SAM|cyt *c*|RC structure demonstrated ~70% RC surface coverage. To understand the limitations in the ET through the linker structure, a detailed energy study of the SAM and cyt *c* was performed using photochronoamperometry, ellipsometry, photoemission spectroscopy, and cyclic voltammetry (CV). Using a simple rectangle energy barrier model, it was found that the electrode work function and the large barrier of the SAM are accountable for the low conductance in the devised linker structure.

4.2. Introduction

The increasing demand for the production of energy without a direct link to combustion of a fossil fuel and the accompanying production of CO$_2$ has brought attention to the deployment of biomolecules for fabrication of bio-photoelectrochemical cells. The bio-photoelectrochemical cell uses technologies that

---

[4] Chapter 4 was published in Journal of Physical Chemistry C (Yaghoubi, H.; Li, Z.; Jun, D.; Lafalce, E.; Jiang, X.; Schlaf, R.; Beatty, J. T.; Takshi, A. The Journal of Physical Chemistry C 2014, 118, 23509.). Permission is included in Appendix A.

exploit biomimetic means of energy conversion by utilizing plant-derived photosystems.[30,31] Different types of protein complexes may be employed to fabricate a bio-photoelectrochemical cell, including reaction centers (RCs) from the *Rhodobacter sphaeroides* bacterium, plant photosystems, and bacteriorhodopsin proteins.[32-34,36-48] Several studies of the *R. sphaeroides* RC have shown promise for the utilization of this RC in bio-photoelectrochemical cells.[32,33,43-45,60,61,63,64] The RC is a transmembrane protein which has nearly 100% quantum yield of primary charge separation--*i.e.*, the formation of charged primary donor (P^+) and final acceptor (Q_B^-)--and an efficient stabilization of separated charges.[24,152,153] Most RC-integrated photoelectrochemical cells fabricated to date have been comprised of a cell with isolated RCs or RCs surrounded with a light harvesting (LH) pigment-protein antenna attached to a working electrode, immersed in an electrolyte with one or more redox mediators.[32,33,35,43,45,61-64] The use of RC-LH pigment-protein by several groups has shown improved photocurrent densities over those obtained with the RC alone.[36,62,80] Although the RC's internal quantum efficiency is very high and the use of LH ring around the RC was shown to enhance the photon absorption,[32,36] the charge transfer between RCs and electrodes is another feature that influences biomolecule-based solar energy conversion.

The RC of *Rhodobacter Sphaeroides* is comprised of three protein subunits called L, M, and H (Figure 4.1(c)). Typically, bio-photoelectrochemical cells have been fabricated using RCs immobilized from either the H-side or the P-side on the surface of one of the cell's electrode.[32,33,44,45,61-65] Upon illumination, a photocurrent can be generated by transferring one of the charges (positive or negative) from the RC to the electrode. The opposite charges are moved to the counter electrode *via* a redox mediator in the electrolyte. The ET rate between the RC and the electrode is higher when RCs are oriented on the electrode's surface from the P-side due to a shorter distance between the RC P^+ site and the electrode.[65] However, the charge transfer at the RC-electrode interface in this orientation is complicated by a bowl on the P-side that introduces a gap between the electrode and the protein (Figure 4.1(c)). A previous work showed a higher photocurrent can be achieved if the bowl of at least some of the RCs may be filled by diffusion of cytochrome *c* (cyt *c*) into the space between a 7-His-tagged (at the C terminus of the RC M protein) RC and a nitrillotriacetic acid (NTA) terminated self-assembled monolayer (SAM) on a Au

electrode.[69] While the work of Lebedev *et al.* pointed to the importance of the bowl problem, the approach relies on the random diffusion of cyt *c* proteins rather than constructing the structure.[69]

The current study is focused on employing a hybrid oligomer-protein linker for immobilizing the wild type RC from the P-side onto an Au electrode and at the same time filling the bowl which resulted in higher peak photocurrent density compared to that in the previous work.[69] This structure was assembled through a layer-by-layer deposition of a SAM with carboxylic acid terminal groups,[111] cyt *c*, and RC proteins. Because the feasibility of immobilizing cyt *c* onto a Au electrode using 6-mercaptohexanoic acid had been demonstrated before,[111,121] we utilized the same molecule to construct the hybrid SAM|cyt *c* linker for RCs (Figure 4.1(a)). The goal was to obtain RC immobilization which occurs *via* the docking interaction between RC and cyt *c*. It was assumed that this mechanism could bring the cyt *c* heme and the RC P cofactor into proximity for an efficient ET. The results presented in this work show that the new structure binds the RC without any need for protein mutation. Additionally, the observed photocurrent density evidenced successful docking between cyt *c* and RC. Furthermore, the energy structure of the hybrid linker was studied in detail and a quantum model was proposed to estimate the electrical conductance along the linker. A schematic of the new structure and the ET events between the RC, cyt *c*, and the SAM-modified Au electrode are illustrated in Figure 4.1(a), with a representation of RC–cyt *c* interaction given in Figure 4.1(b). Additionally, Figure 4.1(c) shows a schematic of the RC protein subunits and the ET pathway through the cofactors. A bowl in the RC is indicated, based on the RC–cyt *c* co-complex crystal structure.[56]
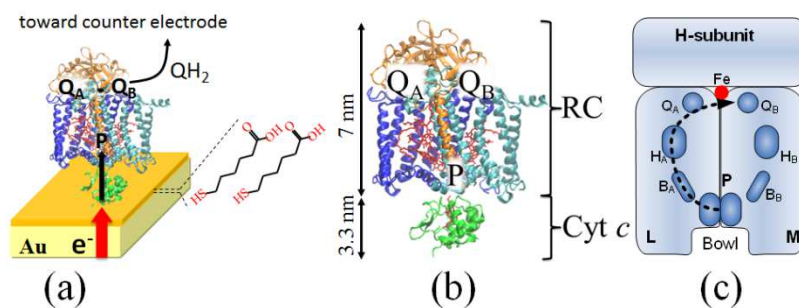
Figure 4.1 (a) ET pathway between the 6-mercaptohexanoic acid-modified Au electrode, cyt c, and the RC in the Au|SAM|cyt *c*|RC structure. The photon-generated electrons acquired at QB are transferred to the counter electrode via diffusion of QH₂ (mediator). (b) The RC–cyt *c* co-complex. The RC subunits are represented as ribbons and colored light blue (L), dark blue (M), and brown (H). Green ribbons show cyt *c*. (c) RC subunit proteins and cofactors. The dashed arrow shows the ET path from P to Q$_B$.

4.3. Electrode Preparation

The Au|SAM|cyt c|RC electrode was fabricated by treating a cleaned Au electrode in a 10 mM 6-mercaptohexanoic acid over five days at room temperature, rinsing the electrode in 0.1 M Tris–HCl (pH 8) buffer, followed by immersing in a 0.8 mM cyt c solution for a day at 4 °C, rinsing with buffer, and immersing in a 1.0 μM solution of RCs at 4 °C for a day. Weakly-bound RCs were removed from the electrode by rinsing the electrode with buffer. The alkanethiol self-assembly was performed as suggested by Love et $al.$[154]

4.4. Results

4.4.1. Photochronoamperometry Analysis

The photocurrent density of the Au|SAM|cyt c|RC structure was measured in both three and two electrode setups with only one diffusible redox mediator (Q) in the electrolyte. As shown in Figure 4.2(a), in a three electrode experiment a cathodic photocurrent was achieved upon illumination. Immobilizing RCs using hybrid SAM|cyt c linker, resulted in peak current density of up to 0.5 µA cm^{-2}, which is at least three times of that using random diffusion of cyt c proteins in a previous work.[69] The photocurrent density stabilized at -185 nA cm^{-2} after 400 s while the working electrode was held at the dark open circuit potential (OCP) of +0.05 V vs Normal Hydrogen Electrode (NHE). There was an initial spike of photocurrent at the onset of illumination similar to what has been observed in a recent work.[62] It was reasoned that this initial spike was originated from a kinetic limitation at the RC's primary acceptor side (Q_B) due to the different rates of P$^+$ reduction and Q_B^- oxidation which results in buildup of negative charges within the protein.[62] Accordingly, the over-oxidation of the redox mediator equilibrates the charge accumulation inside RC.[62]

To confirm the contribution of the protein complexes to the photocurrent generation, control experiments were performed on a cell containing a Au|SAM|cyt c working electrode and Q as the charge carrier, but without any RC protein component. The negligible photocurrent density in the Au|SAM|cyt c structure (black line in Figure 4.2(a)) demonstrates that the photocurrent stems from the charge generation in the RC. The cathodic photocurrent in the Au|SAM|cyt c|RC structure implies ET from the Au electrode to the RC, which likely suggests the protein orientation with the primary donor (P-side) facing the electrode.

Hence, the majority of cyt c molecules likely bound to the P-side of the RC protein complex. Adding more cyt c to the electrolyte did not enhance the photocurrent, which supports the interpretation that the majority of the RCs were docked onto SAM-bound cyt c proteins.
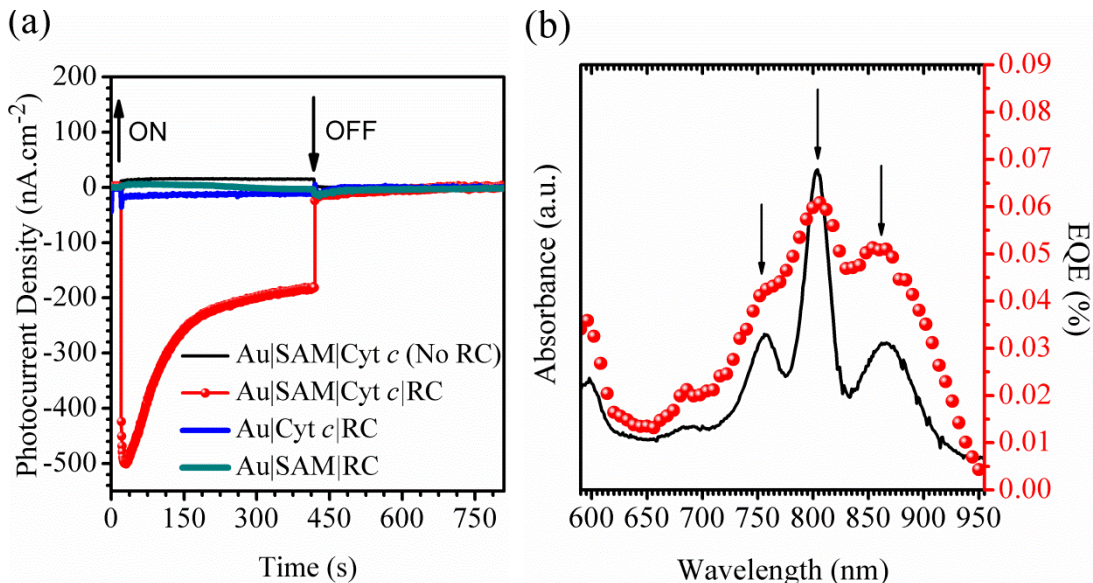
Figure 4.2 (a) Time dependence photo-response of a fabricated bio-photoelectrochemical cell under 80 mW cm^{-2} illumination with coenzyme Q as the single diffusible redox mediator. In the graph the arrows indicate light ON (↑) and OFF (↓), with the current obtained from the configurations shown as nA cm^{-2} according to the key. (b) External quantum efficiency (EQE) of the photocurrent, per incident photon, generated on the Au|SAM|cyt c|RC electrode (red dots), compared to the absorption spectrum of the RC (bold black line).
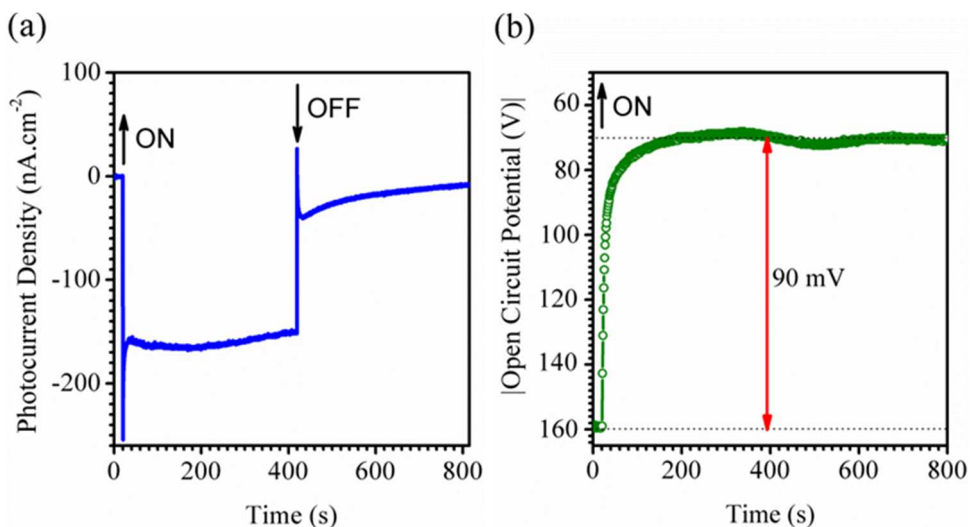
Figure 4.3 (a) Two-electrode photocurrent measurements of the fabricated bio-photoelectrochemical cell. In the graph the arrows indicate light ON (↑) and OFF (↓). (b) Two-electrode OCP measurements of the fabricated bio- photoelectrochemical cell.

The photochronoamperometry study of the two electrode setup resulted in a short circuit steady-state photocurrent density (J_{SC}) of -156 nA cm^{-2} and a steady-state open circuit voltage (V_{OC}) of ~90 mV under continuous illumination (Figure 4.3). As shown in the following text, the energy barrier at the SAM is one of the limiting factors for an efficient charge transfer and energy conversion. However, the very low photocurrent (15 nA cm^{-2}) from an electrode without any SAM (Au|cyt c|RC in Figure 4.2(a)) shows the importance of the linker molecule in a successful use of the incubated cyt c for the RC immobilization. The low photocurrent may be due to variable orientation of cyt c upon adsorption on Au and/or cyt c conformational changes, protein unfolding, and even denaturation on this bare metal electrode as it has been shown in several studies.[155-157]

To further verify that the observed photocurrent in the Au|SAM|cyt c|RC cell stems from the photon absorption and charge generation by RCs, a photocurrent action spectrum was obtained across 590 nm to 950 nm and the EQE was estimated, as well. Figure 4.2(b) shows a substantial match between the RC absorption spectrum and the efficiency of photocurrent generation across this wavelength range. The distinctive triplets of RC cofactor absorptions are clearly present in the EQE spectrum.

The stability of the Au|SAM|cyt c|RC structure was studied further by measuring the photocurrent density of a single cell over a course of five days. As shown in Figure 4.4, the magnitude of the photocurrent density dropped from 185 nA cm^{-2} for a fresh electrode to 102 nA cm^{-2} after four days of storage in aerobic condition. The result suggests that the rate of reduction in the photocurrent density is faster in the first couple of days. This could be due to the degradation of fraction RC complexes, as was shown in an earlier study by Ciesielski et $al.$ for PSI-based photoelectrochemical cells.[41] Extended device lifetime by appropriate sealing and oxygen removal can be achieved as it has been shown earlier.[41] Additionally, these results show that despite the lack of a covalent bond between RC and cyt c, the protein-protein interaction is strong enough to hold more than half of the RCs after four days, in aerobic conditions, while the protein complexes kept their integrity and functionality.
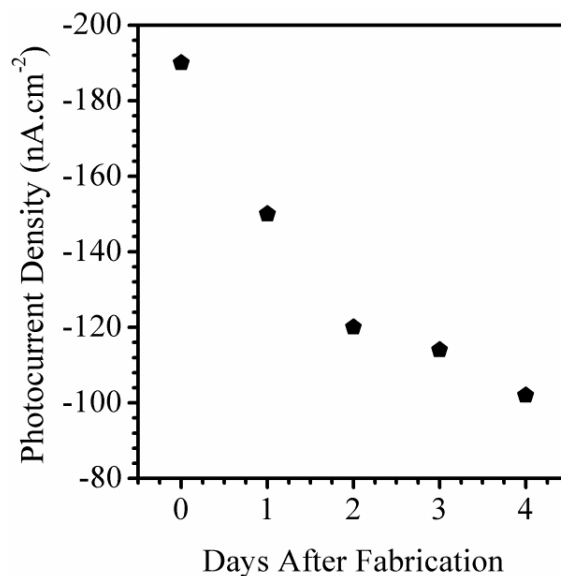
Figure 4.4 The change in the steady-state photocurrent density of a cell, measured over a course of five days (one test each day).

Since the thickness and the energy levels of the SAM and the cyt *c* layer affect the ET rate through the hybrid linker, further studies were carried out to characterize each layer. The thickness of the layers was measured using the ellipsometry technique. The energy levels of the SAM were studied using the photoemission spectroscopy and the UV-Vis absorption methods. Additionally, cyclic voltammetry (CV) was used to investigate the energy level of cyt *c* as well as to estimate the success rate of the cyt *c* and the RC immobilization. The results from these measurements were used to confirm the successful construction of the Au|SAM|cyt *c*|RC structure using the layer-by-layer assembly.

4.4.2. Ellipsometry Analysis

The Au|SAM|cyt *c*|RC structure was further studied by measuring the thickness of the SAM, SAM|cyt *c*, and SAM|cyt *c*|RC layers using ellipsometry. This was performed to confirm that the thickness of each layer is in agreement with the size of employed molecules. As shown in Figure 4.5, the SAM prepared from an ethanolic solution of 10 mM 6-mercaptohexanoic acid showed a ~14 Å thick layer. Assuming a 30º tilt for the alkanethiol chain,[121] the measured thickness is slightly larger than the theoretical thickness expected for a close-packed monolayer oriented to the surface. This has been explained by coverage of a high free energy surface (*i.e.,* Au) with reversibly physisorbed layers of water, hydrocarbons,

and other organic compounds under laboratory ambient conditions.[158] As shown in Figure 4.5, the thickness of the SAM increased by ~33 Å after cyt c immobilization on top, which is in a good agreement with the size of cyt c reported by other groups.[159-161] Upon deposition of the RCs the thickness increased from ~47 Å to ~120 Å, indicating that a monolayer of RCs (thickness ~70 Å) had attached on top of the Au|SAM|cyt c.
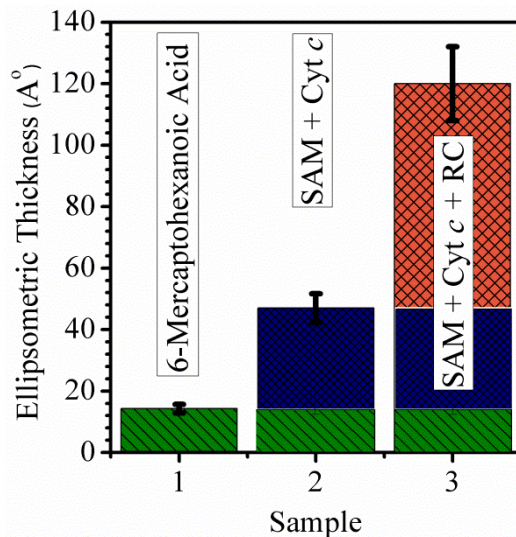
Figure 4.5 Ellipsometric estimation of the thickness of: sample 1 (SAM of 6-mercaptohexanoic acid); sample 2 (SAM|cyt c); sample 3 (SAM|cyt c|RC).

4.4.3. Photoemission Spectroscopy Analysis

In order to evaluate how the energy levels of the SAM affect the ET between the Au electrode and the RC, the highest-occupied-molecular-orbital (HOMO) and the lowest-unoccupied-molecular-orbital (LUMO) of the SAM were measured using low intensity XPS (LIXPS), ultraviolet photoemission spectroscopy (UPS), and UV-Vis absorption spectroscopy methods. Additionally, XPS data provided further evidence for the successful attachment of the desired molecules (Figures 4.8). Figure 4.6 shows the UP spectra measured before and after deposition of the SAM during this experiment. The center panel (Figure 4.6(b)) shows the complete spectra, and the side panels show the secondary edge normalized (Figure 4.6(a)) as well as the valence bands region after background subtraction (Figure 4.6(c)).
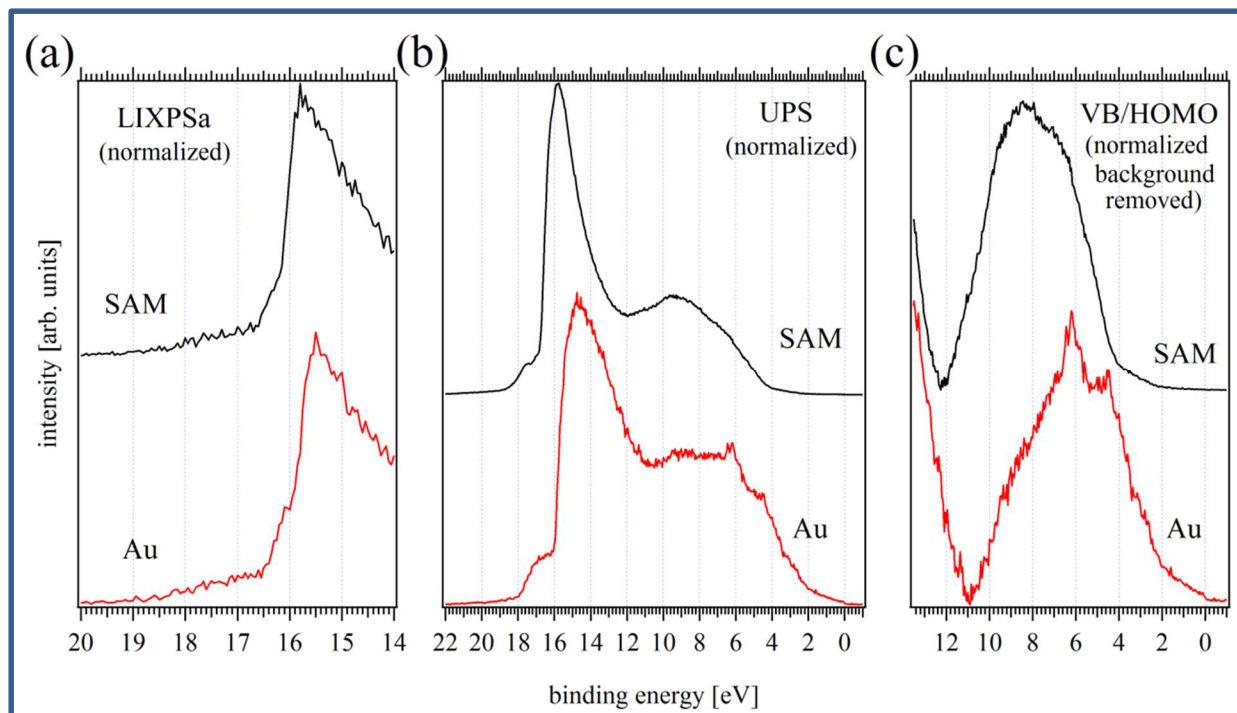
Figure 4.6 LIXPS and UP spectra before (red) and after (black) the deposition of SAM on a clean Au substrate. (a) The normalized secondary edges measured with LIXPS before UPS. (b) The complete normalized UP spectra. (c) The evolution of the VB emission features through the deposition process (black, SAM; red, Au).

The secondary edge spectral cutoffs acquired *via* LIXPS (Figure 4.6(a)) allowed for the determination of the WF of the Au and the Au|SAM substrates. The WF was calculated by subtracting the cutoff binding energy value from the excitation energy (21.2182 eV) and taking the analyzer broadening of 0.1 eV into account. Figure 4.6(b) shows the complete set of normalized UPS. The main emission features include the Fermi level, the valence bands/HOMO (VB/HOMO) density of states, and the secondary edge. The magnified VB/HOMO spectra with background removed are shown in Figure 4.6(c). Before deposition of a SAM, the valence bands and the Fermi level of the Au substrate can be clearly observed. After the deposition of a SAM, these features are suppressed and replaced by features corresponding to the emissions from the SAM. The valence bands maximum (VBM) of the Au electrode coated with a SAM relative to Au alone are shown in the magnified VB/HOMO spectra.

In order to estimate the optical band/HOMO-LUMO gap in the linker molecule, the absorption spectrum of the linker solution (10 mM in ethanol) was measured. As shown in Figure 4.7, the absorption

threshold starts around 300 nm which corresponds to an energy gap of 4.13 eV. From the LIXPS and UPS results the HOMO level is measured to be 7.2 eV below the vacuum level. Hence, the absorption results indicate a LUMO of 3.07 eV below the vacuum level. As explained in the Discussion section, the energy levels in the SAM can be used to draw an energy diagram across the Au|SAM|cyt c|RC to assess the limitations in the ET.
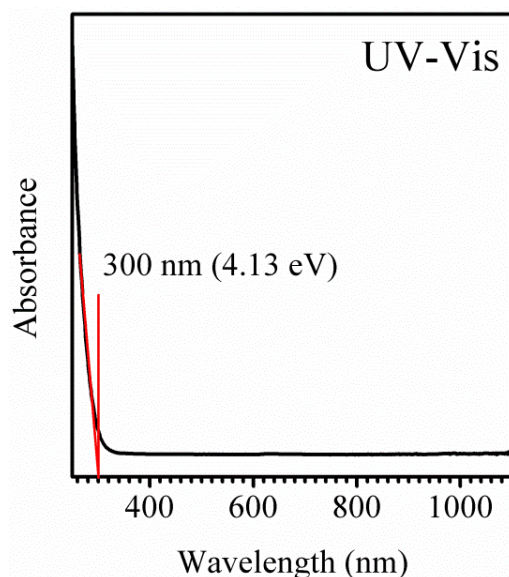
Figure 4.7 The UV-Vis absorption spectrum of the linker solution (10 mM 6-mercaptohexanoic acid).

To analyze the elemental composition on the electrode's surface, we applied X-ray photoelectron spectroscopy (XPS) as a surface-sensitive quantitative spectroscopic technique.[162-164] Also, XPS data provided further evidence for the successful attachment of the desired molecules. Figure 4.8 shows XPS spectra of the O1s, N1s, C1s, and S2p core level lines acquired after each deposition step. The bottom spectra in red were obtained from the bare Au electrode which was free of nitrogen and sulfur, indicated by the absence of a peak in the N1s and S2p lines. Small peaks of O1s and C1s were observed, which we attribute to residual contamination on the Au surface remaining after the chemical cleaning process performed prior to the self-assembly of the alkanethiol layer. The successful self-assembly of alkanethiol molecules on the surface of Au electrodes was confirmed by the emergence of a weak peak in the S2p line, as well as the evolution of well-defined peaks in the O1s and C1s lines. The O1s line in black around 532.3

eV is attributed to C–OH and C=O species in the carboxyl group. The C1s spectrum exhibits a peak around 285.0 eV which arises from the emissions of carbon species in the alkane group. The thiol group as the attachment anchor presents an S2p doublet line around 162.0 eV. Following the deposition of cyt *c* on top of the SAM, the O1s and C1s lines evolved accordingly. The O1s peak in blue has a similar shape and binding energy as from the SAM but of greater amplitude. The O1s line is likely attributed to oxygen atoms in the backbone and side chains of cyt *c*. The C1s emission from cyt *c* shows a different shape and binding energy than that of the SAM alone. The peak around 285.4 eV is thought to arise from the aliphatic side chains of cyt *c*, whereas the weaker peak around 289.0 eV is attributed to the carbon atoms in the protein backbone. The emerging N1s peak in blue (cyt *c*) likely resulted from the N atoms of the peptide bond and N-containing side chains, and validates the adsorption of cyt *c* on the linker layer (which caused the attenuation of S2p photoelectrons from the SAM as shown by the loss of the peak in the S2p line in blue).
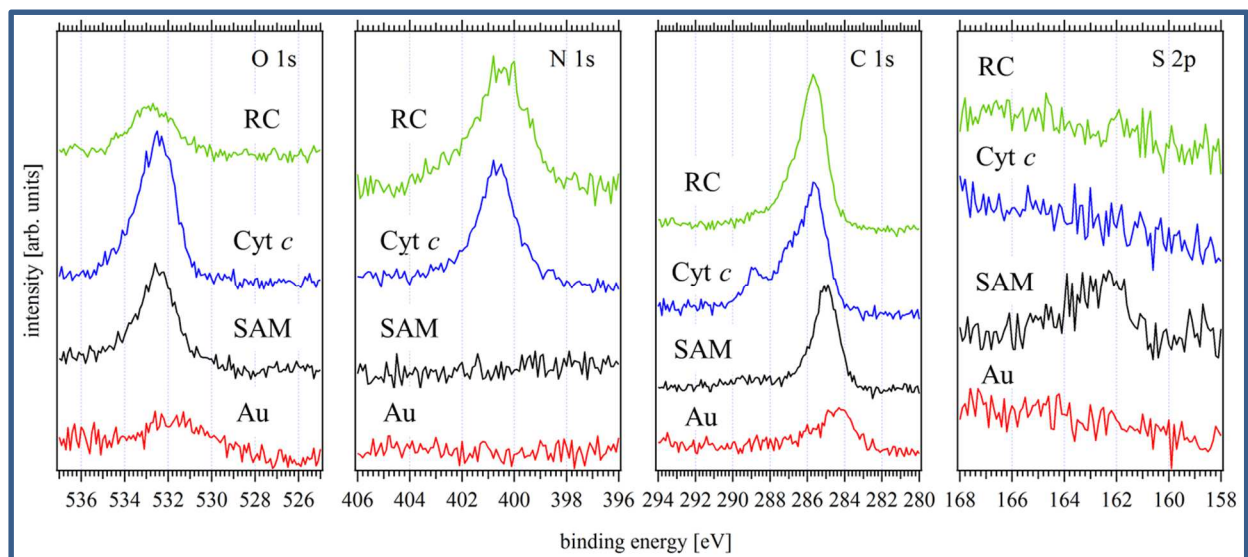
Figure 4.8 XPS spectra of O1s, N1s, C1s and S2p core level emissions for Au, Au|SAM, Au|SAM|cyt *c*, and Au|SAM|cyt *c*|RC samples. The spectra were obtained from: the cleaned Au electrode prior to exposure to the carboxyl-terminated alkanethiol linker (Au, red); after deposition of the carboxyl-terminated alkanethiol linker (SAM, black); after incubation of the SAM-coated electrode with a solution of cyt *c* (blue); after incubation of the cyt *c*-bound, SAM-coated electrode with a solution of the RC (green).

The corresponding core level lines obtained after addition of the RC layer on top of the cyt *c* film are shown in green in Figure 4.8. The photoemission photons from cyt *c* were attenuated by the RC layer

as indicated by the decreased intensity of the O1s peak and the loss of the minor peak in the C1s spectrum around 289.0 eV.
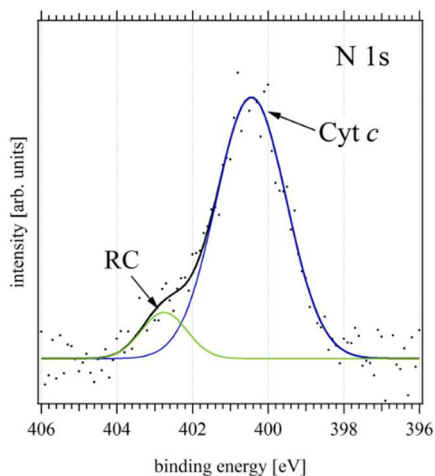
Figure 4.9 Gaussian–Lorenzian fit (blue, attributed to cyt *c*; and green, attributed to the RC) to the RC N1s emission line measured (black) on the Au|SAM|cyt *c*|RC electrode.

The nitrogen species in the RC differ from those in the cyt *c* (Figure 4.9). These spectral changes confirm the attachment of the RC to the Au|SAM|cyt *c*, as opposed to binding of the RC non-specifically, in which case the cyt *c* signal would not be expected to be attenuated.

4.4.4. Electrochemistry Analysis

To estimate the electrochemical midpoint potentials (*i.e.* energy levels) and the surface coverage of the proteins, electrochemical CV was performed for each layer. Figure 4.10(a) shows the CVs of Au, Au|SAM, Au|SAM|cyt *c*, and Au|SAM|cyt *c*|RC electrodes at a scan rate of 0.05 V.s^{-1} at room temperature. As curve ii shows, the Au electrode primed with a layer of 6-mercaptohexanoic acid SAM exhibited no electroactivity in the potential range from 0.1 V to 0.6 V in the 0.1 M Tris–HCl (pH 8.0) background electrolyte. Previous studies have mainly reported the CVs of carboxylic acid-terminated SAM electrodes for positive voltages.[121] When the scan range was extended below 0.0 V *vs* NHE (*i.e.,* the case here) the CV of the SAM showed a pair of peaks corresponding to protonation and de-protonation of the surface COOH groups.[165]
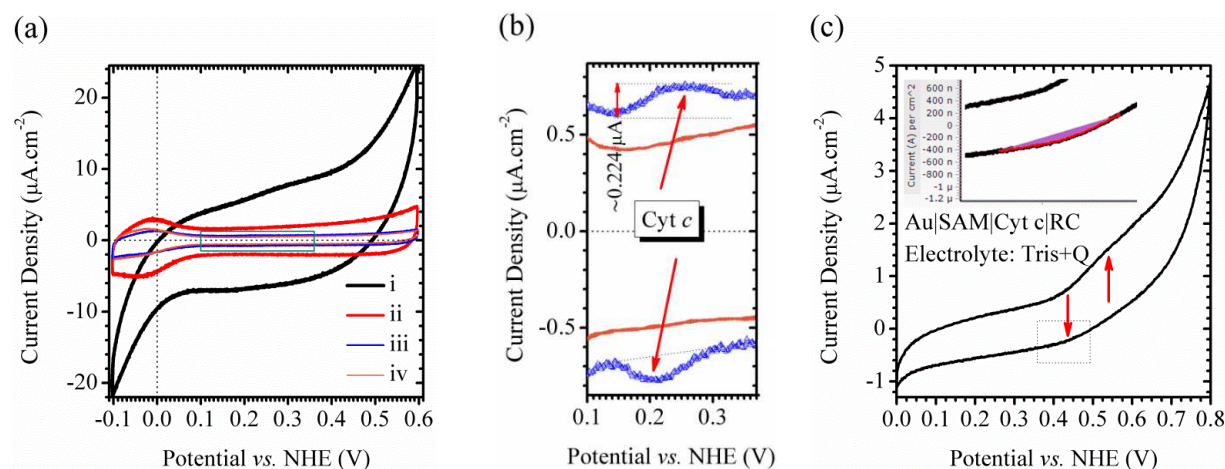
Figure 4.10 (a) CVs of: a Au electrode (i, black trace); Au|SAM electrode (ii, red trace); Au|SAM|cyt c (iii, blue trace); Au|SAM|cyt c|RC (iv, orange trace). The scan rate was 0.05 V.s-1 and the background electrolyte was 0.1 M Tris buffer. (b) Close-up view of the green rectangle in part (a) which shows a pair of quasi-reversible redox peaks attributed to the heme Fe $_{III}$/Fe $_{II}$ couple in cyt c, at ~0.23 V vs NHE (blue trace), wherein the comparative CV for iv is shown in orange. (c) CV of the Au|SAM|cyt c|RC electrode (scan rate of 0.05 V·s^{-1}) in the presence of Q, which shows oxidation-reduction peaks of the RC primary donor (P). The inset shows the anodic peak scaled and colored to emphasize the area of interest. The surface under the peak (purple) was used to estimate the density of immobilized RCs.

After immobilization of cyt c, direct electrochemistry of surface-bound cyt c was achieved (Figure 4.10, curve iii), and a pair of quasi-reversible redox peaks due to the one-electron oxidation and reduction of a heme Fe $_{III}$/Fe $_{II}$ couple was apparent at ~0.23 V vs NHE (Figure 4.10(b)). The surface formal potential of cyt c is nearly identical to the values previously reported for cyt c bound to physiological membranes.[145] From the average of the reduction and oxidation peak potentials, the redox potential of cyt c was measured to be ~0.23 V vs NHE (4.73 eV below vacuum level).

The CV result from RCs in the Au|SAM|cyt c|RC structure in the presence of quinone (Q) in the electrolyte is presented in Figure 4.10(c). Because the immobilized proteins are present as a monolayer, the concentration of RC is very low and the redox peaks in the CV graph are relatively small. Nevertheless the RC P peaks at ~0.4 V and 0.6 V vs NHE were observed, which confirms the successful RC immobilization. The midpoint potential of RC was estimated to be ~+0.45 (vs NHE), which is similar to that reported in previous works.[32,33,63] This confirms that in this structure the RCs are still redox-active, upon docking to cyt c. As explained in the Discussion section, the area under the anodic peak (Figure 4.10(c), inset) has been

used to estimate the total amount of exchanged charges in the redox reaction of RCs, from which the RC density and surface coverage were estimated.

4.5. Discussion

The cathodic photocurrent in Figure 4.2 indicates direction of ET from the Au electrode to the RC protein *via* the SAM|cyt *c* structure, and accordingly confirms the anticipated protein orientation with the P-side facing the electrode. Although the photocurrent result shows the feasibility of immobilizing RCs through cyt *c* proteins, the overall photocurrent depends on the number of the immobilized RCs and the ET rate through the SAM|cyt *c* linker. Assuming a high degree of surface coverage by the SAM,[111] the density of immobilized RCs is limited by the frequency of binding to cyt *c*. Using the results from the electrochemical experiments, we describe in the following text an estimation of the surface coverage of the cyt *c* and the RC layers. Also, the ET rate is estimated from the transient photocurrent response.

For surface coverage estimation of active cyt *c* heme proteins, the total charge was calculated using the CV peak integration (Figure 4.10(b)) after background subtraction.[121] For the Au|SAM|cyt *c* structures, the electroactive surface density of cyt *c* was determined by automatic CV peak integration, using VersaSTAT 4 software. Integrating the area under the peak of photocurrent density *vs* potential gives the charge density (Q_{total}). Using Faraday's Law, the electroactive surface concentration of cyt *c* can be then estimated using Eq. (4.1):[63,121]

$$\Gamma = \frac{Q_{Total}}{nF}$$

Eq. 4.1

where Γ is the electroactive surface density of cyt *c*, *n* is the number of unit charges in the redox reaction of the protein (*n* = 1 in this case), and *F* is the faradaic constant (96485 C mole^{-1}). Considering the surface area of the electrode, the surface density of $\sim 14 \times 10^{-12}$ mole cm^{-2} was estimated for immobilized cyt *c*, which is consistent with a previous report.[121] Bearing in mind the approximate diameter of a cyt *c* molecule, 3.3 nm,[159] the calculated value of the cyt *c* surface concentration corresponds to a $\sim 70\%$ surface coverage of the electrode.

The CV peak integration technique was also applied to estimate the surface coverage of RC using the CV plot in Figure 4.10(c). The measured charge density of ~581 nC (Figure 4.10(c), inset) corresponds to a surface density of RC of 6.02×10^{-12} mol·cm^{-2}. Considering the estimated density of cyt c on the surface (14×10^{-12} mol·cm^{-2}) the number of attached RCs is almost half of the cyt c proteins on the electrode. Despite the lower number of RCs, based on the protein diameter (~5 nm) the RC surface coverage is estimated to be ~70%, which is in the same range as cyt c. Previous research has shown electrostatic interactions between acidic amino acids on the RC periplasmic surface (P-side) and the basic amino acid residues, primarily lysines, surrounding the cyt c heme contribute to inter-protein docking and stability of the RC–cyt c co-complex.[56,166] Our unpublished results shows that $R.$ $sphaeroides$ cyt c_2 and horse heart cyt c are ~30% structurally similar. Additionally, cyt c was found to bind to the proximal position faster, as well as with a higher affinity of the oxidized form to the RC.[167] In the current study, the photocurrent density of the Au|SAM|cyt c|RC structure confirms the binding of cyt c and RC complexes. Additionally, the photocurrent direction proves that cyt c binds to the P-side of the RC protein complex. This binding configuration here can be compared to the mechanism known for the in $vivo$ RC and cyt c proteins bond, as proposed by others.[168-170]

The ET rate between RC and the Au electrode in the Au|SAM|cyt c|RC structure was estimated through the photocurrent transition at the onset of illumination as suggested by Trammell et $al.$[65] Figure 4.11 shows the photocurrent transition (1.4 s) for the RC-modified Au electrode with RC proteins sitting on cyt c-terminated SAMs. Assuming the transient photocurrent follows an exponential profile, the current density, J, was fitted to $J = J_{peak}(1 - e^{-kt})$, where $J_{peak} = -450$ nA cm^{-2} is the peak current density, k is the ET rate, and t is time (t=0 is the onset of the illumination). Based on the fitting curve in Figure 4.11, the ET rate between the RC and the Au electrode was estimated to be $k = 7.1$ s^{-1}.
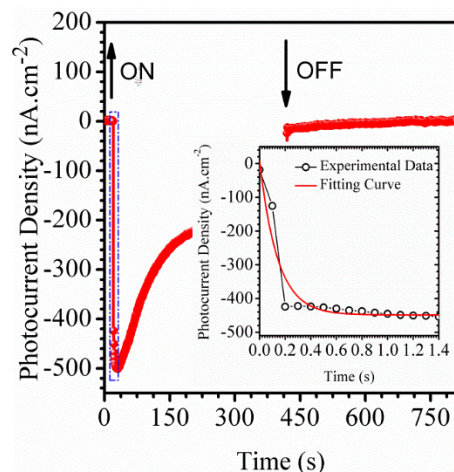
Figure 4.11 Photocurrent transition (inset, close-up view of the dashed rectangle) at the onset of illumination for Au|SAM|cyt *c*|RC electrode (onset of illumination at 0.0 s, and cessation of illumination as indicated by the upward and downward pointing arrows).
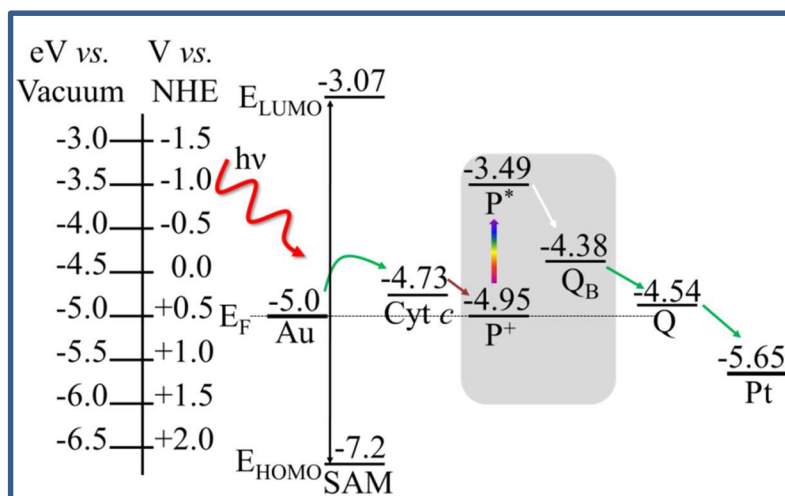
Figure 4.12 The energy diagram of the bio-electrochemical cell with the Au|SAM|cyt *c*|RC structure and the proposed mechanism for operation of the cells with Q as the single diffusible redox mediator. RC complexes are modeled as oriented with the P-side toward the Au electrode. Arrows indicate the route of ET from the Au to cyt *c*, into the P-side of the RC, and through Q to the Pt electrode. The energy level at each layer is relative to the vacuum level. The corresponding electrochemical potentials can be found from the normal hydrogen electrode (NHE) axis at the right.

The relatively low ET rate in the Au|SAM|cyt *c*|RC structure can be explained by an energy diagram of the different layers, shown in Figure 4.12. The electrochemical midpoint potentials of the cyt *c* heme and P$^+$ in RC were measured at 0.23 V and 0.45 V *vs* NHE, respectively (Figure 4.10). The energy levels inside the RC have been studied in detail by others and explained by Blankenship.[51] The midpoint potential of Q at pH 8 was measured in our earlier work as ~0.042 V *vs* NHE.[33] The vacuum potential of Pt and the

electrochemical potential of the Q_B site within the RC were also presented in a previous report.[32] The HOMO and LUMO levels for the SAM were obtained from UPS, LIXPS, and UV-Vis absorption results (Figures 4.6 and 4.7).

The observed cathodic photocurrent implies ET from the Au to P^+ in the RC while the energy diagram in Figure 4.12 shows that the ET is hindered by the energy barrier of the SAM and the unfavorable energy difference between Au and cyt c. Although the Au Fermi level is below the cyt c energy level, the density of electrons above the Fermi level is not zero at room temperature. Additionally, WF measurement of the sputtered Au was performed in vacuum. The WF of a surface can be strongly affected by the condition of the surface. In the event of surface reactions (such as oxidation or reduction), the WF can change considerably. Hence, it is reasonable to assume that there are electrons with enough energy to tunnel through the SAM to the cyt c.

Considering the energy barrier (ΔE_1) of 1.93 eV (the difference between E_F (Au) and E_{LUMO} (SAM)) and the tunneling length (a) of 3.0 nm (Figure 4.5 sample 2 - the distance from the electrode to the middle of cyt c where heme is located), the wave function for an electron tunneling through the SAM experiences attenuation. Using a simple square barrier model for the SAM, the one dimensional conductance, G, through the barrier can be found from Eq. (4.2):[171]

$$G = \frac{2e^2}{h}T(\Delta E_2)$$

Eq. 4.2

where $e = 1.6 \times 10^{-19}$ C is the charge of one electron, $h = 6.626 \times 10^{-34}$ J·s is Planck's constant, and $T(\Delta E_2)$ is the tunneling transmission coefficient between two energy states across the barrier with an energy difference of ΔE_2. For a large barrier the transmission coefficient is estimated by Eq. (4.3):[171]

$$T(\Delta E_2) \approx \frac{16\Delta E_2}{\Delta E_1}exp\left(-\frac{4\pi\sqrt{2m_e\Delta E_1}}{h}a\right)$$

Eq. 4.3

where $m_e = 9.11 \times 10^{-31}$ kg is the electron mass. From Eq. (4.2) and (4.23), the one-dimensional conductance of the barrier is estimated to be $G = 4.65 \times 10^{-23}$ Ω^{-1} which is very low. It should be noted that G is not the

conductance of the SAM, but is the conductance along a single linker molecule (in one dimension). As shown in Figure 4.2, the SAM has a crucial role in the protein immobilization since without the linker no photocurrent was observed (mainly due to the cyt c adsorption orientation). In order to eliminate the charge transfer barrier, a conjugated linker molecule with a HOMO level slightly higher than the energy level in cyt c could be used. In this case, the ET would occur by the charge hopping through the hybrid conjugated molecule-cyt c linker, instead of tunneling. Additionally, a low WF material for the working electrode would greatly increase the ET rate. A detailed study of such approaches is underway in our laboratory and the results will be reported in forthcoming papers. The proposed docking mechanism, described above, may be also exploited for other types of carotenoid-based proteins such as RC-light harvesting (LH) complexes and possibly PSI for intriguing applications in photovoltaic, photonic and optoelectronic devices, and bio-sensors.[27,39,62,114,172,173]

Additionally, we examined the effect of cycling the applied potential on the generated photocurrents to better understand the ET mechanism (Figure 4.13). Figure 4.13 demonstrates that at applied potentials of -0.558 V to 0.050 V (*vs.* NHE), significant cathodic (negative) photocurrent densities were measured whereas at the applied potentials of 0.142 V to 0.542 V (*vs.* NHE), anodic (positive) photocurrent were recorded. The maximum photocurrent density of -2.872 μA cm^{-2} was measured at the applied potential of -0.558 V *vs.* NHE. The change in the photocurrent direction occurred around the applied potential of 0.142 V *vs.* NHE. These observations well correlate with the proposed energy diagram and the operation mechanism for such cells.

Carotenoid-based proteins have shown promise for photovoltaic applications. Several studies have focused on the assembly of PSI onto various substrates such as P-dope silicon and graphene oxide which resulted in enhanced current densities over 100 μA cm^{-2}. Other studies on integration of oriented RC-LH1 complexes, mostly on transparent conductive oxide electrodes, showed several μA current densities,[61,62] with an exception of a recent work on a densely packed monolayer of RC-LH1 complexes on a Au electrode using Langmuir–Blodgett technology which resulted in a 45 μA cm^2 current density.[73]
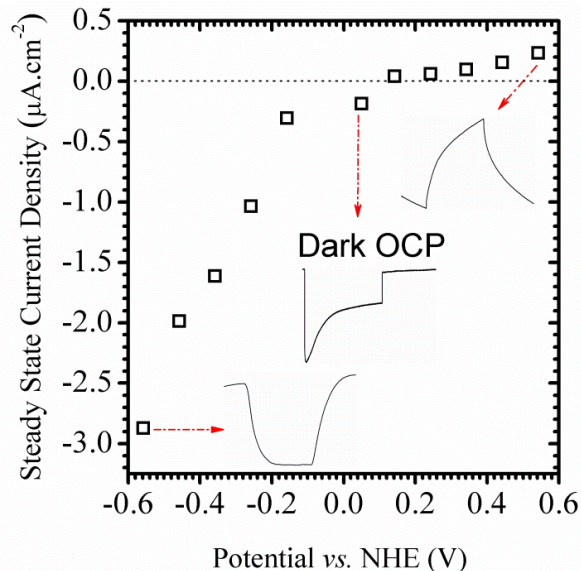
Figure 4.13 Effects of cycling the applied potential on the mean steady state current densities, obtained from the Au|SAM|cyt *c*|RC electrode. The shape of the photocurrent at several applied potential is shown as insets (amplitude is ignored).

Beside carotenoid-based photosystems, bacteriorhodopsin as a robust light-driven proton pump, has found various applications in solar energy conversion,[47,48,98] optoelectronics,[99] and organic field effect transistors.[100] A recent study on fabricating a photovoltaic cell using aqueous bacteriorhodopsin generated a photo-electric response of ~33 µA cm^2. Overall, the tendency towards biomimetic devices and the need for the production of clean energy by mimicking nature brings the light-capturing proteins applications in bio-electronic devices to the forefront of cutting-edge research. The overall effort will advance the application of biological materials in electronic devices with a far reaching impact in the fields of solar cells, bio-sensors, and bio-nanotechnology.

4.6. Conclusions

We have demonstrated the feasibility of utilizing a protein-protein interaction to immobilize the *R. sphaeroides* wild type RC protein from the P-side through a hybrid carboxylic acid-terminated alkanethiol SAM|cyt *c* linker. The new linker structure has demonstrated the ability to control the orientation of the RC with reasonable stability in bonding to the RC protein complex. A simple layer-by-layer deposition/incubation method was applied to build a Au|SAM|cyt *c*|RC structure which resulted in 70% of the surface coverage by RC proteins. The ET rate between the Au electrode and RCs was found to be *k* ≈

112

7.1 s^{-1}. Our detailed energy study of the layers showed a large energy barrier at the SAM which limits the ET rate. These results provide key information about how specific surface modification of an electrode may control the performance of RC complexes in systems suitable for the development of solar energy converters, and other types of photon energy-harvesting biomaterials. This work provides an experimental and theoretical baseline for future work.

CHAPTER 5 : LARGE PHOTOCURRENT RESPONSE AND EXTERNAL QUANTUM EFFICIENCY IN BIO-PHOTOELECTROCHEMICAL CELLS INCORPORATING REACTION CENTER PLUS LIGHT HARVESTING COMPLEXES[5]

5.1. Abstract

Bacterial photosynthetic reaction centers (RCs) are promising materials for solar energy harvesting, due to their high ratio of photogenerated electrons to absorbed photons and long recombination time of generated charges. In this work, photoactive electrodes were prepared from a bacterial RC-light-harvesting 1 (LH1) core complex, where the RC is encircled by the LH1 antenna, to increase light capture. A simple immobilization method was used to prepare RC-LH1 photoactive layer. Herein, we demonstrate that the combination of pretreatment of the RC-LH1 protein complexes with quinone and the immobilization method results in bio-photoelectrochemical cells with a large peak transient photocurrent density and photocurrent response of 7.1 and 3.5 $\mu A\ cm^{-2}$, respectively. The current study with monochromatic excitation showed maximum external quantum efficiency (EQE) and photocurrent density of 0.21% and 2 $\mu A\ cm^{-2}$, respectively, with illumination power of $\sim 6\ mW\ cm^{-2}$ at ~ 875 nm, under ambient conditions. This work provides new directions to higher performance bio-photoelectrochemical cells as well as possibly other applications of this broadly functional photoactive material.

5.2. Introduction

Photosynthesis has been the primary source of energy on earth over the evolutionary history of life.[16] Photosynthetic plants and bacteria convert solar energy into electrochemical energy with high efficiency.[51] Interest in the potential application of biological photosystems has been fueled by the

---

[5] Chapter 5 was published in Biomacromolecules (Yaghoubi, H.* et al. (2015) Large Steady-State Photocurrent and External Quantum Efficiency of Bio-Photoelectrochemical Cells Incorporating Reaction Center Light Harvesting Complexes. Biomacromolecules. 16(4), 1112–1118). Permission is included in Appendix A.

discovery of the 3-D crystal structures of these membrane protein complexes, and the quantitative understanding of the primary ET processes of photosynthesis.[24-26] In the succeeding years, among several intriguing applications of photosynthetic proteins,[27-29] solar energy harvesting has achieved prominence due to an increasing demand for the production of clean energy.[20,30] The reaction center (RC) of the bacterium *Rhodobacter (Rb.) sphaeroides* is the simplest and perhaps the most resilient photosynthetic complex, with ~200 times longer recombination time of the separated charges compared to that in silicon-based devices.[50] Through Förster resonance energy transfer, photon energy initially absorbed by antenna complexes, such as the bacterial light-harvesting complexes 1 and 2 (LH1 and LH2), is transferred to the RC, where a charge-separated state is generated with ~100% quantum efficiency.[51] The RC of *R. sphaeroides* is a transmembrane complex comprised of three protein subunits called L, M and H, with a donor (P) and a acceptor (Q) side. The charge separation in the RC occurs by generation of an excited state in a pair of bacteriochlorophylls (BChls), called the special pair (P). An electron is then transferred to an accessory BChl (B_A), then to a bacteriopheophytin (BPhe), and subsequently to a primary (Q_A) and secondary (Q_B) quinone.[33] The long recombination time and the expected greater than 20% power conversion efficiency of potential devices based on the *Rb. sphaeroides* RC,[60] have inspired several research groups to utilize RCs in photoelectrochemical cells for harvesting solar energy.[3,32-37,43,61,62] In such devices, diffusible mediators were used to transfer light-induced charges from the RCs to the electrodes through reversible redox reactions.[33] However, the limited optical absorption spectrum and extinction coefficient of the RC complex is a concern for achieving high photocurrent in a cell. To enhance the optical absorption, a combination of RC and antenna complexes can be used (the RC-LH1 core complex).[45,75-78] Despite the addition of LH1 and corresponding increase in the absorption spectrum and peak amplitudes, photocurrents in electrochemical cells using an RC-LH1 complex from *Rb. sphaeroides* were lower than expected.[43,45,64,79] Developing a new energy conversion technology that is also sustainable has been an ongoing challenge. *En route*, to achieve the potential of using *Rb. sphaeroides* RC protein complexes in solar energy conversion, several groups proposed different fabrication methods and structures.[32,50,61,62] In the current study we investigated the effect of quinone deficiency on the photocurrent response and the external quantum efficiency (EQE) of bio-

photoelectrochemical cells incorporating RC-LH1 complexes. Hence, we designed the experiments to be carried out in a single diffusible mediator system. The presented results in the current study are among the most promising reported so far, using a single diffusible redox mediator in the electrolyte.[32,50,61,62] However, a recent study shows that using two redox mediators in the electrolyte can further improve the photocurrent.[73] Studies of how RC protein complexes interface with electrodes have focused mainly on the resulting transient peak photocurrent density, with very little attention paid to the associated overall photocurrent response. As the functionality of any solar cell is strongly dependent on its robustness under long illumination, an enhancement in the photocurrent response is also of great importance. In this work, we constructed bio-photoelectrochemical cells using a quinone-treated RC-LH1 dimer (hereafter referred to as Q-treated RC-LH1) as the photovoltaic component, which is comprised of two RC-LH1 cores organized as an S-shape of LH1 complexes.[78] We report on the mean photocurrent density of 3.25 μA cm^{-2}. The fabricated cells showed highly reproducible cycles of charge generation under long times of illumination, which implies a robust functionality of the RCs in this configuration.

5.3. Experimental Section

5.3.1. Preparation of Working Electrodes

Two different batches of RC and RC-LH1 protein complexes were prepared at a final concentration of 15 μM. The RC photoactive electrodes were prepared by drop-casting of 15 μl of a 15 μM RC solution over the surface of the Au electrode. For preparation of the Q-treated RC or RC-LH1s photoactive electrodes, initially 3 μl of a 28.2 mM ethanolic solution of Q was mixed with 15 μl of 15 μM RC or RC-LH1 solutions, and kept at 4 °C for 20 minutes. The prepared mixed solutions were then drop-casted over the Au electrodes. In all cases, the immobilization was performed at 4 °C in aerobic conditions for 15 hours after which the electrode was washed thoroughly three times in de-ionized water and dried in air. Therefore, the proteins were bound to the Au electrode.

5.3.2. Electrochemical Measurements

The photochronoamperometric, CV, and EIS tests were performed in custom built three-electrode setups with the fabricated photoactive Au as the working electrode (area of 0.5 cm^2), Pt counter electrode,

and Ag/AgCl reference electrodes. 0.75 mM Cp_2Fe redox solution was prepared by dissolving Cp_2Fe in 0.1 M Tris buffer and ultra-sonication for 48 hrs and used in all the experiments in which one mediator was added. Because the feasibility of using ferrocene in similar electrochemical cells had been demonstrated in previous work,[50,89] we utilized the same redox mediator. For the experiment with two mediators, the concentrations of Cp_2Fe and Q were 0.75 mM and 0.056 mM, respectively. The current polarity convention was set in a fashion that defined cathodic current as negative. The photochronoamperometric tests were performed at the open circuit potential of system, which was determined for each sample. Illumination was provided using a commercial solar simulator (RST300S (AM 1.0), Radiant Source Technology) at an incident light intensity of 80 mW cm^{-2} at the electrode's surface. Photocurrents and photovoltages were recorded using a VersaSTAT 4 (Princeton Applied Research) potentiostat.

5.4. Results and Discussion

Figure 5.1 shows the superimposed absorption spectra of the *Rb. sphaeroides* RC and the RC-LH1 complex. The distinctive three Q_y RC cofactor peaks, *i.e.,* BPhe, monomeric BChl, and the BChl "special pair", are clear at 760, 804 and 867 nm, respectively (black trace). The RC-LH1, which is comprised of two RC cores encircled with an S-shape of LH1 complexes (Chapter 2), shows the highest light harvesting capacity around 872 nm, arising from the LH1 antenna (Figure 5.1, red trace).[78] The lower-amplitude bands centered around 804 and 760 nm are due to the RC accessory BChl and BPhe cofactors, respectively.
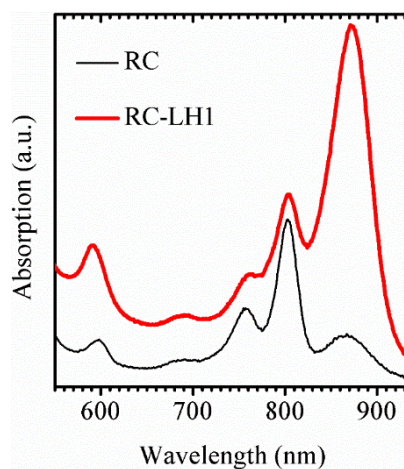
Figure 5.1 The absorption spectra of RC (solid black line) and RC-LH1 dimer (solid red line) complexes.

Figure 5.2 shows the photostability of the RC and the RC-LH1 complexes under 1 hr of continuous illumination using a solar simulator at an incident intensity of 80 mW cm^{-2}.
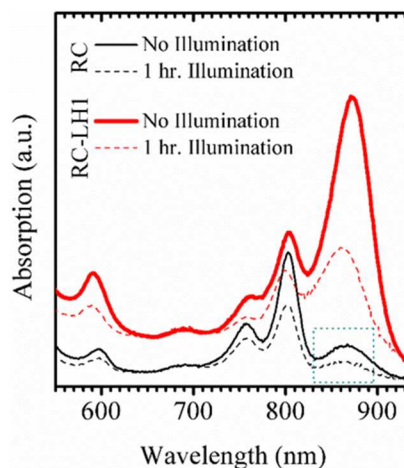
Figure 5.2 The absorption spectra of purified RC (solid black line) and RC-LH1 dimer (solid red line) complexes before 1 hr of illumination. The absorption spectra of the RC and the RC-LH1 complexes after 1 hr of continuous illumination are shown by the dashed lines. The rectangle of green dotted lines around 865 nm signifies the changes in the RC P cofactor absorption after illumination for one hr.

The time-dependent electrical photo-responses of the RC and the RC-LH1 photoactive electrodes were measured in standard three-electrode electrochemical cells with ferrocene (Cp$_2$Fe) in the electrolyte as the added redox mediator (Figure 5.3(a)). To confirm the contribution of the protein complexes to the photocurrent generation, control experiments were performed on cells containing Cp$_2$Fe, but lacking any protein component (Figure 5.3(b)). The negligible 7 nA cm^{-2} anodic (positive) photocurrent density supports the interpretation that the photo-response in the RC- and the RC-LH1-based cells stems from the light harvesting and charge generation in the protein components. In all the other cases with either RC or RC-LH1 photoactive layers, the photo-responses showed cathodic (negative) currents which imply ET from the Au electrode to the P side of the protein.[62,69] The details of the binding and orientation the protein complexes on the Au electrode need an in-depth investigation. However, as in previous work,[50,61,62,64] we define the orientation based on the photocurrent direction, which in our case is from Au to the RC.[32,50,61,73] Therefore, the data indicate that the RC was bound to the electrode with P located within electron tunneling distance from the Au surface. Hypothetically, several mechanisms could control the adsorption orientation,

including heterogeneous hydrophilic characteristics of the complex's surface, which induce adsorption

orientation from the P side,[73] and electrostatic interaction between the electrode and the complex.[24]
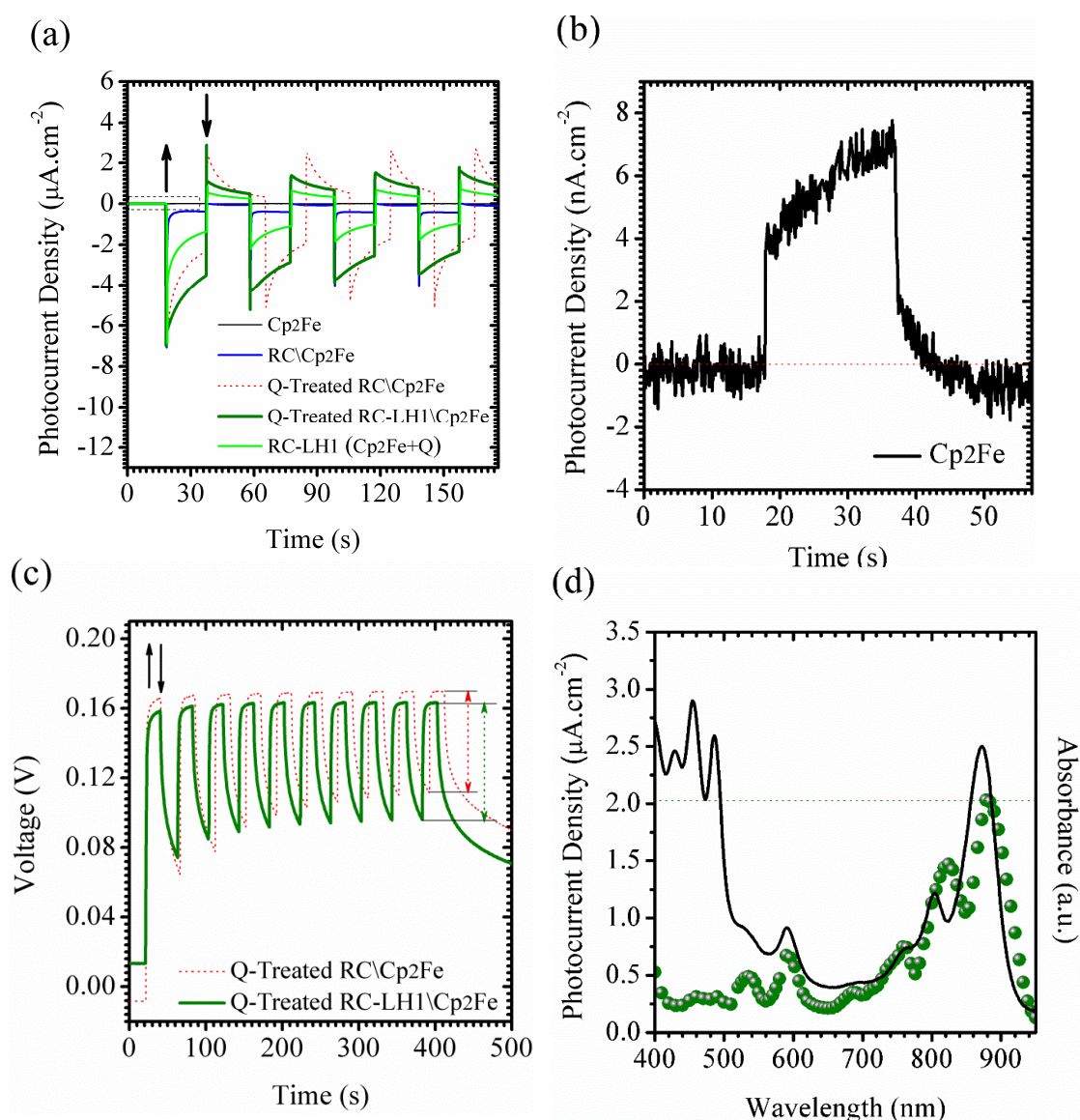
Figure 5.3 (a) Time dependence photo-response of the RC and the RC-LH1 treated electrodes under 80 mW cm^{-2} illumination exposed to light-on/light-off cycles. (↑) and (↓) indicate the onsets of illumination and dark for the first cycle. Measurements with one mediator added were made with and without an RC or RC-LH1 film in a 0.75 mM ferrocene mediator solution with an Ag/AgCl reference electrode and a platinum counter electrode. Measurement with two mediators (light green curve) was made in a 0.75 mM ferrocene and 0.056 mM Q electrolyte solution with an Ag/AgCl reference electrode and a platinum counter electrode. (b) Close-up view of the dashed rectangle in part (a), showing that photocurrent density is negligible in the absence of any protein component. (c) V_{OC} of the Q-treated RC and Q-treated RC-LH1 cells in part (a) in response to cycles of illumination and dark. (d) Action spectrum of the photocurrent amplitude, generated on the Q-treated RC-LH1 treated electrode (with the maximum amplitude of the photocurrent density at each light-on event shown as a green dot), compared to the solution absorption spectrum of the RC-LH1 (bold black line).

119

When an electrode with a layer of the RC bound was tested it showed a peak transient current density of ~7.1 μA cm^{-2} (Figure 5.3(a), blue trace). The photo-response stabilized at ~0.4 μA cm^{-2}. It is worth mentioning that the photo-response was observed in the absence of any linker, with no protein engineering, instead using an immobilization method of protein drop-casting and subsequent washing of the primed electrode. Further improvement in the photocurrent was achieved by devising a new method. In this approach, photoactive RC layers were prepared from protein complexes to which quinone (Q) was added prior to deposition, which led to ~6 times higher photocurrent (Figure 5.3(a); red dashed line, compare with blue trace). Treating the pigment protein complexes with excess Q appears to reconstitute the protein's final electron acceptor (Q_B). Because RC treatment with Q induces a slower decrease of photocurrent, in an effort to increase the photocurrent density to a higher value, RC-LH1 complexes were treated with Q prior to preparation of the photoactive layer. Interestingly, the Q-treated RC-LH1 photo-active electrode yielded ~9 and ~1.5 times higher photocurrent densities compared to that of RC alone and Q-treated RC, respectively. The relatively high value of the photocurrent at the end of the illumination cycles is promising for practical use of the proteins in real applications.

Figure 5.3(a) shows an initial spike of photocurrent at the onset of illumination (t = ~20 s) for the RC, the Q-treated RC, and the Q-treated RC-LH1 photoactive electrodes similar to what was recently reported.[50,62] According to Tan *et al.* this initial spike may be due to a faster rate of P$^+$ reduction relative to Q_B^- oxidation, which results in a buildup of negative charges within the protein.[62] Upon cessation of illumination, transient positive (reverse) currents (Figure 5.3(a)) were observed both for the Q-treated RC and RC-LH1 photoactive electrodes. The positive current is attributed to oxidation and reduction reactions at the photoactive working and the counter electrodes, respectively, which help in dissipating the energy difference between the electrode and the electrolyte to regain a state of equilibrium in the dark.[50,62]

A concern about the Q-treatment method was the possibility of Q acting as a second mediator in the cell, as in previous work that described an increase in the photocurrent when two mediators were used in a device with immobilized proteins.[62] In order to clarify the role of Q, a cell was fabricated with RC-LH1 proteins (no Q-treatment) and Q was added to the electrolyte (Figure 5.3(a), light green curve). The amount

of added Q was the same as in the Q-treated RC-LH1 (see Experimental Section). The RC-LH1 (Cp_2Fe+Q)

curve in Figure 5.3(a) shows the current value was less than 38% of the current in the device with Q-treated

RC-LH1 and a single added mediator. A possible explanation is that the purified RCs were partially or

completely lacking the Q_B quinone, and treating the proteins with Q reconstitutes the Q_B quinone which

enhances the ET from the proteins to the mediator (Cp_2Fe).

The photovoltaic effect was further studied by measuring the open circuit potential (V_{OC}) in the

cells with the electrolyte containing Cp_2Fe as the only added mediator. Figure 5.3(c) demonstrates the V_{OC}

of the Q-treated RC and RC-LH1 cells in response to cycles of illumination and dark. The mediator added

in both cases is 0.75 mM Cp_2Fe. However, it appears that the V_{OC} amplitude--*i.e.,* the difference between

the photo-response under illumination and in the dark--is more stable for the RC-LH1 complexes (ΔV

dropped from 90 mV to 60), than for the RC (ΔV changed from 110 mV to 60 mV) over the course of

experiment. Although the control photochronoamperometric experiment in Figure 5.3(b) indicated that the

observed photo-responses stem from photon absorption and charge generation in the RC and the RC-LH1

complexes, we verified this by obtaining the photocurrent action spectrum of the Q-treated RC-LH1

photoactive electrode using a monochromator to obtain dispersed light across the 400 nm to 950 nm

wavelength range. Figure 5.3(d) shows a compelling match between the Q-treated RC-LH1 solution

absorption spectrum and the photocurrent density across this wavelength range. This match between the

absorption spectrum and the photocurrent confirms that the RC-LH1 complexes were functional and intact.

The results indicate the EQE maximum value of 0.21% with illumination power of ~6 mW cm^{-2} at ~875

nm.

Figures 5.4(a-b) show the average of the photocurrent density response and the transient peak

photocurrent densities for the Q-treated RC-LH1 photoactive electrode in Cp_2Fe solution (one mediator

added) by varying the applied potential to higher and lower figures than the dark V_{OC} (positive and negative

voltages).
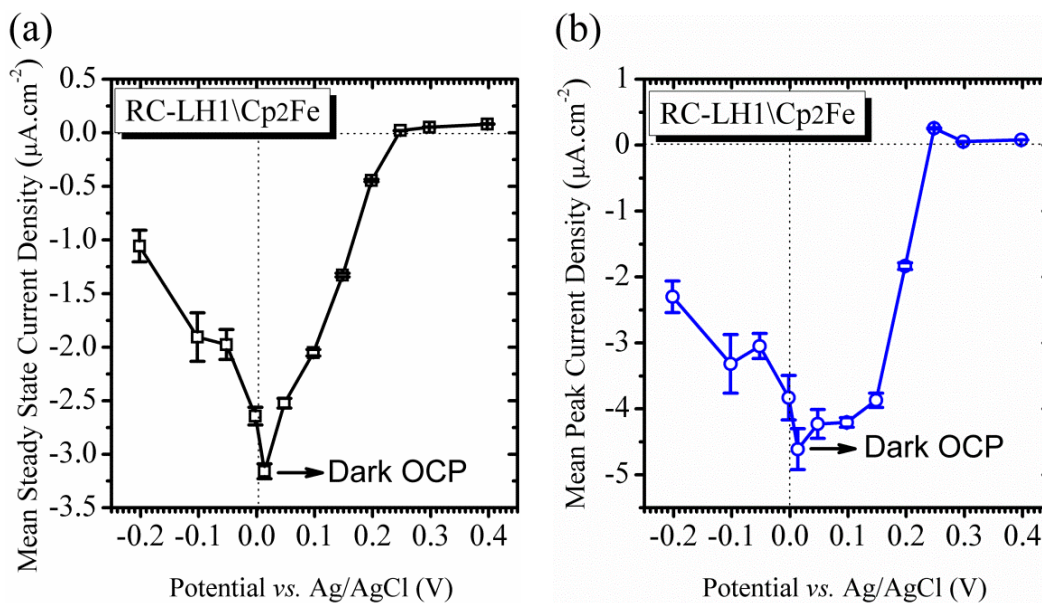
Figure 5.4 Effects of cycling the applied potential on: (a) the mean photocurrent densities (n = 10) and (b) the mean transient current densities (n = 10), obtained from the Q-treated RC-LH1 electrode. The stability of the photo-response is illustrated by the size of the error bars. Error bars represent the standard deviation between samples (n = 10). The photocurrent densities were determined by taking the difference between the current density in the dark and the current density after 20 s of illumination. The OCP value in dark is very close to zero. Hence, positive voltages represents positive bias/positive over potential and negative voltages represents negative bias/negative over potential.

It is clear that at applied potentials of -0.202 V to +0.248 V (*vs.* Ag/AgCl), cathodic photocurrent densities were measured whereas at the applied potentials higher than +0.248 V (*vs.* Ag/AgCl), anodic photocurrents were recorded. The maximum mean photocurrent density and mean peak transient photocurrent density of -3.2 and -4.6 μA cm^{-2} were measured at the dark OCP. The change in the photocurrent direction occurred around the applied potential of 0.248 V *vs.* Ag/AgCl. As discussed in the following text, these observations correlate well with the proposed energy diagram for these cells.

The mechanism for the operation of Q-treated RC-LH1 photoactive cells can be explained by an energy diagram, shown in Figure 5.5(a). The electrochemical midpoint potential of the redox electrolyte-- *i.e.*, containing 0.75 mM Cp_2Fe--was measured at ~0.5 V *vs.* Ag/AgCl (~-4.81 V *vs.* vacuum), as shown in Figure 5.5(b). The energy levels inside the RC have been studied in detail by others and are summarized by Blankenship.[51] The vacuum potential of Pt and the electrochemical potential of the Q_B site within the

RC were given by Tan *et al.*[32] The Fermi level (E_F) of the gold was measured as ~0.697 V *vs.* Ag/AgCl (~-5.0 V *vs.* Vacuum).
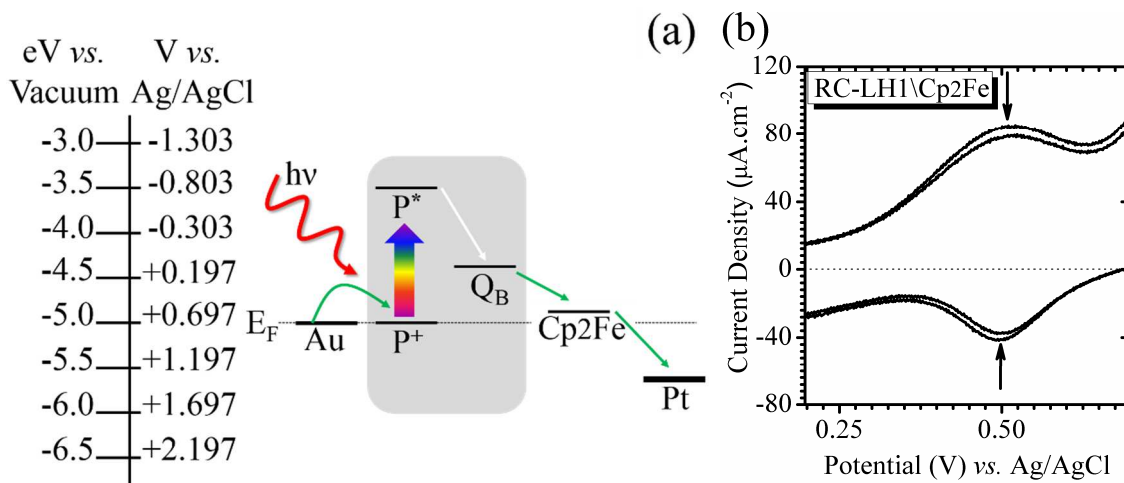
Figure 5.5 (a) The energy diagram of the fabricated bio-electrochemical cell with the Q-treated RC-LH1 photoactive electrode (at no bias) and the proposed mechanism for operation of this cell with Cp$_2$Fe, as the added diffusible redox mediator to the electrolyte. RC-LH1 complexes are modelled as obtaining electrons from the Au electrode. The energy level at each layer is given on the left side of the vertical scale as relative to the vacuum level. The corresponding electrochemical potentials can be found from the Ag/AgCl axis on the right side of the vertical scale. (b) CV of Q-treated RC-LH1 photoactive electrode in 0.75 mM Cp$_2$Fe solution, showing the electrochemical midpoint potential attributed to Cp$_2$Fe centred on 0.5 V *vs.* Ag/AgCl.

The energy diagram in Figure 5.5(a) is consistent with our interpretation that the electrons at the Q$_B$ side of RC-LH1 are transferred to the Pt counter electrode mainly *via* Cp$_2$Fe-mediated redox reactions in the electrolyte, while the photo-oxidized primary donor (P$^+$) is reduced by electrons coming from the Au working electrode.

In order to determine the effect of illumination on the impedance of the RC-LH1 photoactive layer, electrochemical impedance spectroscopy (EIS) was applied in the presence of Cp$_2$Fe as a mediator in the dark and under illumination (Figure 5.6).
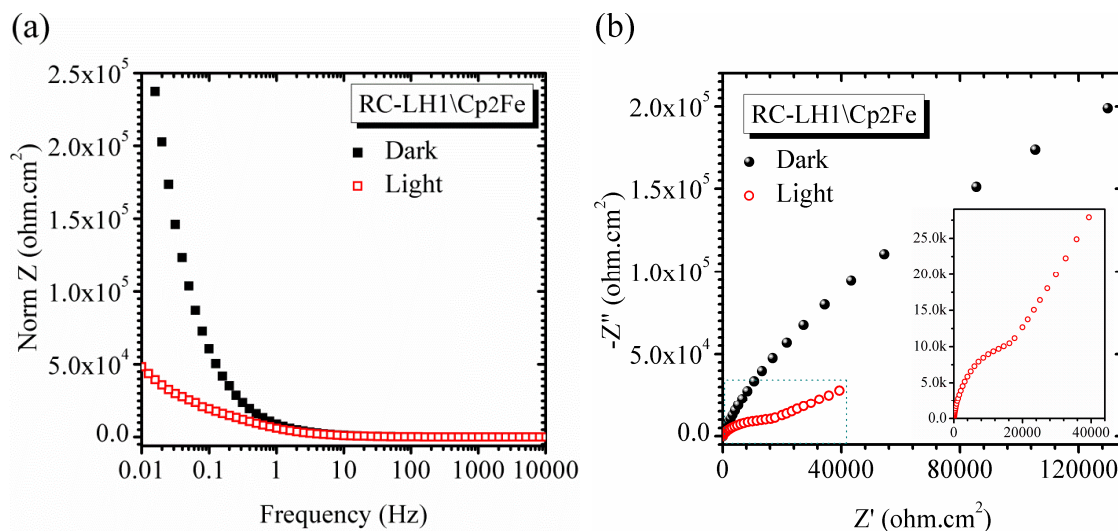
Figure 5.6 (a) Bode and (b) Nyquist plots of samples under dark and light conditions. Inset in part (b) shows the close-up view of the dashed rectangle. EIS was performed using a 10 mV AC voltage over a frequency range of 10^{-2} to 10^5 Hz.

Figure 5.6(a) shows an impedance with an inverted zero around 1 Hz for the RC-LH1/Au electrode in the dark and under illumination which implies the entire composite behaves as a single interface where electrons can be exchanged with the mediator at both the electrode's surface and the active sites (Q_B and P^+) of the RC-LH1 film. Recently, Leblanc *et al.* observed a similar phenomenon for photoelectrochemical solar cells based on PSI photoactive layers.[94] Additionally, we observed a significant decrease in impedance at low frequencies as a result of illumination (Figure 5.6(a)). As was shown by LeBlanc *et al.*,[94] this impedance element reflects the actual electron exchange with the redox mediator, showing that illumination enhances the ET. Also, in the Figure 5.6(b) inset, the changes in the slope of the Nyquist plot for the electrode under illumination suggests that the electrode polarization is due to a combination of diffusion and other processes, while the curve for the electrode in the dark behaves like a simple electrochemical reaction limited by diffusion.[174]

The large photocurrent response and the facile fabrication method using protein drop-casting in this work for making photoactive electrodes from the RC-LH1 complexes are encouraging for developing solar cell technology toward more bio-based devices. In the meantime, these data could be of importance for applications in molecular photonic devices. Besides metal/RC photoactive layers, semiconductor/RC

hybrids and oligomer-protein/RC hybrids have shown promise in solar energy conversion.[3,22,35] In addition to RC and RC-LH1 complexes, other chlorophyll-based proteins such as Photosystem I (PSI) and PSII have also been explored for solar energy conversion application.[40,41,94,95] A recent review summarizes some of these efforts in applications of RC, PSI, and PSII in biological-driven solar power production.[31] A most recent study successfully incorporated large photosynthetic complex trimers into solid-state plastic solar cells that were exclusively prepared by solution processing which resulted in a significant change in the open-circuit voltage.[96] Other applications of light harvesting proteins could be in production of solar fuels such as H_2.[97] The fast-paced activities in exploring new configurations and attaining higher efficiencies of biological solar energy conversion using various photosynthetic proteins,[30,101,102] fuel the idea that mimicking nature is a promising approach for developing a sustainable energy technology.

5.5. Conclusion

We showed that a relatively large photocurrent and external quantum efficiency can be achieved using Q-treated RC-LH1 complexes to fabricate photoactive electrodes. The electrode preparation is based on a simple solution-phase drop casting technique. Using this method, maximum EQE and mean photocurrent density of 0.21% and 2 μA cm^{-2}, respectively, were achieved with an illumination power of $\sim$6 mW cm^{-2} at $\sim$875 nm, which is comparable to the highest reported values in the field.

CHAPTER 6 : CONCLUSION AND FUTURE WORK

In the US, the share of solar energy between various types if sources such as natural gas, coal, and wind has increased significantly in the recent years. This trend is promising for the use of solar energy in electricity generation in much larger scale in near future. However, one of the ignored topics in renewable energy strategies is the sustainability of the renewable energy technology itself. Additionally, various types of technologies for harvesting solar energy should come together to be able to increase the share of renewables in energy production.

Photosynthesis is a natural and sustainable process for solar energy conversion. In photosynthesis the primary energy conversion reactions take place in a RC with nearly 100% quantum yield of primary charge separation and an efficient stabilization of separated charges which implies a great potential in incorporating the RC proteins in a photovoltaic device for solar energy harvesting. Although only a few groups working worldwide on the applications of RCs in bio-inspired systems for efficient light harvesting, the growth in the improvement of efficiency has been remarkable, to date. From the early devices, constructed by Trammell *et al.* in 2004, with photocurrent densities of several nA cm^{-2},[44] the field has been developed notably such that recent efforts demonstrate several µA cm^{-2} photocurrent densities in less than several years.[61,73] The fast-moving activities in fabricating devices with higher efficiencies for biological solar energy conversion using various photosynthetic proteins, fuels the idea that mimicking nature is a promising approach for developing a sustainable energy technology.

This work contributed to the better understanding of bio-hybrid solar cells using photosynthetic reaction centers and photosynthetic reaction centers plus light harvesting complexes and have identified the existed bottlenecks. My specific contributions to the field of bio-photovoltaic technology were: 1- devising the structure of a bio-photovoltaic solar cell by perceiving the key mechanism of charge transfer with a better ET characteristic, the result of which has been filed as a US patent and published as a technical paper

in a high profile journal, as well. 2- Developing a simple structure (Chapter 5, under review work) with relatively large external quantum efficiency that can be eventually scaled up for off-grid applications. 3- Pushing the external quantum efficiency of bio-hybrid devices to 0.21% which is comparable to highest reported figures in the field.[61,73]

6.1. Future Work

As future work in this area to develop a more efficient bio-hybrid device using photosynthetic proteins, one can pursue several areas:

a- Maximizing the conversion efficiency of bio-hybrid devices with improving the ET between the protein complexes and the metal electrodes using conjugated structures. In order to achieve a high ET rate between the biomolecule component (RC) and the electrode, the energy levels at the linker layer (between RC and the electrode shown in the Figure 6.1) must energetically line up with the adjacent layers to avoid charge blockage. In this regard, it is suggested to use organic conductive and/or semiconductive linkers with conjugated structure instead of the insulating linker molecule. The candidate materials can be oligomers of thiophene and ethylenedioxythiophene.
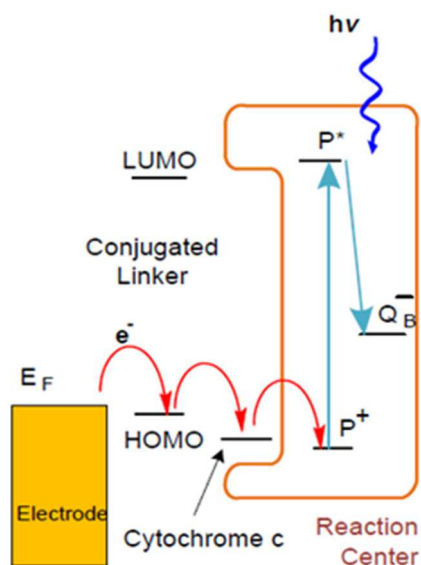
Figure 6.1 A schematic representation of the proposed structure, using a conjugated linker with appropriate HOMO level for an efficient electron transfer to the linker protein and photosynthetic protein.

The HOMO level in regioregular poly (3-hexylthiophene) (rr-P3HT) is close to the energy level at the primary electron donor side of the photosynthetic protein. The use of organic semiconductors as the linker for protein immobilization requires a full study of the interface and a proper alignment of the energy levels along the whole linker structure.

b- One of the possible strategies to increase the EQE in bio-hybrid solar cells is to use porous transparent semiconducting materials as the working electrode instead of metals. Semiconductors with matching energy levels with the proteins can enhance the charge transfer between immobilized proteins and the electrode. A candidate material is ZnO nanowires. Considering the background of the group in growing ZnO nanowires,[175] this approach can expand the synergy between the researchers working in the Bio-Organic Electronics lab.

The biomimetic solar conversion is considered as an ongoing research domain. Scientists have tried various hypotheses to fabricate cheaper and more efficient devices for harvesting the sun's energy. The result, has been mainly shifting from expensive solid devices toward cheaper flexible structures. The recent advanced in replicating what nature has been done for billions of years, has created a relatively new research stream that shows a great potential for revolutionizing the way we harvest solar energy. This trend towards biomimetic devices can be considered a theme that will endure to shape the fabrication of solar cells for the future.

REFERENCES

(1)   Huscher, J. S., D. *THE UNPAID HEALTH BILL: How coal power plants make us sick*, The Health and Environment Alliance (HEAL), 2013.

(2)   Burt, E. O., P.; Buchanan, S. *Scientific Evidence of Health Effects from Coal Use in Energy Generation*, University of Illinois at Chicago School of Public Health, 2013.

(3)   Yaghoubi, H.; Li, Z.; Jun, D.; Lafalce, E.; Jiang, X.; Schlaf, R.; Beatty, J. T.; Takshi, A. *The Journal of Physical Chemistry C* **2014**, *118*, 23509.

(4)   Gratzel, M. *Nature* **2001**, *414*, 338.

(5)   Brattain, W. H.; Garrett, C. G. B. *Bell System Technical Journal* **1955**, *34*, 129.

(6)   Gerischer, H. *Journal of The Electrochemical Society* **1966**, *113*, 1174.

(7)   Behrouznejad, F.; Taghavinia, N. *ChemElectroChem* **2014**, *1*, 944.

(8)   Pazoki, M.; Taghavinia, N.; Hagfeldt, A.; Boschloo, G. *The Journal of Physical Chemistry C* **2014**, *118*, 16472.

(9)   Behrouznejad, F.; Taghavinia, N. *Journal of Power Sources* **2014**, *260*, 299.

(10)   Alimirsalari, S.; Tajabadi, F.; Salehkoutahi, S. M.; Ghahary, R.; Taghavinia, N. *RSC Advances* **2014**, *4*, 45174.

(11)   Ghazyani, N.; Majles Ara, M. H.; Tajabadi, F.; Dabirian, A.; Mohammadpour, R.; Taghavinia, N. *RSC Advances* **2014**, *4*, 3621.

(12)   Pichot, F.; Gregg, B. A. *The Journal of Physical Chemistry B* **1999**, *104*, 6.

(13)   Cahen, D.; Hodes, G.; Grätzel, M.; Guillemoles, J. F.; Riess, I. *The Journal of Physical Chemistry B* **2000**, *104*, 2053.

(14)   van de Lagemaat, J.; Park, N. G.; Frank, A. J. *The Journal of Physical Chemistry B* **2000**, *104*, 2044.

(15)   Vesborg, P. C. K.; Jaramillo, T. F. *RSC Advances* **2012**, *2*, 7933.

(16)   Olson, J. *Photosynth Res* **2006**, *88*, 109.

(17)   Nealson, K. H.; Conrad, P. G. *Life: past, present and future*, 1999; Vol. 354.

(18)   Steger, U., Achterberg, W., Blok, K., Bode, H., Frenz, W., Gather, C., Hanekamp, G., Imboden, D., Jahnke, M., Kost, M., Kurz, R., Nutzinger, H.G., Ziesemer, Th. *Sustainable Development and Innovation in the Energy Sector*; Springer, 2005.

(19)   Field, C. B.; Behrenfeld, M. J.; Randerson, J. T.; Falkowski, P. *Science* **1998**, *281*, 237.

(20)   Blankenship, R. E.; Tiede, D. M.; Barber, J.; Brudvig, G. W.; Fleming, G.; Ghirardi, M.; Gunner, M. R.; Junge, W.; Kramer, D. M.; Melis, A.; Moore, T. A.; Moser, C. C.; Nocera, D. G.; Nozik, A. J.; Ort, D. R.; Parson, W. W.; Prince, R. C.; Sayre, R. T. *Science* **2011**, *332*, 805.

(21)   Hall, D. O. and Rao, K. *Photosynthesis*; Cambridge University Press: Cambridge, 1999.

(22)   Younghye, K.; Seon Ae, S.; Jaehun, L.; Ki Dong, Y.; Ki Tae, N. *Nanotechnology* **2014**, *25*, 342001.

(23)   Alberts, B.; Johnson, A.; Lewis, J.; Morgan, D.; Raff, M.; Roberts, K.; Walter, P. *Molecular Biology of the Cell*; 6th ed.; Garland Science, 2014.

(24)   Feher, G. A., J. P.; Okamura, M. Y.; Ree, D. C. *Nature* **1989**, *339*, 111.

(25)   Deisenhofer, J.; Epp, O.; Miki, K.; Huber, R.; Michel, H. *Nature* **1985**, *318*, 618.

(26)   Deisenhofer, J.; Michel, H. *Science* **1989**, *245*, 1463.

(27)   Terasaki, N.; Yamamoto, N.; Tamada, K.; Hattori, M.; Hiraga, T.; Tohri, A.; Sato, I.; Iwai, M.; Iwai, M.; Taguchi, S.; Enami, I.; Inoue, Y.; Yamanoi, Y.; Yonezawa, T.; Mizuno, K.; Murata, M.; Nishihara, H.; Yoneyama, S.; Minakata, M.; Ohmori, T.; Sakai, M.; Fujii, M. *Biochimica et Biophysica Acta (BBA) - Bioenergetics* **2007**, *1767*, 653.

(28)   Iwuchukwu, I. J.; Vaughn, M.; Myers, N.; O'Neill, H.; Frymier, P.; Bruce, B. D. *Nat Nano* **2010**, *5*, 73.

(29)   Herrero, C.; Quaranta, A.; Leibl, W.; Rutherford, A. W.; Aukauloo, A. *Energy & Environmental Science* **2011**, *4*, 2353.

(30)   Boghossian, A. A.; Ham, M.-H.; Choi, J. H.; Strano, M. S. *Energy & Environmental Science* **2011**, *4*, 3834.

(31)   Yehezkeli, O.; Tel-Vered, R.; Michaeli, D.; Willner, I.; Nechushtai, R. *Photosynth Res* **2013**, 1.

(32)   Tan, S. C.; Crouch, L. I.; Mahajan, S.; Jones, M. R.; Welland, M. E. *ACS Nano* **2012**, *6*, 9103.

(33)   Yaghoubi, H.; Li, Z.; Jun, D.; Saer, R.; Slota, J. E.; Beerbom, M.; Schlaf, R.; Madden, J. D.; Beatty, J. T.; Takshi, A. *The Journal of Physical Chemistry C* **2012**, *116*, 24868.

(34)   Yaghoubi, H., Takshi, A., Jun, D., Saer, R., Madden, J. D., Beatty, J. T. In *The 2011 Materials Research Society (MRS) Fall Meeting* Boston, MA, 2011; Vol. 1414, p mrsf11.

(35)   Takshi, A.; Yaghoubi, H.; Jun, D.; Saer, R.; Mahmoudzadeh, A.; Madden, J. D.; Beatty, J. T. In *MRS Online Proc. Libr.* Boston, MA, 2012; Vol. 1414, p No. mrsf11.

(36)   den Hollander, M.-J.; Magis, J. G.; Fuchsenberger, P.; Aartsma, T. J.; Jones, M. R.; Frese, R. N. *Langmuir* **2011**, *27*, 10282.

(37)   Lu, Y.; Xu, J.; Liu, B.; Kong, J. *Biosensors and Bioelectronics* **2007**, *22*, 1173.

(38)   Katz, E. *Journal of Electroanalytical Chemistry* **1994**, *365*, 157.

(39)   Efrati, A.; Tel-Vered, R.; Michaeli, D.; Nechushtai, R.; Willner, I. *Energy & Environmental Science* **2013**, *6*, 2950.

(40)   LeBlanc, G.; Chen, G.; Gizzie, E. A.; Jennings, G. K.; Cliffel, D. E. *Advanced Materials* **2012**, *24*, 5959.

(41)   Ciesielski, P. N.; Hijazi, F. M.; Scott, A. M.; Faulkner, C. J.; Beard, L.; Emmett, K.; Rosenthal, S. J.; Cliffel, D.; Kane Jennings, G. *Bioresource Technology* **2010**, *101*, 3047.

(42)   Yehezkeli, O.; Wilner, O. I.; Tel-Vered, R.; Roizman-Sade, D.; Nechushtai, R.; Willner, I. *The Journal of Physical Chemistry B* **2010**, *114*, 14383.

(43)   Nagata, M.; Amano, M.; Joke, T.; Fujii, K.; Okuda, A.; Kondo, M.; Ishigure, S.; Dewa, T.; Iida, K.; Secundo, F.; Amao, Y.; Hashimoto, H.; Nango, M. *ACS Macro Letters* **2012**, *1*, 296.

(44)   Trammell, S. A.; Wang, L.; Zullo, J. M.; Shashidhar, R.; Lebedev, N. *Biosensors and Bioelectronics* **2004**, *19*, 1649.

(45)   Kondo, M.; Iida, K.; Dewa, T.; Tanaka, H.; Ogawa, T.; Nagashima, S.; Nagashima, K. V. P.; Shimada, K.; Hashimoto, H.; Gardiner, A. T.; Cogdell, R. J.; Nango, M. *Biomacromolecules* **2012**, *13*, 432.

(46)   Al-Aribe, K. M.; Knopf, G. K.; Bassi, A. S. 2013; Vol. 8615, p 86150Q.

(47)   Bertoncello P, N. D., Paternolli C, Bavastrello V, Nicolini C *IEEE Trans Nanobioscience* **2003**, *2*, 124.

(48)   Zhang, L.; Zeng, T.; Cooper, K.; Claus, R. O. *Biophysical Journal* **2003**, *84*, 2502.

(49)   Van den Brink, J. *J. Chem. Phys.* **1996**, *104*, 1805.

(50)   Mirvakili, S. M.; Slota, J. E.; Usgaocar, A. R.; Mahmoudzadeh, A.; Jun, D.; Mirvakili, M. N.; Beatty, J. T.; Madden, J. D. W. *Advanced Functional Materials* **2014**, *24*, 4789.

(51)   Blankenship, R. E. *Molecular Mechanisms of Photosynthesis*; Blackwell Science, 2002.

(52)   Hashimoto, H. F., R.; Yanagi, K.; Kusumoto, T.; Gardiner, A. T.; Cogdell, R. J.; Roszak, A. W.; Issacs, N. W.; Pendon, Z.; Niedzwiedski, D.; Frank, H. A. *Pure Appl. Chem.* **2006**, *78*, 1505.

(53)   Magis, G. J.; Olsen, J. D.; Reynolds, N. P.; Leggett, G. J.; Hunter, C. N.; Aartsma, T. J.; Frese, R. N. *Photochemistry and Photobiology* **2011**, *87*, 1050.

(54)   Frolov, L.; Wilner, O.; Carmeli, C.; Carmeli, I. *Advanced Materials* **2008**, *20*, 263.

(55)   Roszak, A. W.; Howard, T. D.; Southall, J.; Gardiner, A. T.; Law, C. J.; Isaacs, N. W.; Cogdell, R. J. *Science* **2003**, *302*, 1969.

(56)   Axelrod, H. L.; Abresch, E. C.; Okamura, M. Y.; Yeh, A. P.; Rees, D. C.; Feher, G. *Journal of molecular biology* **2002**, *319*, 501.

(57)   Albert L. Lehninger, D. L. N., Michael M. Cox *Lehninger principles of biochemistry*; W. H. Freeman and Co.: New York, 2008.

(58)   Takahashi, E., Wraight, C. A. *Proc. Natl. Acad. Sci.* **1996**, *93*, 2640.

(59)   Winkler, H. B. G. a. J. R. *Biochimica et Biophysica Acta (BBA) - Bioenergetics* **2010**, *1797*, 1563.

(60)   Das, R.; Kiley, P. J.; Segal, M.; Norville, J.; Yu, A. A.; Wang, L.; Trammell, S. A.; Reddick, L. E.; Kumar, R.; Stellacci, F.; Lebedev, N.; Schnur, J.; Bruce, B. D.; Zhang, S.; Baldo, M. *Nano Letters* **2004**, *4*, 1079.

(61)   Tan, S. C.; Yan, F.; Crouch, L. I.; Robertson, J.; Jones, M. R.; Welland, M. E. *Advanced Functional Materials* **2013**, 5556.

(62)   Tan, S. C.; Crouch, L. I.; Jones, M. R.; Welland, M. *Angewandte Chemie International Edition* **2012**, *51*, 6667.

(63)   Trammell, S. A.; Griva, I.; Spano, A.; Tsoi, S.; Tender, L. M.; Schnur, J.; Lebedev, N. *The Journal of Physical Chemistry C* **2007**, *111*, 17122.

(64)   Kondo, M.; Nakamura, Y.; Fujii, K.; Nagata, M.; Suemori, Y.; Dewa, T.; Iida, K.; Gardiner, A. T.; Cogdell, R. J.; Nango, M. *Biomacromolecules* **2007**, *8*, 2457.

(65)   Trammell, S. A.; Spano, A.; Price, R.; Lebedev, N. *Biosensors and Bioelectronics* **2006**, *21*, 1023.

(66)   Zhao, J.; Liu, B.; Zou, Y.; Xu, C.; Kong, J. *Electrochimica Acta* **2002**, *47*, 2013.

(67)   Zhao, J.; Zou, Y.; Liu, B.; Xu, C.; Kong, J. *Biosensors and Bioelectronics* **2002**, *17*, 711.

(68)   Tiede, D. M. D., P. L. In *Photosynthetic Reaction Center (Deisenhofer, J. & Norris, J. R., eds)*; Deisenhofer, J. N., J. R., Ed.; Academic Press: San Diego, CA, 1993; Vol. 1, p 257.

(69)   Lebedev, N.; Trammell, S. A.; Spano, A.; Lukashev, E.; Griva, I.; Schnur, J. *Journal of the American Chemical Society* **2006**, *128*, 12044.

(70)   Trammell, S. A.; Lowy, D. A.; Seferos, D. S.; Moore, M.; Bazan, G. C.; Lebedev, N. *Journal of Electroanalytical Chemistry* **2007**, *606*, 33.

(71)   Mahmoudzadeh, A.; Saer, R.; Jun, D.; Mirvakili, S. M.; Takshi, A.; Iranpour, B.; Ouellet, E.; Lagally, E. T.; Madden, J. D. W.; Beatty, J. T. *Smart Materials and Structures* **2011**, *20*, 094019.

(72)   Lebedev, N.; Trammell, S. A.; Tsoi, S.; Spano, A.; Kim, J. H.; Xu, J.; Twigg, M. E.; Schnur, J. M. *Langmuir* **2008**, *24*, 8871.

(73)   Kamran, M.; Delgado, J. D.; Friebe, V.; Aartsma, T. J.; Frese, R. N. *Biomacromolecules* **2014**, *15*, 2833.

(74)   Yasuda, Y.; Hirata, Y.; Sugino, H.; Kumei, M.; Hara, M.; Miyake, J.; Fujihira, M. *Thin Solid Films* **1992**, *210–211, Part 2*, 733.

(75)   Sumino, A.; Dewa, T.; Sasaki, N.; Kondo, M.; Nango, M. *The Journal of Physical Chemistry Letters* **2013**, *4*, 1087.

(76)   Crouch, L. I.; Jones, M. R. *Biochimica et Biophysica Acta (BBA)-Bioenergetics* **2012**, *1817*, 336.

(77)   Vasilev, C.; Brindley, A.; Olsen, J.; Saer, R.; Beatty, J. T.; Hunter, C. N. *Photosynth Res* **2013**, 1.

(78)   Qian, P.; Papiz, M. Z.; Jackson, P. J.; Brindley, A. A.; Ng, I. W.; Olsen, J. D.; Dickman, M. J.; Bullough, P. A.; Hunter, C. N. *Biochemistry* **2013**, *52*, 7575.

(79)   Suemori, Y.; Nagata, M.; Nakamura, Y.; Nakagawa, K.; Okuda, A.; Inagaki, J.-i.; Shinohara, K.; Ogawa, M.; Iida, K.; Dewa, T.; Yamashita, K.; Gardiner, A.; Cogdell, R.; Nango, M. *Photosynth Res* **2006**, *90*, 17.

(80)   Magis, G. J.; den Hollander, M.-J.; Onderwaater, W. G.; Olsen, J. D.; Hunter, C. N.; Aartsma, T. J.; Frese, R. N. *Biochimica et Biophysica Acta (BBA) - Biomembranes* **2010**, *1798*, 637.

(81)   Matsuura, K.; Shimada, K. *Biochimica et Biophysica Acta (BBA) - Bioenergetics* **1986**, *852*, 9.

(82)   Deisenhofer, J.; Epp, O.; Sinning, I.; Michel, H. *Journal of Molecular Biology* **1995**, *246*, 429.

(83)   Nogi, T.; Fathir, I.; Kobayashi, M.; Nozawa, T.; Miki, K. *Proceedings of the National Academy of Sciences* **2000**, *97*, 13561.

(84)   Agalidis, I.; Velthuys, B. R. *FEBS Letters* **1986**, *197*, 263.

(85)   Comayras, F.; Jungas, C.; Lavergne, J. *Journal of Biological Chemistry* **2005**, *280*, 11203.

(86)   Janzen, A. F.; Seibert, M. *Nature* **1980**, *286*, 584.

(87)   Seibert, M.; Janzen, A. F.; Kendall-Tobias, M. *Photochemistry and Photobiology* **1982**, *35*, 193.

(88)   Lu, Y.; Yuan, M.; Liu, Y.; Tu, B.; Xu, C.; Liu, B.; Zhao, D.; Kong, J. *Langmuir* **2005**, *21*, 4071.

(89)   Takshi, A.; Madden, J. D. W.; Mahmoudzadeh, A.; Saer, R.; Beatty, J. T. *Energies* **2010**, *3*, 1721.

(90)   Usgaocar, A. R.; Wang, L.; Hong, Z.; Madden, J. D. W. *ECS Transactions* **2013**, *53*, 245.

(91)   Usgaocar, A. R.; Wang, L.; Mahmoudzadeh, A.; Mirvakili, S. M.; Slota-Newson, J. E.; Madden, J. D.; Beatty, J. T.; Takshi, A. *Meeting Abstracts* **2013**, *MA2013-01*, 282.

(92)   Nabiev, I.; Rakovich, A.; Sukhanova, A.; Lukashev, E.; Zagidullin, V.; Pachenko, V.; Rakovich, Y. P.; Donegan, J. F.; Rubin, A. B.; Govorov, A. O. *Angewandte Chemie International Edition* **2010**, *49*, 7217.

(93)   Maksimov, E. G.; Lukashev, E. P.; Seifullina, N. K.; Nizova, G. V.; Pashchenko, V. Z. *Nanotechnol Russia* **2013**, *8*, 423.

(94)   LeBlanc, G.; Winter, K. M.; Crosby, W. B.; Jennings, G. K.; Cliffel, D. E. *Advanced Energy Materials* **2014**, *4*, 1301953.

(95)   Ciesielski, P. N.; Faulkner, C. J.; Irwin, M. T.; Gregory, J. M.; Tolk, N. H.; Cliffel, D. E.; Jennings, G. K. *Advanced Functional Materials* **2010**, *20*, 4048.

(96)   Gordiichuk, P. I.; Wetzelaer, G.-J. A. H.; Rimmerman, D.; Gruszka, A.; de Vries, J. W.; Saller, M.; Gautier, D. A.; Catarci, S.; Pesce, D.; Richter, S.; Blom, P. W. M.; Herrmann, A. *Advanced Materials* **2014**, *26*, 4863.

(97)   Ihssen, J.; Braun, A.; Faccio, G.; Gajda-Schrantz, K.; Thöny-Meyer, L. *Current Protein & Peptide Science* **2014**, *15*, 374.

(98)   Patil, A. V.; Premaruban, T.; Berthoumieu, O.; Watts, A.; Davis, J. J. *The Journal of Physical Chemistry B* **2011**, *116*, 683.

(99)   Prasad, M.; Roy, S. *NanoBioscience, IEEE Transactions on* **2012**, *11*, 410.

(100)   Palazzo, G.; Magliulo, M.; Mallardi, A.; Angione, M. D.; Gobeljic, D.; Scamarcio, G.; Fratini, E.; Ridi, F.; Torsi, L. *ACS Nano* **2014,** *8*, 7834.

(101)   Nguyen, K.; Bruce, B. D. *Biochimica et Biophysica Acta (BBA) - Bioenergetics* **2014**, *1837*, 1553.

(102)   Tel-Vered, R.; Willner, I. *ChemElectroChem* **2014**, *1*, 1778.

(103)   Vanderkooi, J. M., Adar, F., Erecinska, M. *Eur. J. Biochem.* **1976**, *64*, 381.

(104)   Goldsmith, J. O.; Boxer, S. G. *Biochimica et Biophysica Acta (BBA) - Bioenergetics* **1996**, *1276*, 171.

(105)   Jones, M. In *The Purple Phototrophic Bacteria*; Hunter, C. N., Daldal, F., Thurnauer, M., Beatty, J. T., Eds.; Springer Netherlands: 2009; Vol. 28, p 295.

(106)   Kabsch, W.; Sander, C. *Biopolymers* **1983**, *22*, 2577.

(107)   Abresch, E. C.; Axelrod, H. L. A.; Beatty, J. T.; Johnson, J. A.; Nechushtai, R.; Paddock, M. L. *Photosynth Res* **2005**, *86*, 61.

(108)   Yaghoubi, H.; Lafalce, E.; Jun, D.; Jiang, X.; Beatty, J. T.; Takshi, A. *Biomacromolecules* **2015**, *16*, 1112.

(109)   Vasilev, C.; Brindley, A. A.; Olsen, J. D.; Saer, R. G.; Beatty, J.; Hunter, C. *Photosynthesis Research* **2013**, 1.

(110)   Takshi, A.; Yaghoubi, H.; Tevi, T.; Bakhshi, S. *Journal of Power Sources* **2015**, *275*, 621.

(111)   Davis, K. L.; Drews, B. J.; Yue, H.; Waldeck, D. H.; Knorr, K.; Clark, R. A. *The Journal of Physical Chemistry C* **2008**, *112*, 6571.

(112)   Wang, L.; Waldeck, D. H. *The Journal of Physical Chemistry C* **2008**, *112*, 1351.

(113)   Eckermann, A. L.; Feld, D. J.; Shaw, J. A.; Meade, T. J. *Coordination Chemistry Reviews* **2010**, *254*, 1769.

(114)   Wei, J.; Liu, H.; Dick, A. R.; Yamamoto, H.; He, Y.; Waldeck, D. H. *Journal of the American Chemical Society* **2002**, *124*, 9591.

(115)   Wolak, M. u. A.; Balaeff, A.; Gutmann, S.; Helmrich, H. J.; Vosloo, R.; Beerbom, M. M.; Wierzbinski, E.; Waldeck, D. H.; Bezer, S.; Achim, C.; Beratan, D. N.; Schlaf, R. *The Journal of Physical Chemistry C* **2011**, *115*, 17123.

(116)   Schlaf, R.; Murata, H.; Kafafi, Z. H. *Journal of Electron Spectroscopy and Related Phenomena* **2001**, *120*, 149.

(117)   Solov'ev, A. A.; Katz, E. Y.; Shuvalov, V. A.; Erokhin, Y. E. *Bioelectrochemistry and Bioenergetics* **1991**, *26*, 29.

(118)   Lebedev, N.; Spano, A.; Trammell, S.; Griva, I.; Tsoi, S.; Schnur, J. M.; 1 ed.; Kafafi, Z. H., Lane, P. A., Eds.; SPIE: San Diego, CA, USA, 2007; Vol. 6656, p 665614.

(119)   Ciobanu, M.; Kincaid, H. A.; Lo, V.; Dukes, A. D.; Kane Jennings, G.; Cliffel, D. E. *Journal of Electroanalytical Chemistry* **2007**, *599*, 72.

(120)   Carmeli, I.; Frolov, L.; Carmeli, C.; Richter, S. *Journal of the American Chemical Society* **2007**, *129*, 12352.

(121)   Song, S.; Clark, R. A.; Bowden, E. F.; Tarlov, M. J. *The Journal of Physical Chemistry* **1993**, *97*, 6564.

(122)   Ding, X.; Yang, M.; Hu, J.; Li, Q.; McDougall, A. *Microchimica Acta* **2007**, *158*, 65.

(123)   Tarlov, M. J.; Bowden, E. F. *Journal of the American Chemical Society* **1991**, *113*, 1847.

(124)   Niwa, M.; Fukui, H.; Higashi, N. *Macromolecules* **1993**, *26*, 5816.

(125)   Sagara, T.; Niwa, K.; Sone, A.; Hinnen, C.; Niki, K. *Langmuir* **1990**, *6*, 254.

(126)   Mukherjee, D.; May, M.; Vaughn, M.; Bruce, B. D.; Khomami, B. *Langmuir* **2010**, *26*, 16048.

(127)   Takshi, A.; Madden, J. D.; Beatty, J. T. *Electrochimica Acta* **2009**, *54*, 3806.

(128)   Nakanishi, K.; Sakiyama, T.; Imamura, K. *Journal of Bioscience and Bioengineering* **2001**, *91*, 233.

(129)   Gray, J. J. *Current Opinion in Structural Biology* **2004**, *14*, 110.

(130)   Klejin, M. N., W. *Heterogen. Chem. Rev.* **1995**, *2*, 157.

(131)   Norde, W. *Advances in Colloid and Interface Science* **1986**, *25*, 267.

(132)   Norde, W.; MacRitchie, F.; Nowicka, G.; Lyklema, J. *Journal of Colloid and Interface Science* **1986**, *112*, 447.

(133)   Frolov, L.; Rosenwaks, Y.; Carmeli, C.; Carmeli, I. *Advanced Materials* **2005**, *17*, 2434.

(134)   Ciesielski, P. N.; Cliffel, D. E.; Jennings, G. K. *The Journal of Physical Chemistry A* **2011**, *115*, 3326.

(135)   Reiss, B. D.; Hanson, D. K.; Firestone, M. A. *Biotechnology Progress* **2007**, *23*, 985.

(136)   Chan, E. W. L.; Yousaf, M. N.; Mrksich, M. *The Journal of Physical Chemistry A* **2000**, *104*, 9315.

(137)   Bourg, M.-C.; Badia, A.; Lennox, R. B. *The Journal of Physical Chemistry B* **2000**, *104*, 6562.

(138)   Beerbom, M. M.; Gargagliano, R.; Schlaf, R. *Langmuir* **2005**, *21*, 3551.

(139)   Guo, L.-H.; Mukamel, S.; McLendon, G. *Journal of the American Chemical Society* **1995**, *117*, 546.

(140)   Benson, D. E.; Conrad, D. W.; de, R. M.; Lorimier; Trammell, S. A.; Hellinga, H. W. *Science* **2001**, *293*, 1641.

(141)   Mukherjee, D.; May, M.; Khomami, B. *Journal of Colloid and Interface Science* **2011**, *358*, 477.

(142)   Andrade; J.D., H. V., Wei; A.P. *Pure & Appl. Chem* **1992**, *64*, 1777.

(143)   *Physical Chemistry of Biological Interfaces*; Baszkim; A. , N. W., Ed.; Marcel Dekker, Inc.: New York, NY, 2000.

(144)   Grammel, H.; Ghosh, R. *Journal of Bacteriology* **2008**, *190*, 4912.

(145)   Millo, D.; Ranieri, A.; Gross, P.; Ly, H. K.; Borsari, M.; Hildebrandt, P.; Wuite, G. J. L.; Gooijer, C.; Zwan, G. v. d. *The Journal of Physical Chemistry C* **2009**, *113*, 2861.

(146)   Sakata, T.; Suda, Y.; Tanaka, J.; Tsubomura, H. *The Journal of Physical Chemistry* **1977**, *81*, 537.

(147)   Giardi, M. T.; Scognamiglio, V.; Rea, G.; Rodio, G.; Antonacci, A.; Lambreva, M.; Pezzotti, G.; Johanningmeier, U. *Biosensors and Bioelectronics* **2009**, *25*, 294.

(148)   Sepunaru, L.; Tsimberov, I.; Forolov, L.; Carmeli, C.; Carmeli, I.; Rosenwaks, Y. *Nano Letters* **2009**, *9*, 2751.

(149)   Govorov, A. O.; Carmeli, I. *Nano Letters* **2007**, *7*, 620.

(150)   Frolov, L.; Rosenwaks, Y.; Richter, S.; Carmeli, C.; Carmeli, I. *The Journal of Physical Chemistry C* **2008**, *112*, 13426.

(151)   Armstrong, F. A., Hill, H.A.O., Walton, N.J. **1986**, *18*, 261.

(152)   van Grondelle, R.; Dekker, J. P.; Gillbro, T.; Sundstrom, V. *Biochimica et Biophysica Acta (BBA) - Bioenergetics* **1994**, *1187*, 1.

(153)   Kirmaier, C.; Holten, D. *Photosynth Res* **1987**, *13*, 225.

(154)   Love, J. C.; Estroff, L. A.; Kriebel, J. K.; Nuzzo, R. G.; Whitesides, G. M. *Chemical Reviews* **2005**, *105*, 1103.

(155)   Lin, S.; Jiang, X.; Wang, L.; Li, G.; Guo, L. *The Journal of Physical Chemistry C* **2011**, *116*, 637.

(156)   Hobara, D.; Niki, K.; Cotton, T. M. *Biospectroscopy* **1998**, *4*, 161.

(157)   Hildebrandt, P.; Murgida, D. H. *Bioelectrochemistry* **2002**, *55*, 139.

(158)   Bain, C. D.; Troughton, E. B.; Tao, Y. T.; Evall, J.; Whitesides, G. M.; Nuzzo, R. G. *Journal of the American Chemical Society* **1989**, *111*, 321.

(159)   Papadopoulos, S.; Jürgens, K. D.; Gros, G. *Biophysical Journal* **2000**, *79*, 2084.

(160)   Hirota, S.; Ueda, M.; Hayashi, Y.; Nagao, S.; Kamikubo, H.; Kataoka, M. *Journal of Biochemistry* **2012**.

(161)   Khare, N.; Eggleston, C. M.; Lovelace, D. M.; Boese, S. W. *Journal of Colloid and Interface Science* **2006**, *303*, 404.

(162)   Swartz, W. E. *Analytical Chemistry* **1973**, *45*, 788A.

(163)   Lindau, I. P., P.; Doniach, S.; Spicer, W. E. *Nature* **1974**, *250*, 214.

(164)   Paterson, E.; Swaffield, R. In *Clay Mineralogy: Spectroscopic and Chemical Determinative Methods*; Wilson, M. J., Ed.; Springer Netherlands: 1994, p 226.

(165)   Chen, X.; Ferrigno, R.; Yang, J.; Whitesides, G. M. *Langmuir* **2002**, *18*, 7009.

(166)   Adir, N.; Axelrod, H. L.; Beroza, P.; Isaacson, R. A.; Rongey, S. H.; Okamura, M. Y.; Feher, G. *Biochemistry* **1996**, *35*, 2535.

(167)   Moser, C. C.; Dutton, P. L. *Biochemistry* **1988**, *27*, 2450.

(168)   Clark, R. A.; Bowden, E. F. *Langmuir* **1997**, *13*, 559.

(169)   Prince, R. C.; Baccarini-Melandri, A.; Hauska, G. A.; Melandri, B. A.; Crofts, A. R. *Biochimica et Biophysica Acta (BBA) - Bioenergetics* **1975**, *387*, 212.

(170)   Rosen, D.; Okamura, M. Y.; Abresch, E. C.; Valkirs, G. E.; Feher, G. *Biochemistry* **1983**, *22*, 335.

(171)   Davies, J. *The Physics of Low-Dimensional Semiconductors*; Cambridge University Press: New York, 2006.

(172)   Dimonte, A.; Frache, S.; Erokhin, V.; Piccinini, G.; Demarchi, D.; Milano, F.; Micheli, G. D.; Carrara, S. *Biomacromolecules* **2012**.

(173)   Swainsbury, D. J. K.; Friebe, V. M.; Frese, R. N.; Jones, M. R. *Biosensors and Bioelectronics* **2014**, *58*, 172.

(174)   Bard, A. J. L. R. F. *Electrochemical Methods: Fundamentals and Applications* (2 ed.) ed.; Wiley: New York, 2000.

(175)   Ebrahimi, H.; Yaghoubi, H.; Giammattei, F.; Takshi, A. *Electrochimica Acta* **2014**, *134*, 435.

APPENDIX A: COPYRIGHT PERMISSIONS

Below is permission for the use of Figure 1.1.

Diana G Smith <diana@env-health.org>   Jan 12
to me, info

Dear Houman,
Please go ahead and use Figure 1 from the Unpaid health bill report. We would just ask that give full credit to the source of the figure.

Good luck with you dissertation and best wishes,

Diana

--
Diana G. Smith
Communications and Media Adviser
Health and Environment Alliance (HEAL)
Tel: +33 1 55 25 25 84
Mobile: +33 6 33 04 2943
Email: diana@env-health.org
Website: www.env-health.org
Skype: dianagsmith2

Office address:
Health and Environment Alliance (HEAL)
28 Boulevard Charlemagne
B-1000 Bruxelles
Tel: +32 2 234 3640

Below is permission for the use of Figure 1.3, 1.4.

Below is permission for the use of Figure 1.5.

Order Completed

Thank you for your order.

This Agreement between ("You") and Garland Science - Books ("Garland Science - Books") consists of your order details and the terms and conditions provided by Garland Science - Books and Copyright Clearance Center.

License number	Reference confirmation email for license number
License date	May 15, 2015
Licensed content publisher	Garland Science - Books
Licensed content title	Molecular biology of the cell
Licensed content date	Jan 1, 2015
Type of use	Thesis/Dissertation
Requestor type	Academic institution
Format	Print, Electronic
Portion	chart/graph/table/figure
Number of charts/graphs/tables/figures	2
Title or numeric reference of the portion(s)	Figure 12-34a and Figure 14-43
Title of the article or chapter the portion is from	N/A
Editor of portion(s)	N/A
Author of portion(s)	Bruce Alberts, Alexander Johnson, Julian Lewis, David Morgan, Martin Raff, Keith Roberts, Peter Walter
Volume of serial or monograph	N/A
Issue, if republishing an article from a serial	6th
Page range of portion	1-1000
Publication date of portion	2006
Rights for	Main product and any product related to main product
Duration of use	Life of current and all future editions
Creation of copies for the disabled	no
With minor editing privileges	no
For distribution to	Worldwide
In the following language(s)	Original language of publication
With incidental promotional use	no
Lifetime unit quantity of new product	Up to 499
Made available in the following markets	Education
The requesting person/organization	Houman Yaghoubi - University of South Florida
Order reference number	None
Author/Editor	Houman Yaghoubi
The standard identifier	H
Title	Bio-Photoelectrochemical Solar Cells Incorporating Reaction Center and Reaction Center plus Light Harvesting Complexes
Publisher	University of South Florida
Expected publication date	Jun 2015
Estimated size (pages)	140
Billing Type	Invoice
Billing address	Houman Yaghoubi 14434 Caribbean Breeze Dr. #303
	Tampa, FL 33613 United States Attn: Houman Yaghoubi
Total (may include CCC user fee)	0.00 USD

CLOSE WINDOW

Below is permission for the use of Figures 1.6, 2.1, 2.2, and 2.3.

Below is permission for the use of Figure 1.7.

Below is permission for the use of Figures 1.9, 1.10, and 1.11.

144

Below is permission for the use of Figure 1.12.

ELSEVIER LICENSE
TERMS AND CONDITIONS

Jan 12, 2015

This is a License Agreement between Houman Yaghoubi ("You") and Elsevier ("Elsevier") provided by Copyright Clearance Center ("CCC"). The license consists of your order details, the terms and conditions provided by Elsevier, and the payment terms and conditions.

All payments must be made in full to CCC. For payment instructions, please see information listed at the bottom of this form.

Supplier	Elsevier Limited The Boulevard,Langford Lane Kidlington,Oxford,OX5 1GB,UK
Registered Company Number	1982084
Customer name	Houman Yaghoubi
Customer address	14414 Caribbean breeze Dr. #303 Tampa, FL 33613
License number	3546740738314
License date	Jan 12, 2015
Licensed content publisher	Elsevier
Licensed content publication	Electrochimica Acta
Licensed content title	Photoelectric conversion of photosynthetic reaction center in multilayered films fabricated by layer-by-layer assembly
Licensed content author	Jiequan Zhao,Baohong Liu,Yonglong Zou,Chunhe Xu,Jilie Kong
Licensed content date	7 May 2002
Licensed content volume number	47
Licensed content issue number	12
Number of pages	5
Start Page	2013
End Page	2017
Type of Use	reuse in a thesis/dissertation
Intended publisher of new work	other
Portion	figures/tables/illustrations
Number of figures/tables/illustrations	2
Format	both print and electronic
Are you the author of this Elsevier article?	No

Below is permission for the use of Figure 1.13.

146

Below is permission for the use of Figure 1.14.

147

Below is permission for the use of Figure 1.15.

Below is permission for the use of Figure 1.16.

149

Below is permission for the use of Figure 1.17.

Dear Sir/Lady,

I am sending this email to request a permission for using: scheme 1 and Figure 1(a) from the following article:
Lebedev, N.; Trammell, S. A.; Spano, A.; Lukashev, E.; Griva, I.; Schnur, J. *Journal of the American Chemical Society* 2006, *128*, 12044.
I want to reuse the aforementioned figures in my PhD dissertation titled: "Bio-Photoelectrochemical Solar Cells Incorporating Reaction Center and Reaction Center plus Light Harvesting Complexes", publisher: the University of South Florida.

I know it is a short notice but my deadline to submit this dissertation is on Thursday 05/14/2015.

Following is my complete address:

--
--
Houman Yaghoubi, Ph.D.
Bio\Organic Electronics Group, E

NB 351
University of South Florida
4202 E Fowler Ave.
Tampa, FL 33620
Email: hyaghoubi@mail.usf.edu
Webpage: www.houmanyaghoubi.com
Phone: (813) 409-8192

Below is permission for the use of Figure 1.18.

Below is permission for the use of Figures 1.19 and 1.20.

PERMISSION/LICENSE IS GRANTED FOR YOUR ORDER AT NO CHARGE

This type of permission/license, instead of the standard Terms & Conditions, is sent to you because no fee is being charged for your order. Please note the following:

- Permission is granted for your request in both print and electronic formats, and translations.
- If figures and/or tables were requested, they may be adapted or used in part.
- Please print this page for your records and send a copy of it to your publisher/graduate school.
- Appropriate credit for the requested material should be given as follows: "Reprinted (adapted) with permission from (COMPLETE REFERENCE CITATION). Copyright (YEAR) American Chemical Society." Insert appropriate information in place of the capitalized words.
- One-time permission is granted only for the use specified in your request. No additional uses are granted (such as derivative works or other editions). For any other uses, please submit a new request.

If credit is given to another source for the material you requested, permission must be obtained from that source.

BACK   CLOSE WINDOW

Below is permission for the use of Figure 1.21.

153

Below is permission for the use of Figure 1.22.

154

Below is permission for the use of Figure 1.23.

Order Completed

Thank you for your order.

This Agreement between ("You") and Garland Science - Books ("Garland Science - Books") consists of your order details and the terms and conditions provided by Garland Science - Books and Copyright Clearance Center.

License number	Reference confirmation email for license number
License date	May 15, 2015
Licensed content publisher	Garland Science - Books
Licensed content title	Molecular biology of the cell
Licensed content date	Jan 1, 2015
Type of use	Thesis/Dissertation
Requestor type	Academic institution
Format	Print, Electronic
Portion	chart/graph/table/figure
Number of charts/graphs/tables/figures	2
Title or numeric reference of the portion(s)	figure 12-34a and figure 14-43
Title of the article or chapter the portion is from	N/A
Editor of portion(s)	N/A
Author of portion(s)	Bruce Alberts, Alexander Johnson, Julian Lewis, David Morgan, Martin Raff, Keith Roberts, Peter Walter
Volume of serial or monograph	N/A
Issue, if republishing an article from a serial	6th
Page range of portion	1-1000
Publication date of portion	2006
Rights for	Main product and any product related to main product
Duration of use	Life of current and all future editions
Creation of copies for the disabled	no
With minor editing privileges	no
For distribution to	Worldwide
In the following language(s)	Original language of publication
With incidental promotional use	no
Lifetime unit quantity of new product	Up to 499
Made available in the following markets	Education
The requesting person/organization	Houman Yaghoubi - University of South Florida
Order reference number	None
Author/Editor	Houman Yaghoubi
The standard identifier	H
Title	Bio-Photoelectrochemical Solar Cells Incorporating Reaction Center and Reaction Center plus Light Harvesting Complexes
Publisher	University of South Florida
Expected publication date	Jun 2015
Estimated size (pages)	140
Billing Type	Invoice
Billing address	Houman Yaghoubi 14414 Caribbean Breeze Dr. #303 Tampa, FL 33613 United States Attn: Houman Yaghoubi
Total (may include CCC user fee)	0.00 USD

CLOSE WINDOW

155

Below is permission for the use of Figures 1.24-1.25.

Below is the permission for the use of Figures 1.26-1.27.

Copyright Clearance Center

RightsLink®

Home   Account Info   Help   Live Chat

ACS Publications
Most Trusted. Most Cited. Most Read.

Title: Self-Assembled Monolayer of Light-Harvesting Core Complexes from Photosynthetic Bacteria on a Gold Electrode Modified with Alkanethiols

Author: Masaharu Kondo, Yukari Nakamura, Kaoru Fujii, et al

Publication: Biomacromolecules

Publisher: American Chemical Society

Date: Aug 1, 2007

Copyright © 2007, American Chemical Society

Logged in as:
Houman Yaghoubi
Account #:
3000435863

LOGOUT

PERMISSION/LICENSE IS GRANTED FOR YOUR ORDER AT NO CHARGE

This type of permission/license, instead of the standard Terms & Conditions, is sent to you because no fee is being charged for your order. Please note the following:

- Permission is granted for your request in both print and electronic formats, and translations.
- If figures and/or tables were requested, they may be adapted or used in part.
- Please print this page for your records and send a copy of it to your publisher/graduate school.
- Appropriate credit for the requested material should be given as follows: "Reprinted (adapted) with permission from (COMPLETE REFERENCE CITATION). Copyright (YEAR) American Chemical Society." Insert appropriate information in place of the capitalized words.
- One-time permission is granted only for the use specified in your request. No additional uses are granted (such as derivative works or other editions). For any other uses, please submit a new request.

If credit is given to another source for the material you requested, permission must be obtained from that source.

BACK   CLOSE WINDOW

Below is the permission for the use of Figure 1.28.

Below is the permission for the use of Figure 1.29.

Below is the permission for the use of Figure 1.30-1.31.

JOHN WILEY AND SONS LICENSE
TERMS AND CONDITIONS

Jan 12, 2015

This Agreement between Houman Yaghoubi ("You") and John Wiley and Sons ("John Wiley and Sons") consists of your license details and the terms and conditions provided by John Wiley and Sons and Copyright Clearance Center.

License Number	3546850185816
License date	Jan 12, 2015
Licensed Content Publisher	John Wiley and Sons
Licensed Content Publication	Angewandte Chemie International Edition
Licensed Content Title	Generation of Alternating Current in Response to Discontinuous Illumination by Photoelectrochemical Cells Based on Photosynthetic Proteins
Licensed Content Author	Swee Ching Tan,Lucy I. Crouch,Michael R. Jones,Mark Welland
Licensed Content Date	May 23, 2012
Pages	5
Type of use	Dissertation/Thesis
Requestor type	University/Academic
Format	Print and electronic
Portion	Figure/table
Number of figures/tables	2
Original Wiley figure/table number(s)	Figures 1 and 2
Will you be translating?	No
Title of your thesis / dissertation	Bio-Photoelectrochemical Solar Cells Incorporating Reaction Center and Reaction Center plus Light Harvesting Complexes
Expected completion date	Feb 2015
Expected size (number of pages)	200
Requestor Location	Houman Yaghoubi 14621 Grenadine Dr. - Apt.3 Tampa, FL 33613 United States Attn: Houman Yaghoubi
Billing Type	Invoice
Billing Address	Houman Yaghoubi 14414 Caribbean breeze Dr. #303

Below is the permission for the use of Figure 1.32.

Below is the permission for the use of Figure 1.34.

Re: PLS Clear Permission Request - [579] NANOTECHNOLOGY (ONLINE) (13616528)   📁   Inbox ×   🖶 🗗

Permissions <permissions@iop.org>   5:02 AM (9 hours ago) ☆   ↩   ▾
to me ▾

Dear Houman Yaghoubi,

Thank you for your request to reproduce IOP Publishing material in your dissertation.

Regarding:

Figure 5 (Nanotechnology 25 (2014) 342001)
Figures 1c and 4 (Smart Mater. Struct. 20 (2011) 094019)

We are happy to grant permission for the use you request on the terms set out below.

<u>Conditions</u>

Non-exclusive, non-transferrable, revocable, worldwide, permission to use the material in print and electronic form will be granted **subject to the following conditions:**

- Permission will be cancelled without notice if you fail to fulfil any of the conditions of this letter.

- You will make reasonable efforts to contact the author(s) to seek consent for your intended use. Contacting one author acting expressly as authorised agent for their co-authors is acceptable.

- You will reproduce the following prominently alongside the material:

  o   the source of the material, including author, article title, title of journal, volume number, issue number (if relevant), page range (or first page if this is the only information available) and date of first publication. This information can be contained in a footnote or reference note; or

  o   a link back to the article (via DOI); and

  o   if practical and IN ALL CASES for works published under any of the Creative Commons licences the words "© IOP Publishing. Reproduced with permission. All rights reserved"

- The material will not, without the express permission of the author(s), be used in any way which, in the opinion of IOP Publishing, could distort or alter the author(s)' original intention(s) and meaning, be prejudicial to the honour or reputation of the author(s) and/or imply endorsement by the author(s) and/or IOP Publishing.

- Payment of £0 is received in full by IOP Publishing prior to use.

<u>Special Conditions – For STM Signatories ONLY (as agreed as part of the STM Guidelines)</u>

Any permissions granted for a particular edition will apply also to subsequent editions and for editions in other languages, provided such editions are for the work as a whole in situ and does not involve the separate exploitation of the permitted illustrations or excerpts.

If you have any questions, please feel free to contact our Permissions team at permissions@iop.org.

I should be grateful if you would acknowledge receipt of this email.

Kind regards,

Zora Catterick

Publishing Assistant

IOP Publishing

Please note: We do not usually provide signed permission forms as a separate attachment. Please print this email and provide it to your publisher as proof of permission.

Below is the permission for the use of Figure 1.35.

Below is the permission for the use of Figure 1.36, 1.37, and 1.38.

Copyright Clearance Center

RightsLink®

Home | Account Info | Help | Live Chat

ACS Publications
Most Trusted. Most Cited. Most Read.

Title: Photoelectric Performance of Bacteria Photosynthetic Proteins Entrapped on Tailored Mesoporous WO3-TiO2 Films

Author: Yidong Lu, Minjia Yuan, Yuan Liu, et al

Publication: Langmuir

Publisher: American Chemical Society

Date: Apr 1, 2005

Copyright © 2005, American Chemical Society

Logged in as:
Houman Yaghoubi
Account #:
3000435863

LOGOUT

PERMISSION/LICENSE IS GRANTED FOR YOUR ORDER AT NO CHARGE

This type of permission/license, instead of the standard Terms & Conditions, is sent to you because no fee is being charged for your order. Please note the following:

- Permission is granted for your request in both print and electronic formats, and translations.
- If figures and/or tables were requested, they may be adapted or used in part.
- Please print this page for your records and send a copy of it to your publisher/graduate school.
- Appropriate credit for the requested material should be given as follows: "Reprinted (adapted) with permission from (COMPLETE REFERENCE CITATION). Copyright (YEAR) American Chemical Society." Insert appropriate information in place of the capitalized words.
- One-time permission is granted only for the use specified in your request. No additional uses are granted (such as derivative works or other editions). For any other uses, please submit a new request.

If credit is given to another source for the material you requested, permission must be obtained from that source.

BACK | CLOSE WINDOW

Below is the permission for the use of Figure 1.39.

Below is the permission for the use of Table 1.1.

Copyright Clearance Center

RightsLink®

Home   Account Info   Help   Live Chat

ACS Publications
Most Trusted. Most Cited. Most Read.

Title: Photoelectric Performance of Bacteria Photosynthetic Proteins Entrapped on Tailored Mesoporous WO3-TiO2 Films

Author: Yidong Lu, Minjia Yuan, Yuan Liu, et al

Publication: Langmuir

Publisher: American Chemical Society

Date: Apr 1, 2005

Copyright © 2005, American Chemical Society

Logged in as:
Houman Yaghoubi
Account #:
3000435863

LOGOUT

PERMISSION/LICENSE IS GRANTED FOR YOUR ORDER AT NO CHARGE

This type of permission/license, instead of the standard Terms & Conditions, is sent to you because no fee is being charged for your order. Please note the following:

- Permission is granted for your request in both print and electronic formats, and translations.
- If figures and/or tables were requested, they may be adapted or used in part.
- Please print this page for your records and send a copy of it to your publisher/graduate school.
- Appropriate credit for the requested material should be given as follows: "Reprinted (adapted) with permission from (COMPLETE REFERENCE CITATION). Copyright (YEAR) American Chemical Society." Insert appropriate information in place of the capitalized words.
- One-time permission is granted only for the use specified in your request. No additional uses are granted (such as derivative works or other editions). For any other uses, please submit a new request.

If credit is given to another source for the material you requested, permission must be obtained from that source.

BACK   CLOSE WINDOW

Below is the permission for the use of Figure 1.40, 1.41, and Table 1.2.

Request for Permission to Reproduce or Re-Publish ECS Material

Please fax this form to: The Electrochemical Society (ECS), Attn: Permissions Requests, 1.609.730.0629.
You may also e-mail your request to: copyright@electrochem.org. Include all the information as required on this form. Please allow 3-7 days for your request to be processed.

I am preparing a (choose one): ☐ paper ☐ chapter ☐ book ☒ thesis

entitled: Bio-Photoelectrochemical Solar Cells Incorporating Reaction Center and Reaction Center plus Light Harvesting

to be published by: University of South Florida

in an upcoming publication entitled: Bio-Photoelectrochemical Solar Cells Incorporating Reaction Center and Reaction

I request permission to use the following material in the publication noted above, and request nonexclusive rights for all subsequent editions and in all foreign language translations for distribution throughout the world.

Description of material to be used—Indicate what material you wish to use (figures, tables, text, etc.) and give the full bibliographic reference for the source publication. You may attach a separate list, organized by ECS title.

3 Figures and a table including: 1- . Semiconductor-electrolyte interface energy alignment. 2- CVs of SnO2 in presence of various mediators at a scan rate of 10 mV s-1. 3- Sampled current Voltammetry between SnO2 and multiple mediators. Table: Rates of reaction of mediators with F:SnO2 electrode.

Semiconductors as Selective electrodes for Bio-photovoltaic Cells — MA 2013-01 (282) Figures 2,3,4, Table 1

Signature: Houman Yaghoubi   *Digitally signed by Houman Yaghoubi DN: cn=Houman Yaghoubi, o=University of South Florida, ou, email=hyaghoubi@mail.usf.edu, c=US Date: 2015.01.13 00:04:01 -05'00'*   Date: 1/13/2015

Name: Houman Yaghoubi

Address: 4202 E Fowler Ave. ENB 351, Tampa, FL 33620

Telephone: 8134098192   Fax:

E-mail: hyaghoubi@mail.usf.edu

Permission is granted to reproduce the above-referenced material. Please acknowledge the author(s) and publication data of the original material, and include the words: "Reproduced by permission of The Electrochemical Society."

Jan 30, 2015
Date   Ann F. Goedkoop, Publications Production Director

167

Below is permission for the use of Figure 1.42.

**JOHN WILEY AND SONS LICENSE
TERMS AND CONDITIONS**

Jan 13, 2015

This Agreement between Houman Yaghoubi ("You") and John Wiley and Sons ("John Wiley and Sons") consists of your license details and the terms and conditions provided by John Wiley and Sons and Copyright Clearance Center.

License Number	3546870800649
License date	Jan 13, 2015
Licensed Content Publisher	John Wiley and Sons
Licensed Content Publication	Angewandte Chemie International Edition
Licensed Content Title	Fluorescent Quantum Dots as Artificial Antennas for Enhanced Light Harvesting and Energy Transfer to Photosynthetic Reaction Centers
Licensed Content Author	Igor Nabiev,Aliaksandra Rakovich,Alyona Sukhanova,Evgeniy Lukashev,Vadim Zagidullin,Vladimir Pachenko,Yury P. Rakovich,John F. Donegan,Andrei B. Rubin,Alexander O. Govorov
Licensed Content Date	Aug 25, 2010
Pages	5
Type of use	Dissertation/Thesis
Requestor type	University/Academic
Format	Print and electronic
Portion	Figure/table
Number of figures/tables	2
Original Wiley figure/table number(s)	Figures 1 and 2
Will you be translating?	No
Title of your thesis / dissertation	Bio-Photoelectrochemical Solar Cells Incorporating Reaction Center and Reaction Center plus Light Harvesting Complexes
Expected completion date	Feb 2015
Expected size (number of pages)	200
Requestor Location	Houman Yaghoubi 14621 Grenadine Dr. - Apt.3 Tampa, FL 33613 United States Attn: Houman Yaghoubi
Billing Type	Invoice
Billing Address	Houman Yaghoubi 14414 Caribbean breeze Dr. #303

Below is permission for the use of Figure 1.43.

Below is permission for the use of Figure 1.44.

Below is permission for the use of Figures 2.4-2.5 and Chapter 5.

Below is permission for the use of Figures 2.6.

The two permissions below are for the use of material in Chapter 3.

Order Completed

Thank you very much for your order.

This is a License Agreement between Houman Yaghoubi ("You") and Cambridge University Press ("Cambridge University Press"). The license consists of your order details, the terms and conditions provided by Cambridge University Press, and the payment terms and conditions.

Get the printable license.

Below is permission for the use of Chapter 4.

Copyright Clearance Center

RightsLink®

Home   Create Account   Help   Live Chat

ACS Publications
Most Trusted. Most Cited. Most Read.

Title: Hybrid Wiring of the Rhodobacter sphaeroides Reaction Center for Applications in Bio-photoelectrochemical Solar Cells

Author: Houman Yaghoubi, Zhi Li, Daniel Jun, et al

Publication: The Journal of Physical Chemistry C

Publisher: American Chemical Society

Date: Oct 1, 2014

Copyright © 2014, American Chemical Society

LOGIN

If you're a copyright.com user, you can login to RightsLink using your copyright.com credentials. Already a **RightsLink user** or want to learn more?

PERMISSION/LICENSE IS GRANTED FOR YOUR ORDER AT NO CHARGE

This type of permission/license, instead of the standard Terms & Conditions, is sent to you because no fee is being charged for your order. Please note the following:

- Permission is granted for your request in both print and electronic formats, and translations.
- If figures and/or tables were requested, they may be adapted or used in part.
- Please print this page for your records and send a copy of it to your publisher/graduate school.
- Appropriate credit for the requested material should be given as follows: "Reprinted (adapted) with permission from (COMPLETE REFERENCE CITATION). Copyright (YEAR) American Chemical Society." Insert appropriate information in place of the capitalized words.
- One-time permission is granted only for the use specified in your request. No additional uses are granted (such as derivative works or other editions). For any other uses, please submit a new request.

BACK   CLOSE WINDOW

ABOUT THE AUTHOR

Houman Yaghoubi earned his B.Sc. and M.Sc. in Materials Science and Engineering in 2007 and 2010, respectively. He earned his Ph.D. in Electrical Engineering at the University of South Florida where he worked on several research domains including photosynthetic bio-hybrid electrochemical solar cells, CO_2 photoconversion to solar fuels using novel semiconductor nanocatalysts, electrochemical energy storage devices, and synthesis and characterization of nanomaterials. Houman has received several awards including 2014-15 University of South Florida Dissertation Completion Fellowship, 2013-14 Allan R. Gondeck Memorial Scholarship, 2013 Da Vinci Engineering Award, and The 2012 Inter-Continental Advanced Materials for Photonics (I-CAMP) award to participate in I-CAMP 2012 School on Renewable and Sustainable Energy where he was trained on various topics including: Solar Fuel Materials, Catalysts, Artificial Photosynthesis, Enzymatic and Bacterial Production of Biofuels, Nanoscale Photovoltaics, Chemical, Macromolecular, and Nanostructure Synthesis, Charge Transport and Recombination Kinetics, Light Trapping and Optical Control, and Photovoltaic Upscaling and Manufacturing Next Generation Strategies to Maximize Photon Harvesting in Organic Photovoltaic. He has a strong commitment to teaching and mentorship and have demonstrated this in various efforts. Namely, he was the instructor for the Foundations of Engineering course in the fall of 2011 at the University of South Florida and co-instructor for an upper level graduate course, Compound Semiconductor Materials. His students' work on the fabrication of solar ovens from scratch and his method of teaching was recognized by the Florida Energy Systems Consortium and published in the University of South Florida Clean Energy Research Center (CERC) newsletter.